Pan African University
Institute of Water and Energy Sciences

PAN-AFRICAN UNIVERSITY
INSTITUTE FOR WATER AND ENERGY SCIENCES
(including CLIMATE CHANGE)

Master Dissertation

Submitted in partial fulfillment of the requirements for the Master degree in

[Water Engineering]

Presented by

Attikora, Kouadio Ulrich ETCHE

FLOOD INUNDATION MODELING IN THE GOUROU WATERSHED OF CÔTE D'IVOIRE, WEST AFRICA

Defended on 02/09/2019 Before the Following Committee:

Chair	GEMOU Bouabdallah	Ph.D	University Center Belladj Bouchaid | Algeria
Supervisor	Amos T. Kabo-bah	Ph.D	University of Natural Resources | Ghana
External Examiner	Prof. Abdelkrim KHALDI	Professor	University of Sciences and Techniques of Oran
Internal Examiner	Benadda LOTFI	Ph.D	University Abou Bekr Belkaïd | Algeria

ACADEMIC YEAR: 2018-2019

DECLARATION

I, ETCHE Attikora Kouadio Ulrich, hereby declare that this thesis represents my personal work, realized to the best of my knowledge. I also declare that all information, material, and results from other works presented here, have been fully cited and referenced in accordance with the academic rules and ethics.

Signed: 

Name Attikora Kouadio Ulrich, ETCHE Date : 15 September 2019

APPROVAL

This thesis has been submitted with my approval as the supervisor

Signed 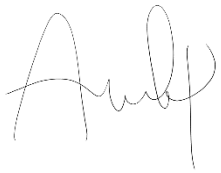 Date: 15 September 2019

Dr. Amos T. Kabo-bah

University of Energy and Natural Resources

Head, Energy and Environmental Engineering Department

DEDICATION

To my family

ABSTRACT

Nowadys, floods and droughts are becoming more and more frequent all other the world. According to the Emergency Events Database, Africa is the third continent most affected by flood events in terms of occurrence, total deaths, injured, affected and homeless. This report showed that since 1989, Côte d'Ivoire has experienced floods in 1996, 2007, 2008, 2010, 2014, 2015, 2016, and recently in 2017 and 2018. Those floods caused 169 deaths and around 40000 affected people. Floods occur principally in Abidjan. Their occurrences and amplitudes will increase due to climate change and the increasing urban population. The study was conducted to construct hydrological and hydrodynamics models couple with GIS for flood inundation mapping in Gourou watershed in Côte d'Ivoire. HEC-HMS and HEC-RAS models were used to achieve the specified objective. The result of hydrological modeling showed that the HEC-HMS model simulated fairly well the peak discharges. A sensitivity analysis of the HEC-HMS model parameters used in this study showed that the model outputs are more sensitive to Curve Number compared to the percentage of impervious area and lag time. From the result of hydrodynamics model, it was obvious that the floodplain inundated areas increase with the magnitude of flow within the modeled network confirming the high flood hazard level for settlements and activities near the main canal in Gourou watershed. The WSE profile showed a great variability as water is moving from upstream toward downstream. The obtained flood inundation map for 5-, 10-, 20-, 50-, 100-years illustrated that most of the inundated areas are built-up areas. Thus, flood inundation maps developed in this study can be used for decision making, along with strategies for flood preparedness.

Keywords: Flood, inundation mapping, hydrological modeling, hydrodynamics models, Curve number, HEC-HMS, HEC-RAS.

RESUME

Durant ces dernières décennies, les inondations et les sécheresses sont devenues de plus fréquentes dans le monde. Selon le rapport l'agence de gestion de la base de données des catastrophes naturelles, l'Afrique est le troisième continent le plus affecté par les inondations en termes d'occurrence, nombre de mort, personnes blessées et sans abri. Ce même rapport montre que depuis 1989, la Côte d'Ivoire a connu des inondations notamment en 1996, 2007, 2008, 2010, 2014, 2015, 2016 et dernièrement en 2017 et 2018. Ces inondations ont causé 169 morts et environ 40000 personnes affectés. Les inondations interviennent généralement dans la ville d'Abidjan. Leurs fréquences et intensités augmentent à cause du changement climatique et de l'augmentation de la population. Cette étude avait pour but de construire un modèle hydrologique et hydrodynamique basé l'utilisation des systèmes d'information géographiques pour la modélisation des inondations dans le bassin versant du Gourou. Pour atteindre cet objectif les modèles HEC-HMS et HEC-RAS ont été utilisé respectivement pour la modélisation hydrologique et hydraulique. Les résultats de la modélisation hydrologique ont montré que le modèle HEC-HMS est capable de simuler le ruissellement dans le bassin versant. Par ailleurs, l'analyse de la sensitivité des paramètres du model a montré que les résultats du modèle sont plus sensibles au Curve Number comparé au pourcentage de surface imperméable et le lag time. Les résultats de la modélisation hydraulique ont quant à eux montré que la surface de zones inondables augmente lorsque les débits d'écoulement augmentent. La largeur au miroir maximal en cas de débordement peut atteindre 166 m. Les cartes des zones inondables pour les périodes de retour de 5-, 10-, 20-, 50-, et 100 ans montrent que la plupart des zones inondables sont des habitations, les routes. Les cartes d'inondation produites lors de cette étude peuvent être utilisés dans les prises de décision à comme moyen de sensiblisation pour une meilleure gestion des inondations.

Mots clés : Inondation, carte d'inondation, model hydrologique, model hydrodynamique, Curve Number, HEC-HMS, HEC-RAS.

ACKNOWLEDGMENT

After twenty-four months, finally, here it is! It went slow, but with the help of several people and organizations, I managed to finish this M.Sc Thesis.

Though space is limited, here, I would like to express my thanks to:

- The African Union Commission for the scholarship they provided to support my studies as young African in Algeria;
- Pan African University, Institute of Water and Energy Sciences administration, for all the efforts they do to support the program and make it successful;
- My supervisor Dr. Amos KABO-BAH for his assistance and encouragement. I am deeply indebted to him for his ideas, and methodologies, especially in the field of flood hazards, GIS solutions and hydrological modeling;

I also want to acknowledge M. GOUGOU Antoine, Chief of "Programme d'Aménagement et de Gestion Intégrée du Bassin Versant du Gourou" and His staff especially Mrs KOUADIO Marie called kindly "Mother Marie", for their kind cooperation and for the materials provided during my study and internship. It has been really precious and worth wile to me.

I am very grateful to the people who gave me suggestions and support for the advancement of the thesis. As there are: LEKOMBO Claude Sara, KONAN N'Guessan Aimé, ZAUCYN David, KONE Aminata, N'GOM Leopold, ABOURAMANE Amadou, ESSOSSNINAM Emmanuel, GADO Abdel Aziz, EKPE Sévérin.

The blessings of my parents and family enabled me to come across all the hurdles. My deepest regards to them.

LIST OF ABREVIATION

ALOS	: Global Digital Surface Model
ASECNA	: Agency for Aerial Navigation Safety in Africa ann Nadagascar
ASTER	: Advanced Spaceborne Thermal Emission and Reflection Radiometer
BNETD	: Bureau National d'Etude Technique et de Developpement
CN	: Curve Number
DEM	: Digital Elevation Model
EM-DAT	: Emergency Events Database
GDEM	: Global Digital Elevation Model
GIS	: Geographical Information System
GPS	: Global Positioning System
HEC-GeoHMS	: Hydrology Engineers Centre – Geographical Hydrology Modeling System
HEC-HMS	: Hydrology Engineers Centre – Hydrology Modeling System
HEC-RAS	: Hydrology Engineers Centre – River Analysis System
hr	: Hour
IDF	: Intensity-Duration-Frequency
IPCC	: Intergovernmental Panel of Climate Change
LOB	: Left Overbank
NGO	: Non Governmental Organization
NSE	: Nash-Sutcliffe Efficiency
OLI	: Operational Land Imager
PEPF	: Percentage Error in Peak Flow
PWRMSE	: Peak-Weighted Root Mean Square Error
ROB	: Right Overbank
ROI	: Regions of Interest
SCS-CN	: Soil Conversation Service - Curve Number
SODEXAM	: Société d'Exploitation et de Développement Aéroportuaire, Aéronautique et Météorologique
SRTM	: Shuttle Radar Topography Mission
TIN	: Triangulated Irregular Network
TIRS	: Thermal Infrared Sensor
USACE	: United State Army Corps of Engineers
USGS	: United States Geological Survey
WSE	: Water Surface Elevation

TABLE OF CONTENTS

LISTE OF TABLES

LIST OF FIGURES

1 INTRODUCTION

1.1 Background

During the last decades, floods and droughts are becoming more and more frequent all other the world. According to the Emergency Events Database (EM-DAT, 03 Jan 2019), Africa is the third continent most affected by floods events in terms of occurrence, total deaths, injured, affected and homeless. This report showed also that since 1989, Côte d'Ivoire has experienced floods in 1996, 2007, 2008, 2010, 2014, 2015, 2016, and recently in 2017 and 2018. Those floods caused 169 deaths and around 40000 affected people. Floods occur principally in Abidjan (Capital city). Their occurrences and amplitudes will increase due to climate change and the increasing urban population (IPCC,2007).

Floods can be defined as an accumulation of water in places which are normally dry after a storm event. Depending on the origin of water and the generation processes, one can distinguish river flood, urban flood, ice jam flood, hurricanes, and flash flood. Cause of availability of water and the economic advantages that their offer, humans tend to settle in flood-prone areas. In Africa countries south of the Sahara, almost 72% of urban inhabitants live in slums (Aimé, 2018). Thus, the consequences of floods events can be worse in the absence of mitigation measures. There is then a need to set up flood mitigation measures. In terms of flood mitigation measures, there are two main methods which are structural methods and nonstructural methods. Nowadays, the importance of using nonstructural mitigation measures instead of structural measures is crucial cause their economic and environmental aspects.

Many studies have been conducted for the development of flood forecasting and early warning systems as one of the most important nonstructural flood mitigation tools (Ghalkhani *et al*., 2012). Those nonstructural measures include the use of Geographical Information System (GIS) for hydrologic and hydraulic modeling in order to determine flood-prone areas, inundation maps as well as to do a flood risk assessment.

Hydrologists and scientists in different field of competences have made many studies to understand the hydrologic cycle (rainfall-runoff process) in the watersheds. Those researches came out with

the development of hydrologic and hydraulic models to support decision making. These models with different approaches are used as tools for water resources management and development. The choice of any one of these models depends on the availability of the requires data and budget constraints. Among those models, GIS-based hydrological models are widely used in flood studies. HEC-HMS and HEC-RAS are widely used by engineers for rainfall/runoff and flood wave routing in a channel respectively. They are both developed by the US Army Corps of Engineers. Several applications of HEC-HMS and HEC-RAS models to determine the extent of inundation resulting from a given flood have been reported. A study carried out in Kabul River in Pakistan by (Shahzad *et al.*, 2015) showed that HEC-RAS is suitable in simulating water surface profiles and determining the extent of inundation under different return period. *Paresh et al., (2011)* used a GIS-based HEC-HMS and HEC-RAS modeling to estimate the peak discharges and obtain runoff volume/timing in the Woldiya watershed in Ethiopia. They found that GIS-Based Hydrological modeling reduces the analysis time and improves the accuracy of the analysis with the spatial data describing the watershed of interest. The advantage of using HEC-HMS and HEC-RAS is because they are free of charge, able to represent and study the hydrological process in a given watershed as much other software like MIKE DHI package.

1.2 Problem definition

Abidjan which is the capital city of Côte d'Ivoire faced urban flood on 11th May 2018 and 19th June 2018. The flood originated from a heavy rainfall event. A study conducted by (Aimé, 2018) shows that one of the causes is that the runoff, as a result of those rainfall events, exceeds the capacity of the drainage system. Referred specifically as "***pluvial flood***", urban floods are caused by the insufficence of drainage system to carry water sometimes due to the high rate of urbanization. In urbanized area, the soil has a little capacity of water storage, then almost all the precipitation (rainfall in our case) need to be conveyed through the drainage system. Pluvial floods, therefore, occur when rainfall events exceed the capacity of stormwater drains. This is usually associated with short storm events and high rainfall intensities, but may also occur for longer events with lower intensities, especially if the ground surface is impermeable, saturated, or frozen (Houston *et al.*, 2011). The case of Abidjan is very critical. In fact, due to the uncontrolled urbanization process, the population used to settle in flood-prone areas. Thus, almost all the natural

water bodies are transformed into artificial canal where the sections are sometimes small to convey the excess rainfall. This impact the equilibrium of water bodies system and can be a threat to the environment. Due to the economic and social damages related to flood, many different method and approach have been developed to support flood studies. Information regarding flood event is primordial for water resources management and future development. It will help to support decision making by providing ideas to choose some adapted strategies for flood risk management. Several studies pertaining to the flood hazard problem of Gourou watershed have been done. Nevertheless, research on the integration of GIS and hydrologic modeling has not been done in the area.

1.3 Objective of the study

The study seeks to construct hydrological and hydrodynamics models couple with GIS for flood inundation mapping in Gourou watershed in Côte d'Ivoire. The specific objectives are:

- To calibrate and validate HEC-HMS model for Gourou watershed
- To estimate the flood hydrographs in the watershed and used them as the inputs of the hydrodynamics model;
- To develop floods extent map for a return period of 5, 10, 50 and 100 years with associated water depth;
- To recommend mitigation measures for flood disaster risk management in the watershed.

1.4 Research questions

This research will be guided by the following questions:

- How accurate can the observed peak discharge be simulated by the selected modeling approach?
- How does the inundation pattern vary along the canal?
- What are the causes of the frequent occurrence of flood in Gourou watershed?
- What type of measure (structural and non-structural) would work best to alleviate the flood risk in the study area?

1.5 Structure of the study

This study is divided into six chapters. Chapter 1 provides a brief introduction and background of the study area. Chapter 2 will deal with the literature review. In this section, a detailed description of the two models used in the study, as well as application of GIS Techniques, are provided. Chapter 3 will present the datasets and the method used in this study. Thus, chapter four will be more focused on the description and explanation of the main findings. Chapter 7 presents the conclusion and recommendations.

2 LITERATURE REVIEW

2.1 Overview on flood

Flood is a natural process that occurred when the water rises to overflow land that is not normally submerged (Ward, 1978). Those lands are sometimes referred as floodplain. Floods are among the most devastating natural (and sometimes human-produced) threats on Earth (Ohl *et al.*, 2000), which involve inundations, i.e., submerged land from overflowing rivers and lakes when water overtops or breaks levees, from the sea because of high tides, and/or develop in otherwise dry areas due to accumulation of heavy rainfall. They can be categorized in different type according where the water comes from and on their generated processes. One can distinguish river floods, flash floods, dam-break floods, ice-jam floods, glacial-lake floods, urban floods, coastal floods, and hurricane-related floods. Indeed, most types of flood are driven and modulated by climate, through precipitation and temperature and also the landscape (Shroder *et al.*, 2015). This research will be focus on urban flood as, during the recent year, Abidjan, the city in which our study area is located has been subject to many flood events.

2.2 Hydrological modeling

A hydrological model usually refers to the use of mathematical and logical expressions defining the existing relationships between flow characteristics (outputs) and its endogenous and exogenous conditional factors (inputs) (Devia *et al.*, 2015). It is an essential tool in understanding watershed dynamics because we are not able to measure every parameter we would like to know about the hydrologic system. Hydrological modeling allows us to provide some answers to the frequently asked question in hydrologic such as:

- How much water do we have?
- When do we have water?
- For how long do we have water?
- How high will the flood be?
- What are the dynamics of runoff in the given watershed?

This study is will be more oriented on the last two questions. The following table 2.1 provides a description of the different classification of hydrologic models.

Table 2. 1*: Categorization of hydrological model Adapted from (Scharffenberg, 2016)*

Category	**Description**
Event or continuous	This distinction applies primarily to models of watershed-runoff processes. An *event model* simulates a single storm. The duration of the storm may range from a few hours to a few days. A *continuous model* simulates a longer period, predicting watershed response both during and between precipitation events.
Lumped or distributed	A *distributed model* is one in which the spatial variations of characteristics and processes are considered explicitly, while in a *lumped model*, these spatial variations are averaged or ignored.

***Table 2.1**: Categorization of hydrological model _Continued*

Category	**Description**
Empirical (System theoretic) or conceptual	This distinction focuses on the knowledge base upon which the mathematical models are built. A *conceptual model* is built upon a base of knowledge of the pertinent physical, chemical, and biological processes that act on the input to produce the output. An *empirical model* is built upon observation of input and output, without seeking to represent explicitly the process of conversion.
Deterministic or stochastic	If all the inputs in a model are considered free of random variation and known with certainty, then the model is a *deterministic model*. If instead the model describes the random variation and incorporates the description in the prediction of output, the model is a *stochastic model*.
Measured-parameter or fitted-parameter	A measured-parameter model is one in which model parameters can be determined from the system properties, either by direct measurement or indirect methods that are based upon the measurements. A fitted-parameter model, on the other hand, includes parameters must be found by fitting the model with observed values of the input and the output.

2.3 Model selection

For selecting an appropriate modeling tool in any research, there are various criteria which can be applied to choose the most suitable model. According to (Cunderlik *et al*., 2004) the choice mainly depends on the requirements and needs of the research or project under interest. Cunderlik *et al*,. (2004) cited the following criteria for model selection:

- ✓ Required outputs of the model;
- ✓ Availability of input data;
- ✓ Prices and availability of the model and the model structures.

Based on the budget allocated to this research, the time constraint and the availability of the data, HEC-HMS with his GIS extension HEC-GeoHMS and HEC-RAS were selected as hydrologic and hydraulic model respectively for this research. These models are free of charge and they have been widely used in many researches.

2.4 HEC-HMS hydrological model

HEC-HMS (Hydrology Engineers Centre – Hydrology Modeling System) is a software designed by the US Army Corps of Engineers (USACE). The software is developed to simulate the rainfall-runoff process in dendritic watershed. It is developed such that it can be applied in a wide range of geographic areas. This includes large river basin water supply and flood hydrology, and small urban or natural watershed runoff.

Hydrographs produced by the program are used directly or in conjunction with other software for studies of water availability, urban drainage, flow forecasting, future urbanization impact, reservoir spillway design, flood damage reduction, floodplain regulation, and systems operation. The mass and energy flow in the watershed are represented by a mathematical model. Each mathematical model included in the program is suitable in different environments and under different conditions. Thus, the choice of the model to be applied require the knowledge of the watersheds, the goals of the hydrologic study, and engineering judgment.

The software is composed of the following component:

- an analytical component which allows the calculation of overland flow runoff as well as the channel routing;
- a user graphical interface for the hydrologic system illustration and displaying the model outputs;
- a system for data storing and management.

Figure 2.1 shows the representation of rainfall-runoff process in a given watershed (Arlen, 2000).

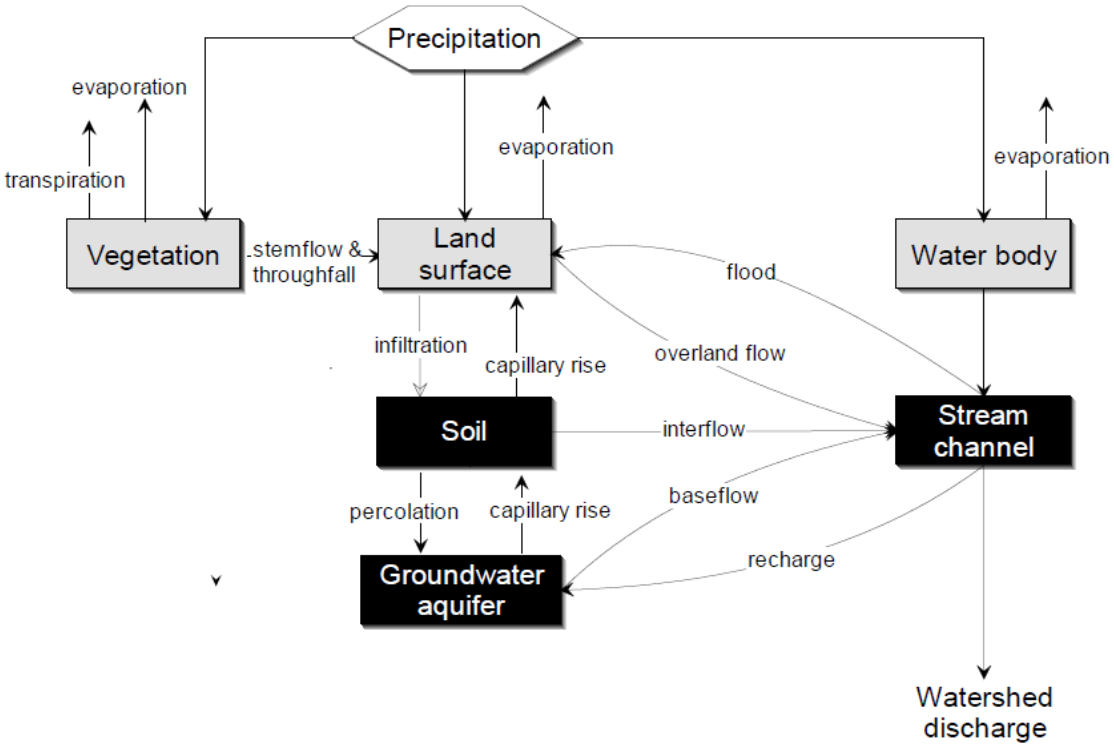

***Figure 2. 1**: Representation of the rainfall-runoff process in HEC-HMS*

The above figure is the HEC-HMS representation of the hydrologic cycle. In simple conceptualization, the precipitation can fall on the watershed vegetation, land surface, and water bodies such as streams and lakes. Water that falls in those different areas returns into the atmosphere through evaporation and transpiration.

HEC-HMS uses a separate model to represent each component of the runoff process showed in the above figure. Therefore, based on the available data, the watershed characteristics, the modeler can choose the suitable model.

The description of the models and their methods are in table 2.2.

Table 2. 2: *HEC-HMS models for runoff*

Models	**Methods**
Runoff-Volume models	Initial and constant-rate
	SCS curve number (CN)
	Gridded SCS CN
	Green and Ampt (also gridded)
	Deficit and constant rate (also gridded)
	Soil moisture accounting (also gridded)
	Gridded SMA
Direct-runoff	User-specified unit hydrograph
	Clark's unit hydrograph
	Snyder's unit hydrograph
	SCS unit hydrograph
	ModClark
	Kinematic wave
	User-specified s-graph
Baseflow	Constant monthly
	Exponential recession
	Linear reservoir
	Nonlinear Boussinesq
Channel Routing	Kinematic wave
	Lag
	Modified Puls
	Muskingum
	Muskingum-Cunge
	Straddle Stagger

2.4.1 Runoff-Volume models

HEC-HMS computed runoff volume by computing the volume of water that is intercepted, infiltrated, stored, evaporated, or transpired and subtracting it from precipitation.

Interception, infiltration, storage, evaporation, and transpiration are referred to as losses. The program assumes that all of the land and water in a watershed are categorized as:

- Directly-connected impervious surface: the portion of watershed for which the precipitation runs off (no infiltration, evaporation or others losses);
- Pervious surface: subject to losses.

Among the different model of runoff-volume model, the SCS Curve Number (SCS-CN) was selected for this study.

The Curve Number model was developed by the Soil Conservation Service (SCS) in 1972. The model allows the estimation of excess precipitation as a function of cumulative precipitation the soil type, the vegetation and the antecedent moisture condition of the watershed (Arlen, 2000). The depth of excess rainfall or direct runoff from a storm is computed by the model using the following equation:

$$\mathbf{P_e = \frac{(P - I_a)^2}{P - I_a + S}} \quad (\mathbf{2.1})$$

Where $\mathbf{P_e}$ = accumulated precipitation excess at time t,

P = accumulated rainfall depth at time t,

$\mathbf{I_a}$ = the initial abstraction (initial loss),

S = potential maximum retention, a measure of the ability of a watershed to abstract and retain storm precipitation.

Following some studies done by the SCS in many small watersheds, an empirical relation has been developed between $\mathbf{I_a}$ and **S**:

$$\mathbf{I_a = 0.2S} \quad (\mathbf{2.2})$$

Thus,

$$\mathbf{P_e = \frac{(P - 0.2S)^2}{P + 0.8S}} \quad (\mathbf{2.3})$$

The watershed characteristics and the potential maximum retention are related to the Curve Number as follows:

$$\mathbf{S = \frac{25400 - 254\ CN}{CN}} \quad (\mathbf{2.4})$$

The CN takes the values ranging from 0 to 100 and has no physical meaning. It is estimated as a function of land use, soil type, and antecedent moisture condition. The appendix A show the CN tables developed by the SCS and published in the Technical Report (commonly known as TR 55). In the watershed where there is different land use, soil type, a composite curve number is calculated as follows:

$$\boldsymbol{CN_{composite} = \frac{\sum A_i CN_i}{\sum A_i}} \quad (\mathbf{2.5})$$

In which $CN_{composite}$= the composite CN used for runoff volume estimation; i = index of watershed subdivision with homogenous land use and soil type; CN_i the curve number of the watershed i, and A_i = the drainage area of the subdivision i.

2.4.2 Direct runoff model

The model allows the transformation of excess precipitation into point runoff. Only the SCS unit hydrograph model, used in this study as a transform model will be described. The model is based upon averages of Unit Hydrograph (UH) derived from gaged rainfall and runoff for a large number

of small agricultural watersheds throughout the US (Arlen, 2000). The SCS suggests that the UH peak and time of UH peak are related by:

$$\boldsymbol{U_P = C\frac{A}{T_P}} \quad \boldsymbol{(2.6)}$$

In which A = watershed area, C = conversion constant (2.08) and T_P is the time to the UH peak. The time of peak is related to the duration of the unit of excess precipitation by the following equation:

$$\boldsymbol{T_P = \frac{\Delta t}{2} + t_{lag}} \quad \boldsymbol{(2.7)}$$

Where Δt = the excess runoff duration and t_{lag} = the basin lag. A good definition of the ordinates on the rising limb requires that the computation interval Δt less than 29% must be used (Arlen, 2000).

2.4.3 Channel flow routing

The model includes several methods for channel flow routing. Among those models, the Muskingum model for flood routing was selected for this research due to the availability of required data. The Muskingum method uses a simple finite difference approximation of the continuity equation:

$$\left(\frac{I_{t-1} + I_t}{2}\right) - \left(\frac{O_{t-1} + O_t}{2}\right) = \left(\frac{S_t + S_{t-1}}{\Delta t}\right) \ \boldsymbol{(2.8)}$$

Storage in the reach is modeled as the sum of prism storage and wedge storage. The storage is defined by the model as:

$$S_t = KO_t + KX(I_t - O_t) = K[XI_t + (1 - X)O_t] \ \boldsymbol{(2.9)}$$

Where **K** = travel time of the flood wave through routing reach, and **X** = dimensionless weight ranging from **0 to 0.5**. The quantity $XI_t + (1 - X)O_t$ is a weighted discharge. When the storage in the channel is controlled by downstream conditions, such that storage and outflow are highly

correlated, X=0.0. Thus, $S = KO$ and it is the linear reservoir model. If X=0.5, the inflow, and outflow have the same weight which means that the wave does not attenuate when moving through the reach. By substituting equation (2.9) in (2.8) and rearranging to isolate the unknown values at time t, we have:

$$\boldsymbol{O_t = \left(\frac{\Delta t - 2KX}{2K(1-X) + \Delta t}\right) I_t + \left(\frac{\Delta t + 2KX}{2K(1-X) + \Delta t}\right) I_{t-1} + \left(\frac{2K(1-X) - \Delta t}{2K(1-X) + \Delta t}\right)} \quad (\mathbf{2.10})$$

2.5 HEC-RAS hydraulic model

HEC-RAS is a hydrodynamic model developed by the Hydrologic Engineering Center of the US Army Corps of Engineers. The hydraulic model offers both one and two-dimensional hydraulic modeling capacity. HEC-RAS is widely used to simulate flood routing in river systems (Hicks *et al.,* 2005;); (Timbadiya *et al.,* 2011). It is designed to perform one-dimensional (1D), two-dimensional (2D), or combined 1D and 2D hydraulic calculations for a full network of natural and constructed channels (Brunner *et al*., 2016).

The model has the following capabilities:

- A user interface which allows users to be more focused on the design while still maintaining a high level of efficiency;
- River analysis components for steady flow water surface profiles, unsteady flow simulation, sediment transport, and movable boundary computations, water quality analysis;
- Data storage and management component;
- Graphics and reporting to display the outputs of the calculations.

In his past version, the water surface profile calculated during the modeling were converted into flood inundation maps by using HEC-GeoRAS. Since the version 5.0.5, HEC-RAS has an integrated geospatial capabilities component called “RAS Mapper” which allows the creation of flood inundation maps directly in HEC-RAS. RAS Mapper is intended to provide visualization of HEC-RAS simulation results along with pertinent geospatial data to assist in the improvement of

hydraulics models. Based on these capabilities and to the fact that the software is free of charge, HEC-RAS has been widely used in many flood studies.

2.5.1 Governing equation

Water surface profiles are computed from one cross-section to the next by solving the energy equation with an iterative procedure called the standard step method. The energy equation is written as follows (figure 2.2):

$$\boldsymbol{Z_2 + Y_2 + \frac{\alpha V_2}{2g} = Z_1 + Y_1 + \frac{\alpha V_1}{2g} + he} \quad \boldsymbol{(2.11)}$$

Where:

- Z_1, Z_2 = elevation of the main channel inverts,
- Y_1, Y_2 = depth of water at cross-sections,
- V_1, V_2 = average velocities (total discharge/ total flow area)
- α_1, α_2 = velocity weighting coefficients,
- g = gravitational acceleration,
- he = energy head loss

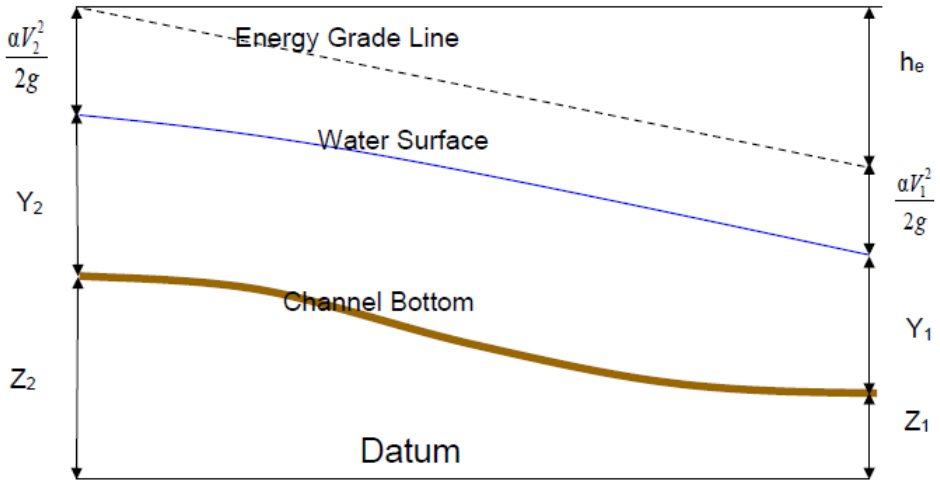

***Figure 2. 2**: Energy equation representation in HEC-RAS*

The energy head loss (he) between two cross-sections is comprised of friction losses and contraction or expansion losses. The equation for the energy head loss is as follows:

$$h_e = L\bar{S}_f + C\left|\frac{\alpha_2 {V_2}^2}{2g} - \frac{\alpha_1 {V_1}^2}{2g}\right| \quad (2.12)$$

Where:

- **L** = discharge weighted reach length
- $\bar{S}_f$ = representative friction slope between two sections
- C = expansion or contraction loss coefficient.

2.5.2 Cross-section subdivision for conveyance calculation

The determination of total conveyance and velocity coefficient for a cross-section requires that flow be subdivided into units for the velocity is uniformly distributed. The approach used in HEC-RAS is to subdivide flow into the overbank areas using the input cross-section n-value breakpoints (locations where n-values change) as the basis for subdivision (figure 2.3). Conveyance is calculated within each subdivision from the following form of manning's equation:

$$Q = KS_f^{\frac{1}{2}} \quad (2.13)$$

$$K = \frac{1.486}{n} AR^{2/3} \quad (2.14)$$

Where:

- K = conveyance for subdivision
- n = Manning's roughness coefficient for subdivision
- A = flow area for the subdivision
- R = hydraulic radius for subdivision (wetted perimeter)
- S_f = slope of the energy grade line.

The program sums up all the incremental conveyances in the over banks to obtain a conveyance for the left overbank and the right overbank. The main channel conveyance is normally

computed as a single conveyance element. The total conveyance for the cross-section is obtained by summing the three subdivision conveyances: left, channel, and right (Brunner *et al*, 2016).

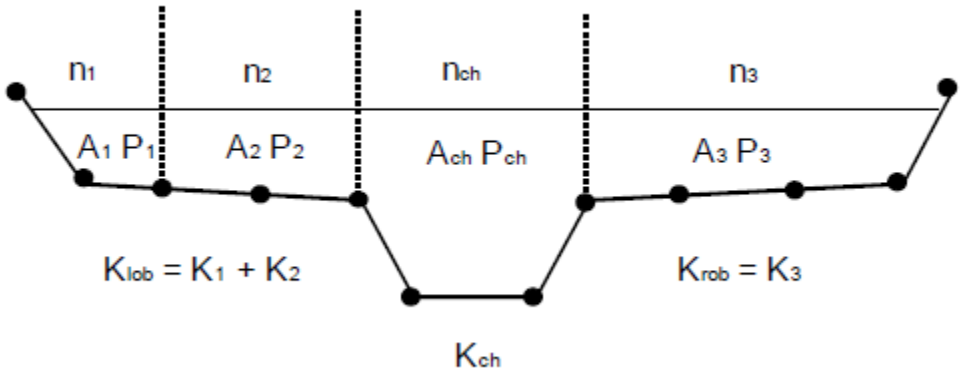

Figure 2. 3: *Cross-section subdivision for conveyance calculation*

2.5.3 Water surface profile computation and data requirement

The primary procedure for computing water surface profile for steady, gradually varied flow between two cross-sections is called the standard step method (Paresh *et al.*, 2011). According to (Brunner *et al.*, 2016), the computation procedure can be summarized as the following:

a. Assume a water surface elevation at the upstream cross-section (or downstream is the flow is subcritical);
b. Determine the area, hydraulics radius, and velocity based on the cross-section profile;
c. Computed the associated conveyance and velocity head values;
d. Calculate friction slope, friction loss, and contraction/expansion loss;
e. Solve the energy equation for the water surface elevation at the upstream cross-section;
f. Compared the computed water surface elevation with the one assumed in step (a);
g. Repeat steps (a) through (f) until the assumed and computed water surface elevations are within a predetermined tolerance.

Therefore, for the computation of water surface profile, HEC-RAS needs some basic data to be entered:

- **River system schematic**: Required for any geometry data set within the HEC-RAS system. It defines how reaches, storage areas, and 2D flow area are connected, as well as establishing a naming convention for referencing all the other data.
- **Cross-section geometry**: Located at intervals along the stream to characterize the flow carrying capacity of the stream and its adjacent floodplain. Indeed, in HEC-RAS the properties of the section are defined by some points called "Station". The stations are defined by the horizontal distance from the left river bank and the bottom elevation above the datum.
- **Energy loss coefficient**: The Manning's n is an important coefficient which influences the computation result. Therefore, it is important to select an appropriates manning's value to get more accurate water surface elevation. The best method to estimate manning's value is by calibration whenever it is possible to get observed water surface elevation information. Due to the fact that it is possible to get such information, several references can be found in the literature which is useful for estimating manning's value. The most used are those found in Chow's book (Chow *et al.*, 1988). Also, the expansion and contraction coefficient need to be entered as the change of cross-section cause energy loss within the reach. For gradual transitions and supercritical flow, Brunner *et al.*, (2016) suggest using values of 0.01 for contraction and 0.03 for expansion. When the change in river cross-section is small, and the flow is subcritical, coefficients of contraction and expansion are typically on the order of 0.1 and 0.3 respectively. When the change in effective cross section area is abrupt such as at bridges, contraction and expansion coefficients of 0.3 and 0.5 are often used.

2.6 Geographical Information System for hydrologic and hydraulic modeling

The recent development of Geographic Information System (GIS) technologies and remotes sensing help in understanding and dealing with the pressing problems of water and related resources management by changing how the different studies are accomplished (Lynn, 2014). One of the main characteristics of watershed runoff process is the spatial variability. Therefore, GIS is

an important tool to organize the data and the formulate hydrologic models to support decision making. The availability of the elevation model (DEM and TIN), land use data, radar-rainfall, and satellite imagery have brought a strong contribution in understanding the spatial distribution of hydrologic processes. The user environment provides engineers an opportunity to view real-world systems of interest, which in turn assists them to rectify errors and make informed decisions in the model development (Ackerman *et al.*, 2010).

HEC Geo-HMS uses ArcView and Spatial Analyst to develop a number of hydrologic modeling inputs. Analyzing digital terrain information, HEC-GeoHMS transforms the drainage paths and watershed boundaries into a hydrologic data structure that represents the watershed response to precipitation. As stated before, HEC-RAS has an integrated GIS component (RAS Mapper) for flood inundation visualization, water depth and velocity displayed. A widely used approach is watershed modeling that divides the drainage basin into discrete units possessing similar rainfall-runoff and physical characteristics. This approach reduces model complexity and spatially distributed data requirements in basin-scale models (Beighley *et al*., 2005). Based on the objectives of the study, GIS will play an important role in watershed physical characteristic extraction and in the development of basin model.

3 METHODS

3.1 Physical environment and landscape characteristic of the Study area

The District of Abidjan is located in the south part of Côte D'Ivoire (a country located in West Africa) between latitude 5° 10' and 5° 38' North and longitude 3° 4' and 5° 21' West. It was established as Autonomous District in 2001 by the application of the Law No. 2001-476 of the 9th August 2001 relative to the general orientation of the territorial administration. The territory of the Autonomous District of Abidjan is composed by 13 municipalities from which 10 constitute the city of Abidjan, namely: Abobo, Adjamé, Attécoubé, Cocody, Koumassi, Marcory, Plateau, Port-Bouët, Treichville, and Yopougon (figure 3.1). The three (03) others are surrounding municipalities: Anyama, Bingerville, and Songon.

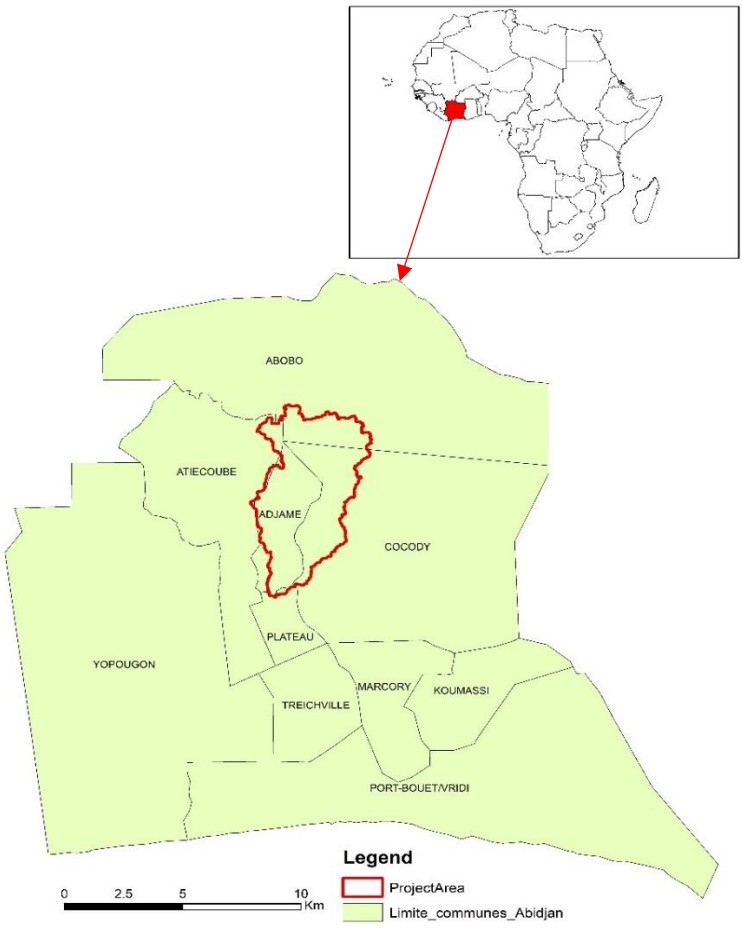

***Figure 3. 1**: Location of Gourou watershed in Abidjan/Côte d'Ivoire*

3.1.1 Location of the watershed and its boundaries

The Gourou watershed is located in the city of Abidjan. It drains the flows produced by its hydrographic network in the Cocody lagoon via a roundabout called “roundabout of Indénié”. The area is bordered on the west part by the railway line “Adjamé-Anyama”, which runs along the National Park of Banco, on the east by the extension of “Latrille Boulevard” to the “II Plateaux” district, and to the north by neighborhoods of “Abobo”. According to the literature, the watershed can be represented by a rectangle with the length of 9km and a width of 3 km. The surface area is then approximately 27 km^2.

3.1.2 Hydro-climatologic context

3.1.2.1 Different seasons

Gourou watershed is located in Abidjan, southern part of Côte d’Ivoire. The movement of the Inter-Tropical Convergent Zone (ITCZ) determines the climate in Côte d’Ivoire (Saley *et al.*, 2005). The climate in the study area is equatorial type. It is characterized by four (04) seasons:

- a long dry season from December to March with few rainy days. The rainfall depth varies from 26.1 mm in January to 308.39 mm in May;
- a long rainy season from April to the mid of July with a rainfall depth varying from 170.5 mm in April to 572 mm in June. The rainy days range from 12 to 16.
- a short rainy season from mid-September to November: characterized by high temperatures and a long duration of the sunshine. During this season the rainfall depths vary from 164,8 mm to 149,4 mm for 18 to 13 of rainy days;
- a short dry season from mid-July to the mid of September: It is characterized by a low duration of the sunshine and a high number of rainy days but the amount rainfall depth is low. The monthly rainfall depth is between 26.6 mm and 63.9 mm.

3.1.2.2 Rainfall

The study conducted by ASECNA allowed to distinguish three (03) different type of months in a year (Aimé, 2018):

- **Months with low rainfall**: (Average rainfall depth less than 100 mm)
  These are the months of December, January, and February. They characterize the long dry season. The number of rainy days does not exceed four (04) days. The maximum daily rainfall depth for each of the month is less than 20 mm.
- **Months with intermediate rainfall**: (Average rainfall depth between 100 and 200 mm)
  These are the months of March and April. These intermediate months preceded the long rainy season. The increase in rainfall depth is considerable in the whole area. It is in the month of April that rainfall depth becomes more important with a daily rainfall depth more than 40 mm. The months of September and October are also included in this range. This period of the year corresponds to the short rainy season.
- **Months with high rainfall** (Average rainfall depth between 200 and 600 mm)
  The months of May, June, and July are the rainiest of the year in the Ivorian forest region. The highest rainfall amounts are recorded on the coast. This situation is most noticeable in the month of June when the rains sometimes exceed 500 mm. It is the long rainy season.

The minimum, maximum and mean values of rainfall in the district of Abidjan from 1961 to 2017 are shown in table 3.1**.**

Table 3. 1: *Rainfall variation in Abidjan city*

	Jan	Feb	Mar	Apr	May	Jun	Jul	Aug	Sep	Oct	Nov	Dec
Min (mm)	0	0	6.5	17	116.5	158.6	6.7	2.1	1.8	3.5	47.4	2.2
Mean (mm)	20.44	46.26	99.36	162.18	289.04	526.6	180.86	32.89	67.66	161.19	156.69	73.88
Max (mm)	154.5	174	245.4	508.4	669.6	990.6	936.1	238.1	411.1	491.2	294	261

3.1.2.3 Temperature

Over the period 1961-2015, the average monthly temperatures in the district of Abidjan are less than 30°C. The monthly minimum and maximum values vary from 22.7°C (month of August) to 30°C (month of March). As shown in figure 3.2 below, the period from November to April is the hottest period with minimum and maximum monthly temperature superior to 27.1°C and 30°C.

One can see that the months of May, June, July, August, September, and October are less hot. This due to the rainfall that occurs during this period.

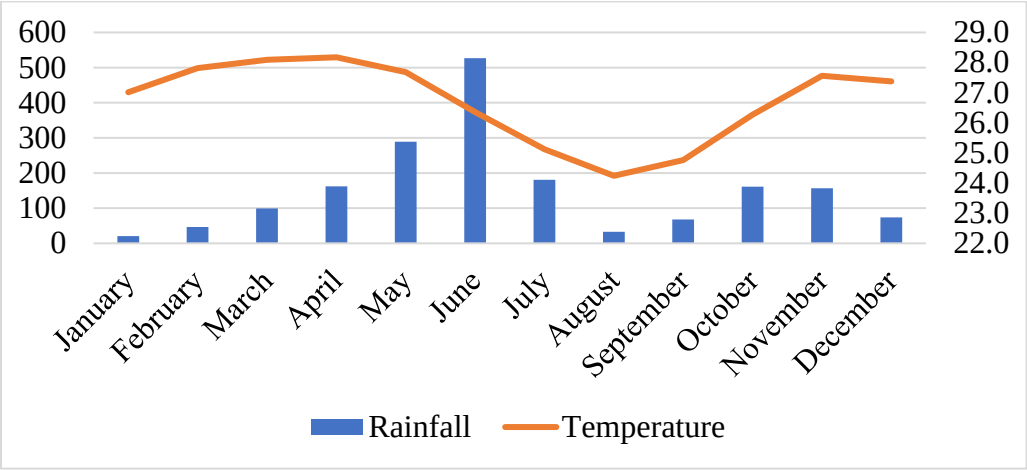

Figure 3. 2: *Annual average variation of temperature and rainfall*

3.1.2.4 Potential evapotranspiration

The average potential evapotranspiration calculated over the two last decades (1990-2011) show an increase PET according to the SODEXAM. Indeed, it varies from 1650 mm/year for the period 2003-2011 to 1518 mm/year between 1990-2003.

3.1.2.5 Hygrometry

The relative humidity varies inversely with temperature and sunshine. It is quite high in the region as the monthly average values range from 80.21% in December to 87,78% in August.

3.1.2.6 Relief and geomorphology

The District of Abidjan, in which our area of study is, presents globally a little contrasted and monotonous relief. Indeed, we have three (3) units geomorphologically individualized (Tastet *et al.*, 1982) which are:

- the shoreline (East and West part);
- the lagoons and island (Island of Bassam, Island of Boulay);
- the plateau (plateau; plateau of Banco forest, Cocody and Abobo).

3.1.2.7 Geology

The geological context of the town of Abidjan is that of the sedimentary basin of Côte D'Ivoire. The sedimentary basin in Abidjan is characterized by a length of 350 km from the east to the west and a north-south width, very reduced, which lies between 10 and 40 km. The successive layers are in monocline position and the dip in direction of the ocean.

3.1.2.8 Pedology

The soils of Abidjan belong to the class of desaturated lateritic soils, depleted-modal, on tertiary sand (continental terminal) according to (Saley *et al.*, 2005). They are ferralitic and hydromorphic soils. The ferralitic soils are found on the low and high plateau. Almost all of the primary minerals, except for quartz, have been subject to total hydrolysis. The settlement of this pedological texture comes from the process of ferralitisation developed under the influence of the paleoclimatic factors and the very old types of vegetation. Due to the influence of rainfall and temperature, the horizons of the soil are the following:

- the first horizon is not very thick horizon, poor in humus and rich in organic matter;
- the second horizon, very thick, is generally enriched iron and alumina and also strongly colored with the presence of red and brown color;
- the third horizon is clayey, compact and less permeable.

The hydromorphic soils are the second type of soil found in Abidjan. Those soils were formed because of a pedological evolution due to the excess of water.

3.1.2.9 Hydrography

The main stream in the study watershed is called "Gourou". The water flows from the Northern to the Southern part of the watershed in the Cocody bay, outlet of the watershed. Actually, it is no more a natural stream, because of the high rate urbanization, it has been transformed in an open channel (figure 3.3) made with concrete. There are many other tributaries that are connected to the main channel. Some of those tributaries are still naturals and some have been transformed in

concrete channel. Gourou and its tributaries are not permanent, the discharge is intermittent and depends on the rainfall depth that falls.

3.1.2.10 Hydrogeology

The sedimentary basin of Abidjan is composed by homogeneous and highly permeable aquifers. One can distinguish three (30) categories of aquifer within the basin.

- Quaternary aquifer;
- Abidjan's aquifer;
- Fossil aquifer.

Abidjan's aquifer is the one which is found in the study area. It is bordered in the South part by Ebrié lagoon, in the West part by "Agnéby" and "Niéké" (rivers), in the East part by "La Mé" and Potou lagoon. The surface area of this aquifer is 1750 Km^2, with a maximum length (from East to West) of 70 Km and with a width of about 25 Km (from North to South). This aquifer is composed of four (04) horizons:

- horizon 1: gravelly sand mixed with clay (0 to 20 m)
- horizon 2: black clay and sandy-clay soil (0 to 10 m)
- horizon 3: coarse sand (0 to 90 m)
- horizon 4: lateritic cuirass which covers locally sandy clay soil (0 to 70 m).

This aquifer is principally recharged by the water from Banco's and Anguédédou forest. It is the main source for water supply in the district of Abidjan. But, due to the high rate of urbanization and human activities, it is exposed to contamination.

Figure 3. 3*: Gourou canal, initially a natural stream*

3.1.2.11 Vegetation

Gourou watershed is located in the forest zone of Côte d'Ivoire. In detail, cause of geological factors, one can distinguish many features: mangrove swamp, savanna, marshy forest.

3.1.2.12 Cocody bay: Outlet of the watershed

The bay of Cocody, the outlet of Gourou watershed, is the lagoon which the edge is oriented towards the municipality of Adjamé, commonly called "Roundabout of Indénié". It is limited to the East by the commune of Cocody, to the West by the municipality of Plateau and to the South by the bridge General De Gaulle. The bay receives wastewater from domestic, industrial activities and also water from runoff generated in the watershed that contains large amount of organic matters. The degradation of those organic matters by the micro-organisms leads to the eutrophication that we observe on water surface. Recently, a project financed by Morocco Kingdom has been launched for the valorization of Cocody bay.

3.2 Datasets

3.2.1 Hydrological and flow data

The hydro-meteorological and flow data are critical input for this research. The flow data were obtained from the organism in charge of the management of the watershed called *Unité de Gestion du Bassin versant du Gourou*. The flow data, with a time step of 1 hour, are the discharge of the different storm events occurred on 11th of May 2018 and 19th June 2019 (Storm events which have occurred since the flow station has been installed). Concerning the hydrological data, the design rainfall depth for 6-hour was taken from the IDF curve developed for the study area base on the rainfall data. Figure 3.4 illustrates the design rainfall depth for different flood return period used in this study.

3.2.2 Topographic data

In this study, one can distinguish different types of topographic data: The Digital Elevation Model (DEM) obtained from satellite and on other hand the channel geometry which was obtained from a survey (figure 3.5) and Lidar data (1m resolution). The availability of global coverage digital surface models has had a positive impact on scientific researches over the past decade as they provide a fairly good base dataset with low production time and expense (Józsa *et al.*, 2014). DEMs are very useful today in hydrologic modeling especially in the areas where there is lack of detailed topographic map and because those data are expensive. Several DEMs are available freely online namely the Shuttle Radar Topography Mission (SRTM), the Advanced Spaceborne Thermal Emission and Reflection Radiometer (ASTER) Global Digital Elevation Model (GDEM) and the ALOS Global Digital Surface Model "ALOS World 3D - 30m (AW3D30)". A 30m by 30m grid SRTM DEM format covering the entire district of Abidjan was obtained from USGS Explorer website. And the one covering the study area was obtained by clipping the main DEM.

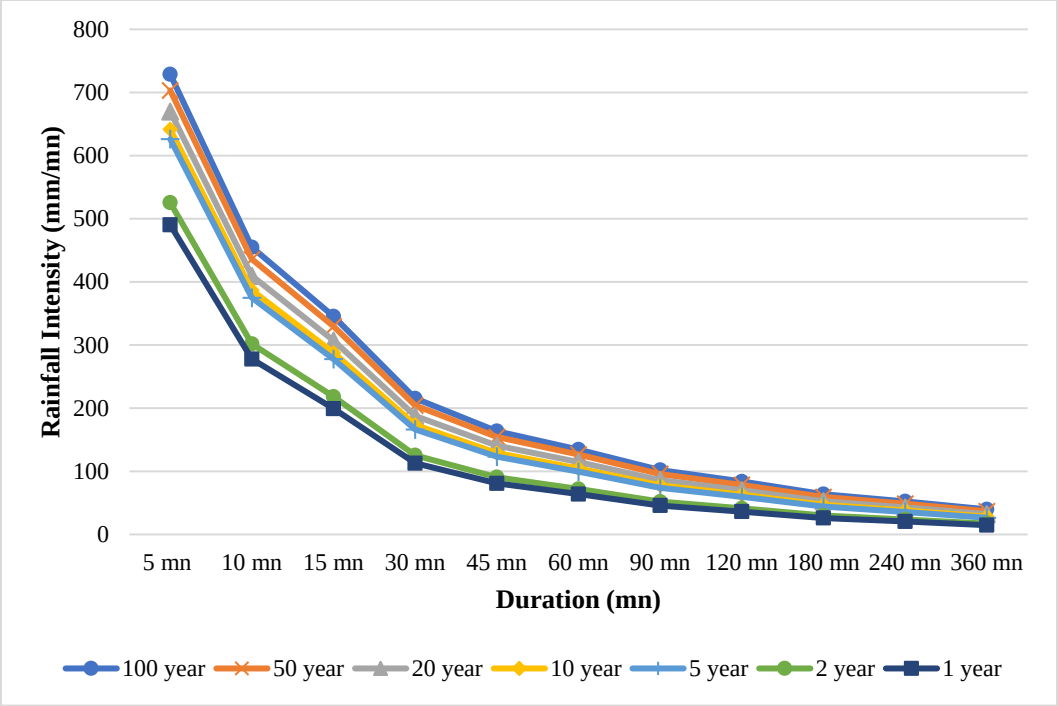

***Figure 3. 4**: Intensity-Duration-Frequency curve – 6 hours*

***Figure 3. 5:** Topographic survey*

3.2.3 Soil, Land Use, and Land cover data

The soil data used in this study were obtained from BNETD (National Bureau for Technical Study and Development) in shapefile format. As covering all the country, it was processed to extract the area of interest.

Land Use and Land Cover data were obtained from USGS explorer website. The data are images from Landsat8 satellite. Launched on the 11th February 2013; Landsat8 is the most recent Landsat satellite. The overall mission objectives of this new spacecraft of the Landsat program are:

- Provide data continuity with Landsat 4, 5, and 7;
- Offer 16-day repetitive Earth coverage, an 8-day repeat with an L7 offset;
- Build and periodically refresh a global archive of Sun-lit, substantially cloud-free land images.

Landsat8 has two types of sensors: Operational Land Imager (OLI) and Thermal Infrared Sensor (TIRS). OLI sensors allowed the acquisition of nine (09) shortwave spectral bands with a 30 meter (m) spatial resolution for all bands except the 15 m Pan band. The TIRS sensor collects image data for two thermal bands with a 100 m spatial resolution. Thus, the Landsat8 data used in the study is composed of 11 bands with follows sequence of fixed ground tracks: Path 195 and Row 56. *The retained image was the one acquired the 25th December 2017 because the scene cloud cover and land cover cloud were the smallest (both are less than 3%)*.

3.2.4 Channel resistance factor

In hydraulic modeling and simulation, the channel resistance factor is a critical input as it has a direct influence on the accuracy of the computed water surface elevations. The channel resistance factor is a coefficient used by HEC-RAS to evaluate energy loss. The value of Manning's n is highly variable parameter, which depends upon a number of factors like the surface roughness, the vegetation, the channel irregularities, the channel alignment, obstructions, size and shape of the channel. For this study, due to the lack of available water surface profile for Manning's value calibration, the channel resistance factor for the main channel and the over banks were estimated

from Chow's book "Open-Channel Hydraulics" (Chow *et al.*, 1988) after a field visit of the study area (figure 3.5).

3.3 Methodology: Modeling approach

Different methodologies have been applied in this study in order to achieve the goals of this research. The methodology comprises three (03) phases:

- Terrain preprocessing using the Digital Elevation Model (DEM), HEC-GeoHMS and Arc-Hydro for the preparation of hydrographic features, watershed delineation and development of the HEC-HMS model;
- HEC-HMS model development;
- HEC-RAS model development.

The following chart (figure 3.6) illustrates the overall methodology used in this study.

3.3.1 Terrain preprocessing and HEC-HMS inputs extraction

The preprocessing of the terrain was done using HEC-GeoHMS. HEC-GeoHMS is an extension of HEC-HMS model within Arc view GIS. It is the first step which has to be accomplished to be able to use properly the DEM. The aim is to extract the physical characteristics of the watershed and the creation of the basin model which are the most important inputs of HEC-HMS model.

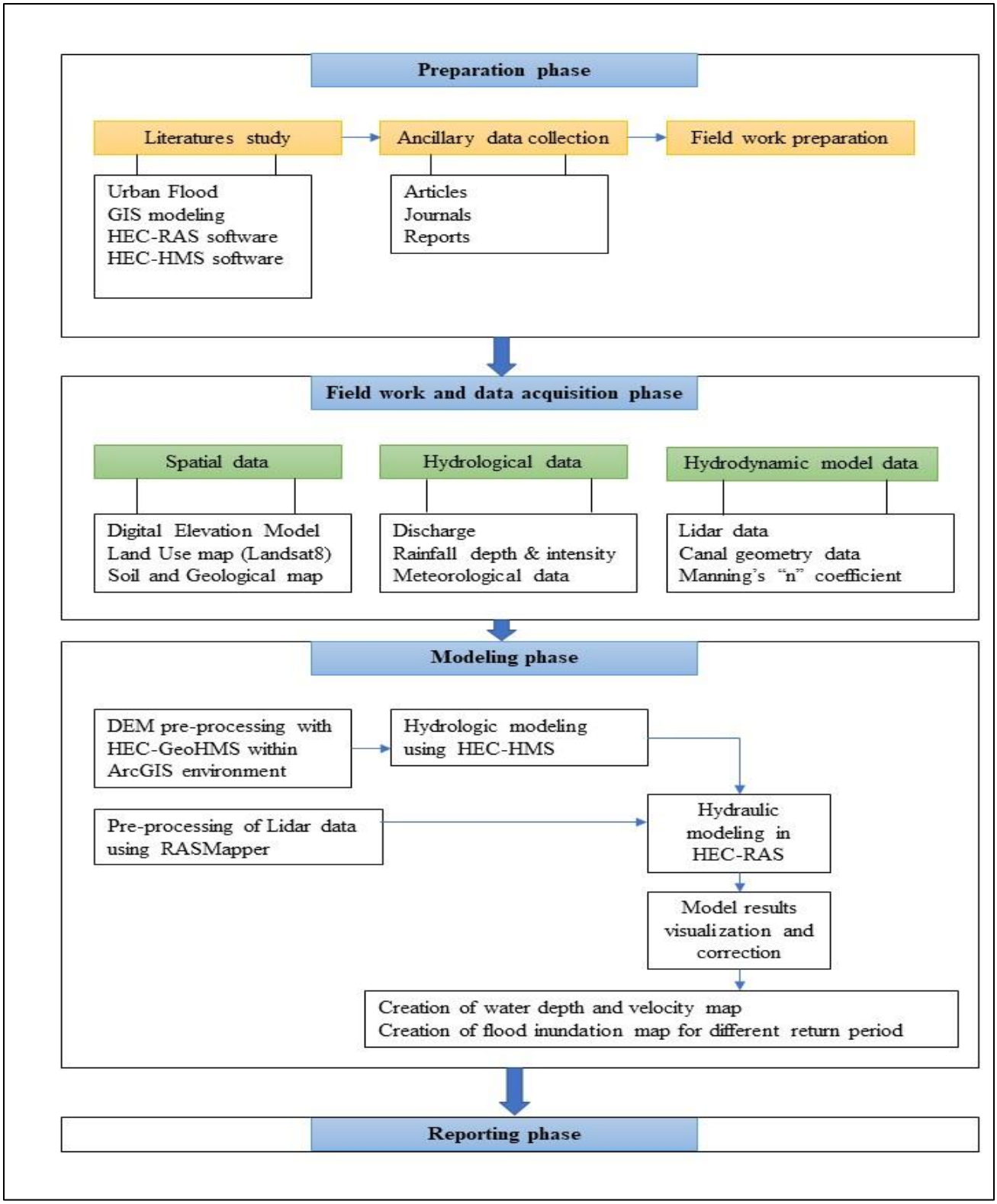

***Figure 3. 6**: Methodology chart*

3.3.2 Rainfall-runoff model: HEC-HMS

The floods hydrographs required for the hydraulic modeling were simulated using HEC-HMS model. The software is designed to simulate the rainfall-runoff process in a complex dendritic watershed. The version of HEC-HMS used in this case study is version *4.2*. The simulation of rainfall-runoff model required to specify the loss method, the transform method and the routing method used in this study.

3.3.2.1 Loss method

Among the different method for computing loss resulting from a rainfall event, the SCS Curve Number was selected due to data scarcity in the study area. The required parameters for loss computation are: The Curve Number (CN), the percentage of imperviousness and the initial abstraction.

The CN for each sub-basin were developed with HEC-GeoHMS and imported into HEC-HMS during the exportation of the basin model. Due to time constraint, it was impossible to do a survey for the percentage of imperviousness calculation. Therefore, the percentage of imperviousness was assigned on the basis of the knowledge of the watershed and after a field visit. Regarding the initial abstraction, no data were entered, then HEC-HMS estimates as follows:

$$\boldsymbol{I_a = 0.2 \times S \; with \; S = \frac{25400 - 254 \times CN}{CN}} \qquad (\mathbf{3.1})$$

3.3.2.2 Transform method

Basin lag time parameter values were computed during data processing using the HEC GeoHMS application in ArcGIS environment and stored in the attributes table of the sub-basin data layer. Basin Lag time in hours for each sub-basin was computed using equation (3.2) (Arlen, 2000) and then converted to minutes by multiplying by sixty.

$$\boldsymbol{Lag = \frac{L^{0.8}(S+1)^{0.7}}{1900 \times Y^{0.5}}} \qquad (\mathbf{3.2})$$

Where **S** = Maximum retention

Lag = basin lag time (hours)

L= hydraulic length of the watershed (longest flow path)

Y = Basin slope (%).

3.3.2.3 Routing method

The Muskingum method was used for flood wave routing. The details are presented in the literature review section. Muskingum X ranges from 0 to 0.5. In this study, the value of 0.05 was assigned at each sub-basin. The values of K for the sub-basins were determined by trial and error and technique until all the reaches were stable. Also, the reaches were divided into two (02) sub-reaches to ensure the stability of the computation during the routing process.

3.3.2.4 HEC-HMS model calibration and validation

The calibration estimates some model parameters that cannot be estimated by observation or measurement, or have no direct physical meaning (Cunderlik *et al.*, 2004). The estimated initial parameters were adjusted until the model result match acceptably the observed data. The quantitative measure of the match was performed by the objective function which measures the degree of variation between computed and observed hydrographs. The model calibration was done by using the Univariate Gradient optimization package and Peak-Weighted Root Mean Square Error (PWRMSE) objective function because of its simplicity and performance (Deng et al., 2010, cited by (Tassew *et al.*, 2019)**)**. In this study, two (02) storm events (one for calibration and one for validation) recorded in 2018 were selected for calibration and validation purpose. The events are the storm that created flood since the discharge station has been installed (table 3.2).

The Peak-weighted root mean square error (PWRMSE) was developed by the USACE in 2001. It is an objective function which uses a weighting factor and gives greater overall weight to error near the peak discharge. It is calculated as follow:

$$PWRMSE = \sqrt{\frac{\sum_{t=1}^{N}\left(Q_o(t) - Q_M(t)\right)^2 \frac{Q_o(t) + Q_A}{2Q_A}}{N}};\ Q_A = \frac{1}{N}\sum_{t=1}^{N} Q_o(t) \quad (\mathbf{3.3})$$

Where Q_o and Q_M are observed and modeled flow at time t_i and Q_A is the average observed flow.

Table 3. 2*: Peak discharge for calibration and validation*

Station Name	Date of the storm event	Peak discharge (m^3/s)	Time of peak	Use
Monument des Matyrs (Monument of Matyrs)	11th May 2018	103.4	10:00	Calibration
	19th June 2018	165.7	5:00	Validation

During the optimization procedure, HEC-HMS computes automatically the Nash-Sutcliffe Efficiency (NSE). The NSE, statistical method developed by Nash and Sutcliffe was used to evaluate the model performance in representing the rainfall-runoff process and the selected loss and transform methods. NSE is sensitive to strong flows. In practice, studies have considered that Nash is acceptable from the value 0.6 (Nash and Sutcliffe, 1970). Based on these considerations, it will be assumed that the simulation is of poor quality when the Nash criterion is low (<0.6), it is satisfactory when it is between 0.60 and 0.80 and good when it is greater than 0.90. The Nash criterion is computed as follows:

$$NSE = \left[1 - \frac{\sum(Q_{o,i} - Q_{m,i})^2}{\sum(Q_{o,i} - Q_o)^2}\right] \quad (\mathbf{3.4})$$

After the optimization, the optimized parameters were used to simulate the storm event of the 19th June 2018. This is known as the validation procedure when doing hydrological modeling.

3.3.3 Hydraulic model: HEC-RAS

An integrated approach using hydraulic modeling software and GIS software has been used to generate the flood model. HEC-RAS software, version 5.0.7, was used to perform, to compute water surface elevation, flow characteristics at the various cross-section and to develop 3D perspective for floodplain analysis. Regarding the geometric data, which is a critical input to perform the spatial analysis, RAS Mapper (integrated GIS component of HEC-RAS) has been applied to obtain the geometric data needed in this study. In this section, a number of issues regarding the generation of the river flood model will be elaborated. In each HEC-RAS project,

one can distinguish three (03) required components which are: Geometry data, Flow data, and Plan data.

3.4 HEC-HMS model development

3.4.1 DEM preprocessing: HEC-GeoHMS Application

In the past years, the delineation of watershed was done manually by using topographic maps and those techniques are still be used. But, nowadays, with the development of remote sensing and GIS techniques, engineers and water sector professional use more and more DEM of different resolution for watershed delineation. HEC-GeoHMS has been developed as a geospatial hydrology toolkit for engineers and hydrologists with limited GIS experience. It allows the visualization of spatial information, document watershed characteristic, performs spatial analysis, delineates subbasins and streams, constructs inputs to hydrologic models. The use of HEC-GeoHMS in this study allows the creation of hydrologic inputs which are directly use with HEC-HMS software. The different steps for watershed delineation include: fill sinks, flow direction, flow accumulation, stream definition, and segmentation. The result is shown in Appendix B. Based on the flow direction and stream segmentation grid, the corresponding watershed for each stream segment was delineated. Figure 3.7 illustrated the watershed which is the study area. The watershed has a surface area of 27 km2 and the perimeter is 106.36 km.

3.4.2 Watershed physical characteristics extraction

The extraction of the watershed physical properties can be assimilated as HEC-HMS initial parameters estimation. The 31 subbasins were merged based on the knowledge of the study area. Finally, we remained with 9 subbasins with various surface. Thereafter, the subbasins characteristics were determined using HEC-GeoHMS functions. For each sub-basin, the basin slope, the perimeter, the longest flow path, the LagMethod, and the Transform method were estimated by HEC-GeoHMS. Regarding the different reaches, the Reach length, the slope, the routing method were also generated. All the computed characteristics were stored in the attribute table of the different sub-basins and reaches (Appendix C).

3.4.3 Curve Number grid preparation

In a given basin or watershed, precipitation loss is one of the main factors that influence direct runoff. Precipitation loss is used to estimate the relationship between rainfall and excess rainfall (Model *et al.,* 2009). Excess rainfall is a part of rainfall that contributes directly to runoff. It is neither retained in storage nor is lost as infiltration, interception, and evapotranspiration (Mujumdar *et al.*, 2012). When dealing with flood study, two procedures may be used for estimating flood runoff and flood peaks. These procedures are: Rational method and Soil Conservation Service (SCS) curve number method. In this research, we used the SCS CN method developed by the Soil Conservation Service in 1972 for runoff estimation. Soil and land use data of the study area were prepared and used to create a curve number grid using HEC-GeoHMS.

3.4.3.1 Soil data preparation

As mentioned above in section 3.2.3, the soil data was obtained from BNETD. Thus, the soil data of the study area was clipped by using the watershed boundary as a clip feature. As this study uses the SCS CN for runoff estimation, it is required to define the hydrologic soil group based on soil data. One can distinguish four (04) hydrologic soil groups described below according to (Chow *et al.,* 1988):

- **Group A**: Deep sand, deep loess, aggregated silts (soils having the highest infiltration rates);
- **Group B**: Shallow loess, sandy loam (soils having moderate infiltration rates);
- **Group C**: Clay loams, shallow sandy loam, soils low in organic content, and soils usually high in clay (soils having low infiltration rates);
- **Group D**: Soils that swell significantly when wet, heavy plastic clays, and certain saline soils (soils having very low infiltration rates).

Table 3.3 gives the general description of different type of soil found in Abidjan.

***Table 3. 3**: General description of different type of soil found in Abidjan*

Type of Soil	% Sand	% Silt	% Clay	Texture
Hydromorphic Soil	33	28.9	38.1	Sandy-Clay
Ferralitic soil highly unsaturated in high pluviometry zone; Tropical ferruginous soil	87.1	6.9	6	Loamy-Sand
Soil over magmatic rocks and cuirass zones	20.6	48	31.4	Clay-Loam
Ferralitic soil highly unsaturated in low pluviometry zone; Ferralitic soil middling saturated	75.4	9.4	12.2	Sandy-Loam

Source: Adapted from Aimé, *2018*

After analyzing the clipped soil data, its related attribute table and based on the previous study done by (Aimé, 2018), the soil type of the study area is mainly ferralitic highly desaturated. But due to the variation in clay and sand content, the watershed is classified into to two hydrologic soil group: **B** in the upstream part of the watershed and **C** in the downstream part (figure 3.7).

After assigning the soil hydrologic group, the percentage of A (PctA), B (PctB), C (PctC) and D (PctD) in each polygon were defined. For example, PctA defined what percentage of a given polygon has a soil group A. Regarding the soil group of the study area, we only have one soil group for the different polygon.

The following table 3.4 shows the summary of the soil data preparation.

***Table 3. 4:** Hydrologic soil group of the Gourou watershed*

FID	Soil Type	Area (Km^2)	Soil Group	PctA	PctB	PctC	PctD
0	Ferralitic highly desaturated (Clay<10 %)	20	B	0	100	0	0
1	Ferralitic highly desaturated (Clay>10 %)	7	C	0	0	100	0

3.4.3.2 Land Use data preparation

The Land Use data was obtained by performing a supervised classification of the Landsat 8 satellite using the maximum likelihood classification technique. Eight (08) Regions of Interest (ROI) were defined:

- Four (04) ROIs were used for calibration
- The other 04 were used for the classification validation. The ROIs were defined through the analysis of the Google Earth image and the geographic map of the whole country.

The image was then classified in the following areas of interest: Forest, Mixed Agriculture, Urban area and water bodies. The classified image was then imported into ArcGIS and polygonized. The land use data of the study area was clipped according to the watershed boundary (figure 3.8).

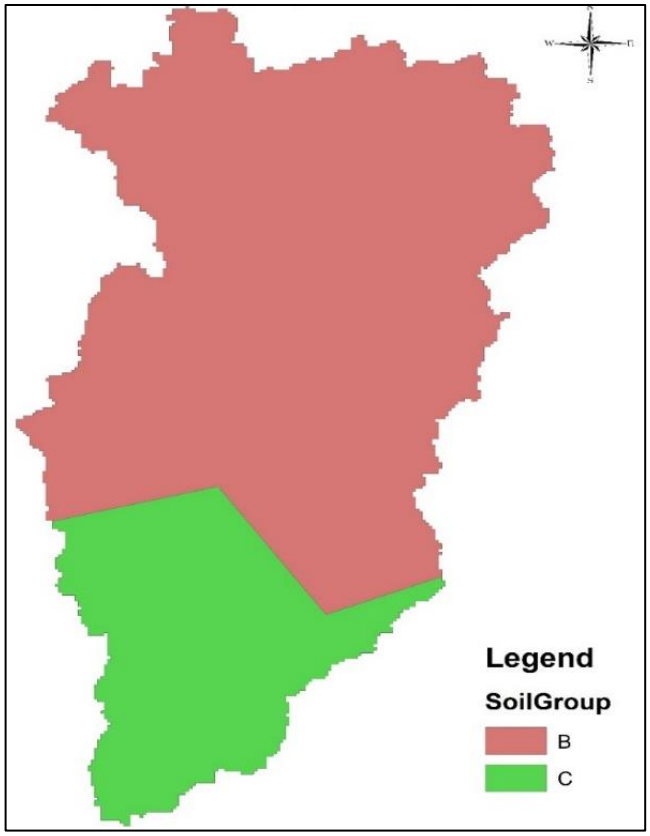

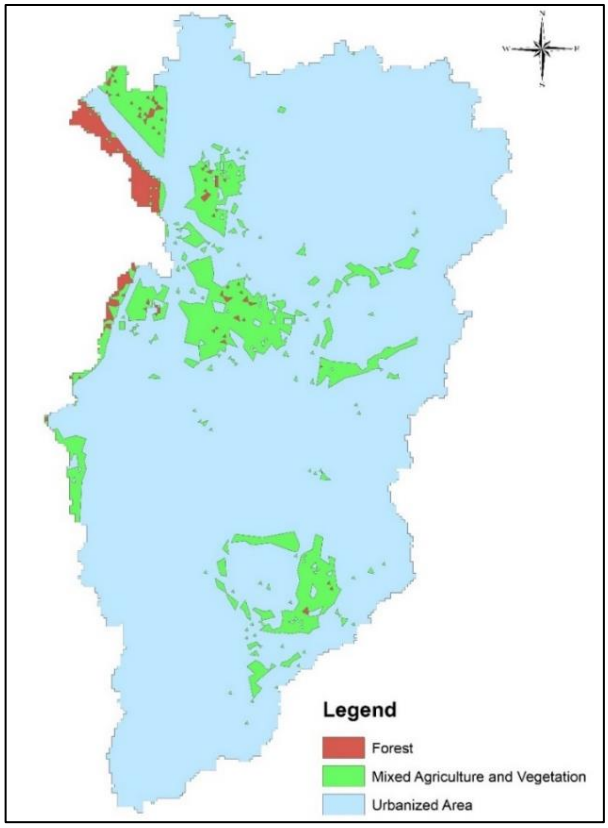

Figure 3. 7*: Soil group map*

Figure 3. 8: *Land Use classification*

The classification result was assessed by a confusion matrix which compares the obtained image with a ground truth region of interest. These ground truth region of interest correspond to the validation ROIs defined in above section. The validation areas were spread on the image to consider the spectral reality of each class in the image. The matrix was then calculated from pixel correctly/incorrectly classified in the validation zones. The confusion matrix was computed using ENVI software. The overall accuracy of the classification is 1384367 pixels correctly classify out of 1505174 pixels which give in terms of percentage 91.9739% of success. The detailed result is shown in appendix D.

3.4.3.3 SCS Curve Number generation with HEC-GeoHMS

The creation of the curve number grid was done by using HEC-GeoHMS. For this purpose, the soil data file and the Land Use (LU) file were merged (Union process in ArcGIS) to create a single shapefile. Thereafter, a correspondence table that gives the CN value for each combination of land use – soil hydrologic group was created (table 3.5). The values of CN were obtained from SCS TR 55.

***Table 3. 5**: Standard Curve Number* (Soil Conservation Service, 1986)

Table

cnlookup_thesis

FIELD1	LUVALUE	DESCRIPTION	A	B	C	D
0	1	Forest	30	58	71	78
0	2	Mixed Agriculture and Vegetation	67	77	83	87
0	3	Urbanized Area	57	72	81	86

Source: HEC-GeoHMS project, Thesis Ulrich ETCHE, 2019

The merged soil and land use data were combined with the DEM of the study area to create a curve number grid. The resulting CN grid is shown in the following figure 3.10. The curve number is a parameter that ranges from 0 (meaning that all the rainfall is accounted for losses, highly dry condition) up to 100, meaning that all the rainfall is transformed into runoff (Mujumdar *et al.* 2012). For the study area, as one can see in the figure 3.9, the curve numbers lie between 58 to 83 which indicate that we are in moderately wet condition and the watershed is susceptible to generate much runoff during the rainy season. After the creation of the data files described in the previous sections, the data were exported into the HEC-HMS model structure. When exporting, the data were checked to be sure that there are no conflicting names, stream reaches are within a watershed boundary, each sub-basin has a unique centroid, all stream reaches are connected and that the outlet point is valid.

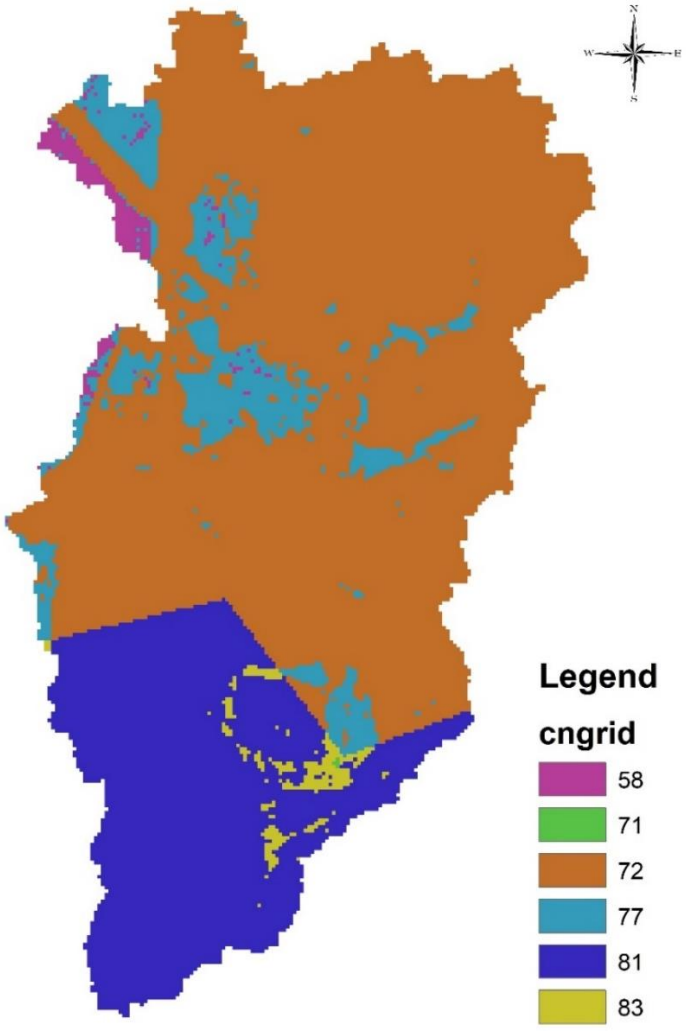

Figure 3. 9: *Curve Number grid*

3.4.4 Basin model of the study area

The physical representation of the hydrographic network is accomplished with a basin model. The hydrological elements are connected in a network to simulate the runoff process. The available elements are: sub-basin, junction, reservoir, source, and outlet. The calculation proceeds from upstream elements to downstream. The hydrological model of the Gourou watershed developed with HEC-GeoHMS and imported in HEC-HMS is represented by nine (09) sub-watersheds illustrated in figure 3.10. The basins model is composed of different reaches and junctions which allow the simulation of water from different sub-basins towards the outlet.

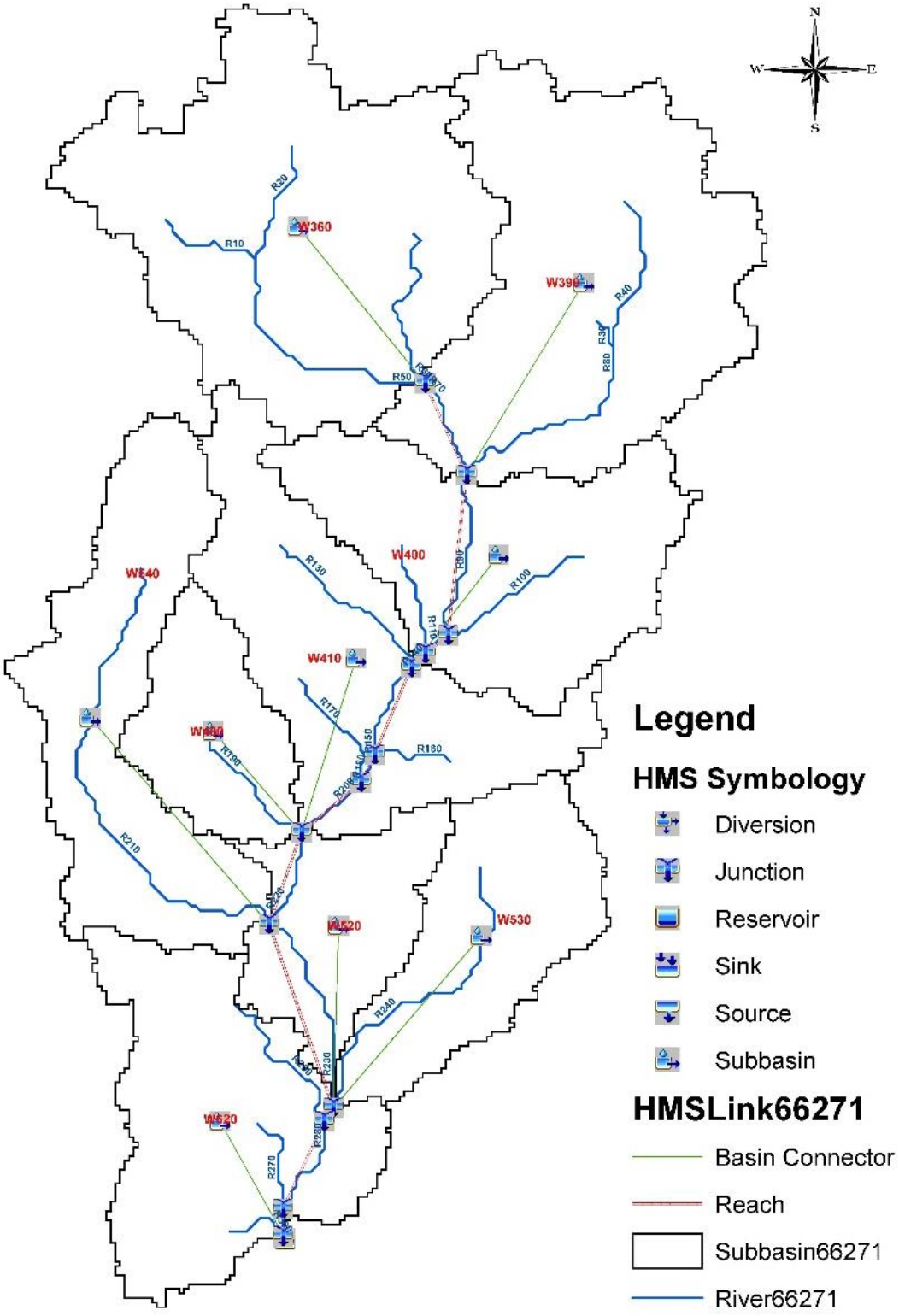

Figure 3. 10: *Basin model of Gourou Watershed*

3.4.5 Estimated initial parameter computed HEC-GeoHMS

Table 3.6 below summarizes all the model initial parameter estimated by HEC-GeoHMS using GIS environment and all other initial parameter required by the model such as: potential retention, percentage of impervious.

Table 3. 6: *Initial parameters value use for simulation*

Sub-basins	Initial Curve Number (CN)	Potential Retention (S)	Initial Abstraction (Ia)	%Impervious	Lag Time (min)
W360	71.91	99.20	19.84	35	99.473
W390	72.12	98.21	19.64	45	132.17
W400	72.80	94.88	18.98	40	59.834
W410	72.71	95.36	19.07	50	85.361
W480	74.15	88.56	17.71	60	49.545
W520	79.43	65.79	13.16	30	64.955
W530	76.78	76.81	15.36	35	65.747
W540	75.64	81.78	16.36	60	94.806
W620	81.01	59.56	11.91	60	70.621

3.5 HEC-RAS model development

3.5.1 Geometric data input

3.5.2 RAS Mapper application

Geometric data consist of establishing the connectivity of river system. It is composed by cross-sectional cut lines, junction, river, reaches, cross-sectional bank station, the flow path, downstream reach lengths between two cross-sections for the left overbank, main channel, and right overbank. Those data were obtained through the application of RAS Mapper which allows the creation of the river schematic and the extraction of the different attributes from an existing Triangulated Irregular Network (TIN).

As said previously, topographic data is a critical input in hydraulic modeling. In this study, a Lidar data for the study area (1m resolution) was used. The contours were converted into grid file (supported format of RAS Mapper) through ArcGIS spatial analyst tool. Thereafter, the grid file was brought into RAS Mapper to create a Terrain of the study area (figure 3.11) after the georeferencing. The georeferencing of the grid file is an important step when using RAS Mapper for flood study because it allows the visualization of water surface elevation, velocity on a map. The terrain file was used to develop the geometric data.

3.5.2.1 RAS themes creation

The RAS themes are generally, the file data in RAS Mapper used to develop geometric data. For this study, they are essentially lines themes:

- **Stream centerline (03)**: Three canals (Dokui reach, Zoo reach and the Main canal called "Gourou canal" were represented by the centerlines. The centerlines were drawn in the direction of the flow from upstream (North) to downstream (South). RAS Mapper created automatically a junction at the confluence of the canals. For accuracy, the TIN was superimposed on google satellite imagery during the creation of the centerline. The created centerlines are represented in blue in figure 3.12.

- **Main channel banks (03)**: The main canal banks (in red, figure 3.12) were specified for each reach. As the centerlines, there are drawn from upstream to downstream looking the flow direction. The banks allow the separation of the main canals from the over banks.
- **Flow path centerlines (06)**: There have been used to identify the hydraulic flow path in the left overbank, main channel and right overbank. The extent of the flow path determines the extent of the floodplain area. In total, six (06) flow paths were defined (one for each canal). Again, the flow paths are used to determine the reach lengths between two consecutive cross-sections.
- **Cross-sectional cut lines (57)**: The location, position, and expanse of the cross-sections have been represented by the cross-section cut lines defined in green in figure 3.12. The cross-section cut lines were drawn from left to right, from the perspective of looking downstream and perpendicular to the stream centerline (River) to meet the recommendation of the RAS Mapper user manual. The total number of cross-sections is 57. While the cut lines represent the planar location of the cross-sections, the station elevation data has been extracted along the cut line from the terrain.

3.5.2.2 Themes attributing

Following, the RAS themes creation, a number of required attributes in the model were created. Indeed, all the cross-sections (XS) attribute which include: the distance of the left overbank, main canal and right overbank between an upstream cross-section and the downstream one (reach lengths), the banks stations positions were calculated.

After these different steps, the created geometry has been opened into HEC-RAS geometry editor for his completion

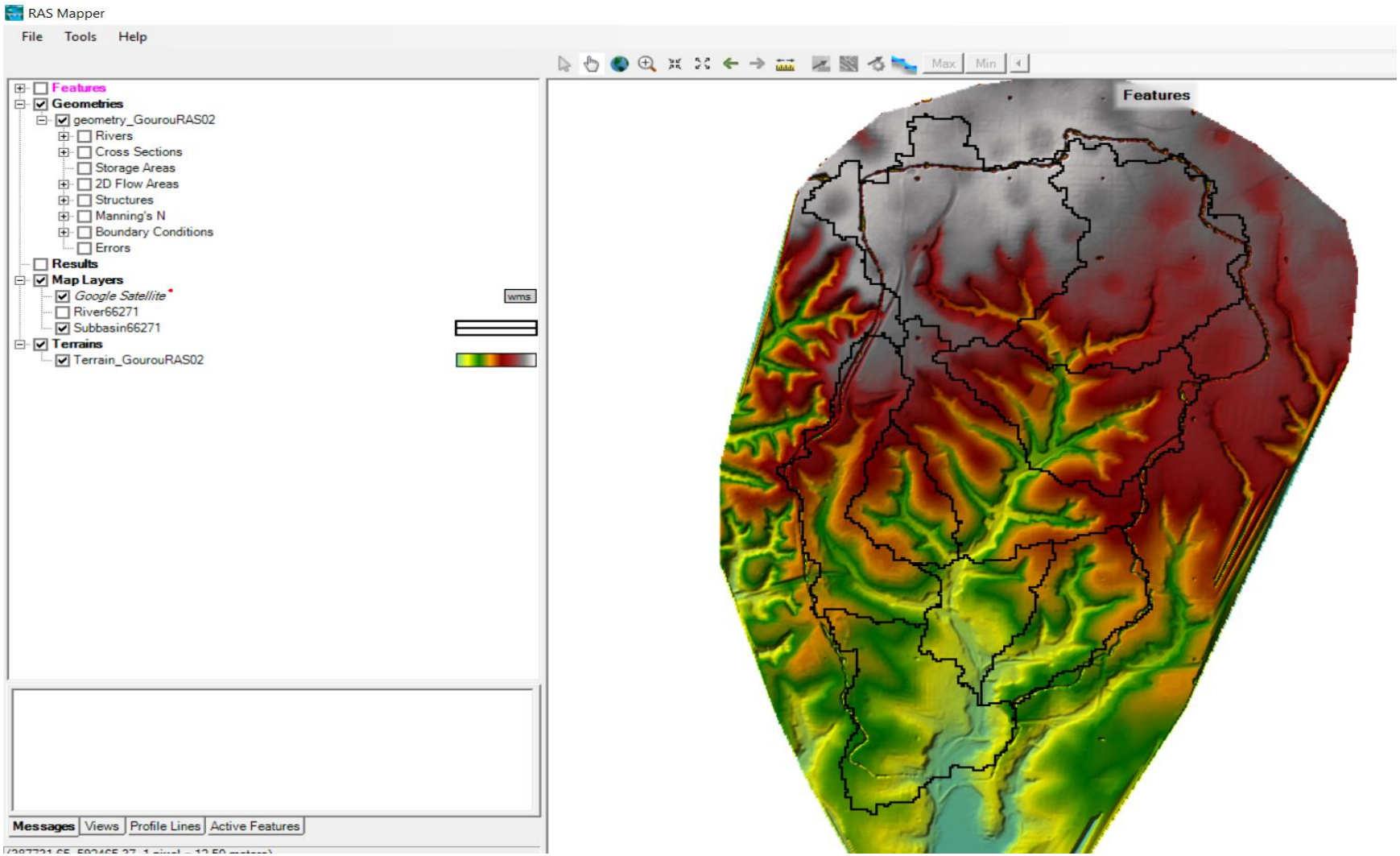

Figure 3. 11: *Terrain model created with RAS Mapper*

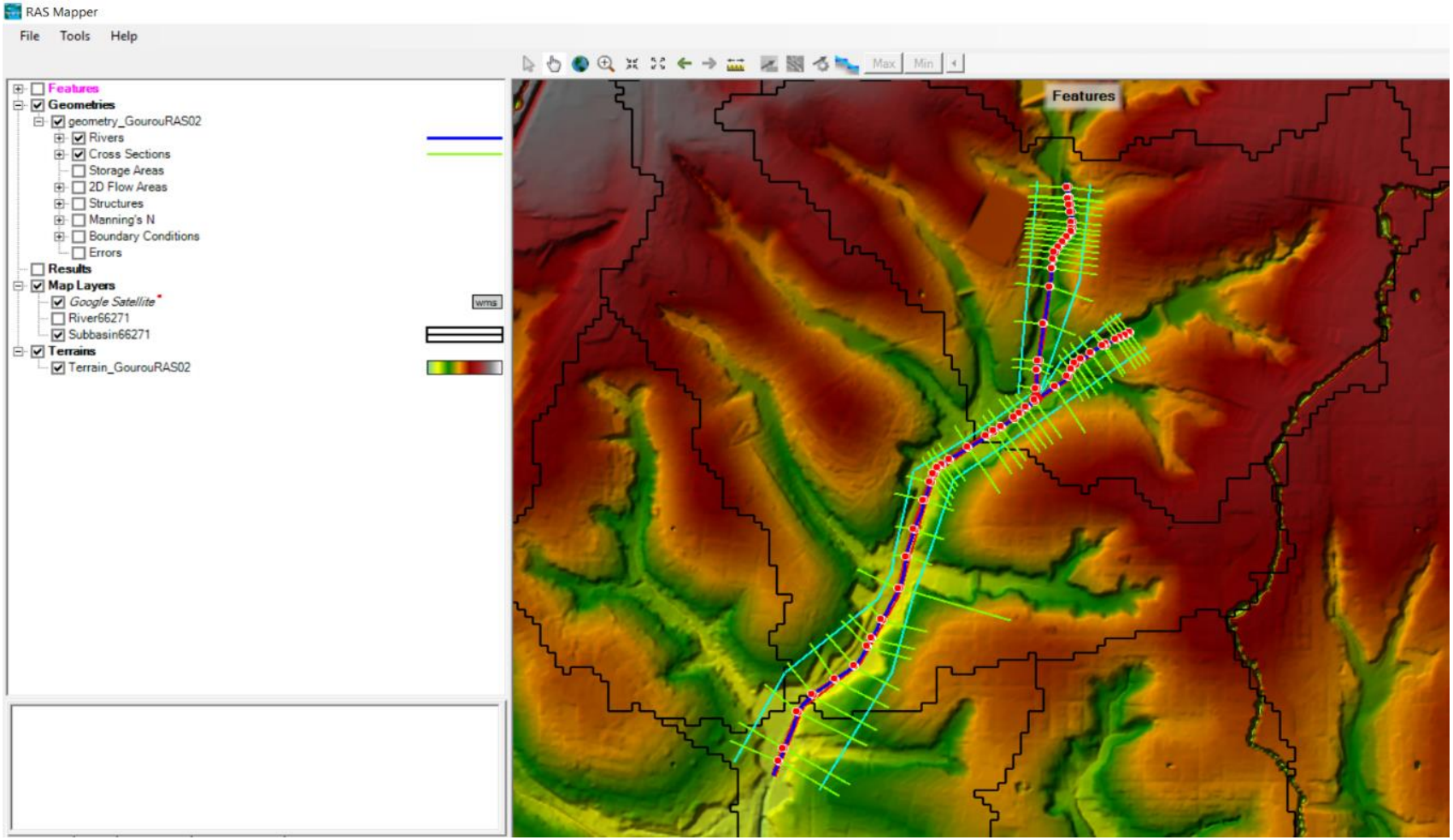

***Figure 3. 12**: RAS Mapper themes*

3.5.2.3 Geometric data editing

At this level, the geometric data editing is about the canal cross-section editing, assigning Manning coefficient and defining expansion and contraction coefficients. Regarding the canal cross-section editing, the cross section drawn in RAS Mapper were checked and adjusted based on the surveyed cross-cross section profile done with a differential GPS to better reproduce the geometry of the canal. All the 57 cross-sections drawn in RAS Mapper were adjusted. Figure 3.13 shows an example of an adjusted cross-section.

Once the canal cross-section editing was done, the Manning roughness coefficients were entered for the different overbank of each stream. The roughness parameters (Manning's Roughness coefficient) cause energy loss during flows along the canal, leading to the attenuation of the flood wave (Mukolwe, 2016). Channel roughness is a sensitive parameter in the development of a hydraulic model. It is a highly variable parameter, which depends upon a number of factors like the surface roughness, the vegetation, the channel irregularities, the channel alignment. In this work the different Manning's coefficients were assigned base on the land use types in the over banks. Each land-use types were allocated a Manning coefficient with reference to (Chow *et al*., 1988). As the main canals are made of concrete, a manning value of 0.013 was assigned to the three modeled canals. From visual observation, over banks had some vegetation and bare soil, the appropriate manning’s n value selected was 0.25.

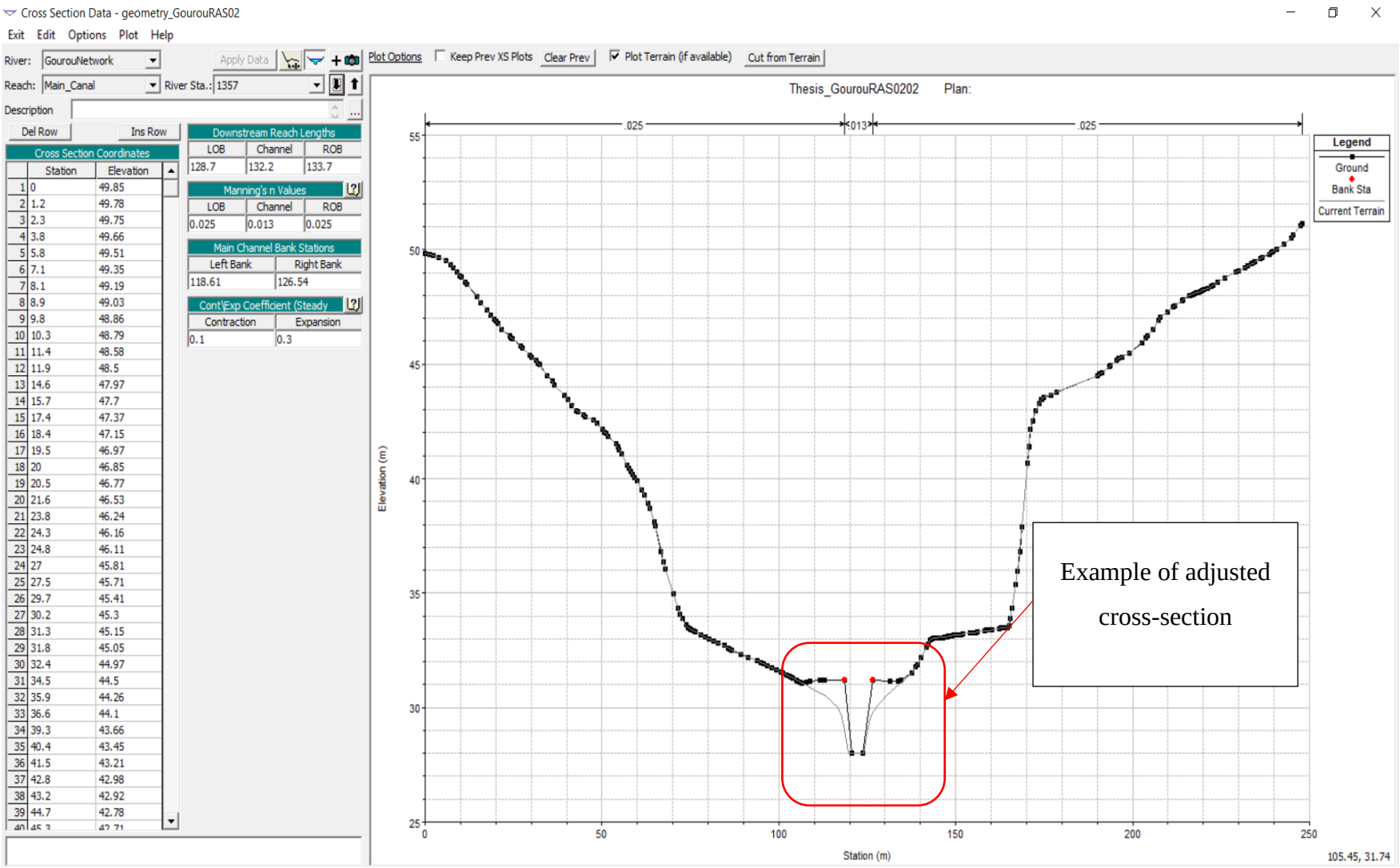

Figure 3. 13: Example of Edited cross-section in HEC-RAS

An example of the storage and editing of the Manning values in HEC-RAS is shown in figure 3.15.

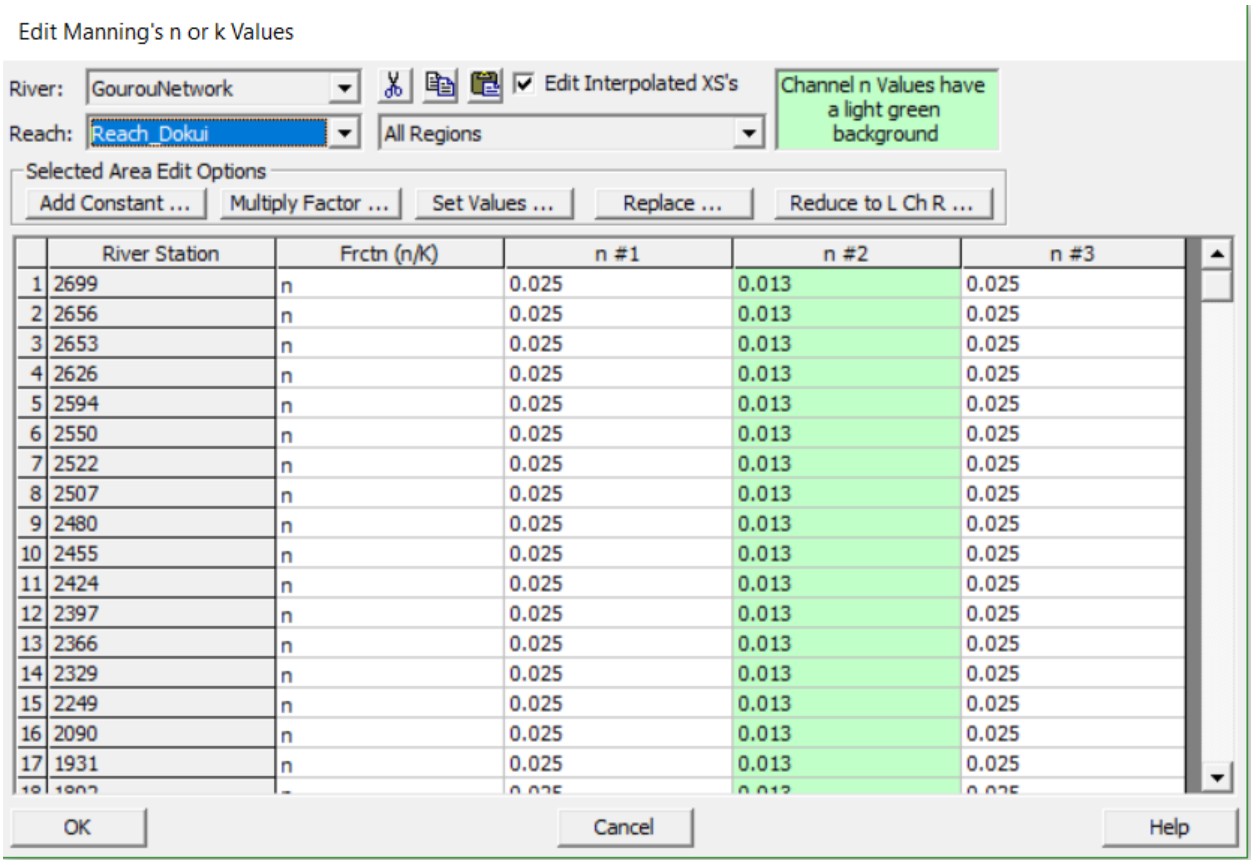

	River Station	Frctn (n/K)	n #1	n #2	n #3
1	2699	n	0.025	0.013	0.025
2	2656	n	0.025	0.013	0.025
3	2653	n	0.025	0.013	0.025
4	2626	n	0.025	0.013	0.025
5	2594	n	0.025	0.013	0.025
6	2550	n	0.025	0.013	0.025
7	2522	n	0.025	0.013	0.025
8	2507	n	0.025	0.013	0.025
9	2480	n	0.025	0.013	0.025
10	2455	n	0.025	0.013	0.025
11	2424	n	0.025	0.013	0.025
12	2397	n	0.025	0.013	0.025
13	2366	n	0.025	0.013	0.025
14	2329	n	0.025	0.013	0.025
15	2249	n	0.025	0.013	0.025
16	2090	n	0.025	0.013	0.025
17	1931	n	0.025	0.013	0.025

Figure 3. 14*: Manning's n value*

However, in this work, the channel bottom width was kept uniform for the respective reaches. Indeed, the change in bottom at some part of the different canal was less than 0.5 m and due to the time constraint, it was not possible to survey all the small changes. That why this assumption was made. Therefore, based on the recommendation of HEC-RAS manual (Brunner *et al*, 2016), the values of 0.1 and 0.3 were used respectively for contraction and expansion. In HEC-RAS, for steady flow hydraulic computations, a junction can be modeled by either the energy equation or the momentum equation. The energy equation does not consider the angle of any tributary coming in or leaving the main stream, while the momentum equation does (Brunner *et al*, 2016). In most cases, the amount of energy loss due to the angle of the tributary flow is not significant and using the energy equation to model the junction is more than adequate. Thus, the junction in this study is modelled by the energy equation.

3.5.2.4 Flow data and boundary conditions

After completing the geometry of the different canal, the hydischarges were entered into the model. This was done through the HEC-RAS steady flow component. The steady flow condition was selected because what we are interested in, in this study, is flood extent and depth and any damage that could be caused. However, in case of retention ponds design at the upstream side, one should consider the unsteady flow simulation because the volume of floods becomes important (Aimé, 2018). Based on this choice, HEC-RAS requires flows to be entered at all upstream boundaries. In addition, flow changes were specified along the main canal where some secondary canals are connected to the main canal. Flows were provided to the model for the 5-, 10-, 20-, 50- and 100-year recurrence interval storm events. These flow data were obtained from HEC-HMS simulation result.

The model boundary conditions in HEC-RAS can be the normal depth, a rating curve, a known water surface elevation, or critical depth. A critical depth was specified for the upstream of Dokui and Zoo canal and the normal depth at the downstream of the main canal. The normal depth option requires an energy slope to be entered by the user and the program then back-calculates a starting water surface elevation using Manning's equation. The energy slope was assumed to be the same as the main canal bottom slope (steady flow condition), thus estimated directly by HEC-RAS. The bottom slope is 0.008. The figures 3.15 and 3.16 summarize the boundary conditions and flow data entered in HEC-RAS for this study. After all the required data were entered, the steady flow analysis component has been selected to run our model.

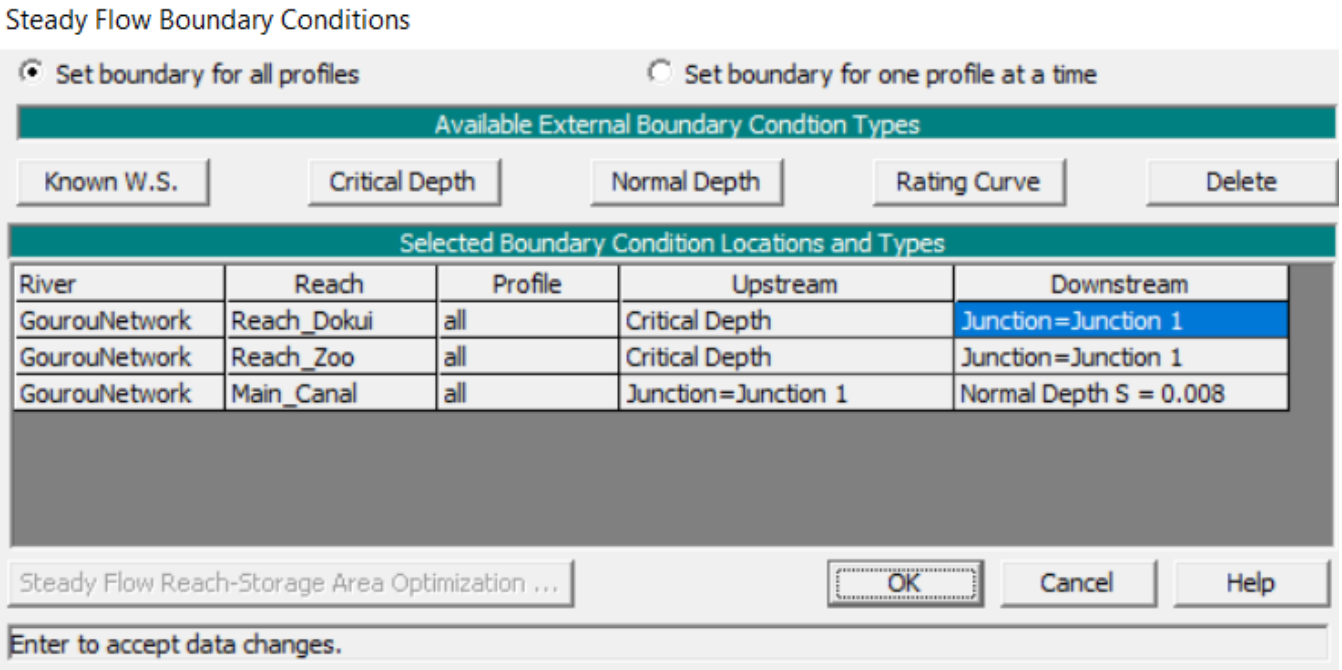

***Figure 3. 15**: Boundary condition of the developed HEC-RAS model*

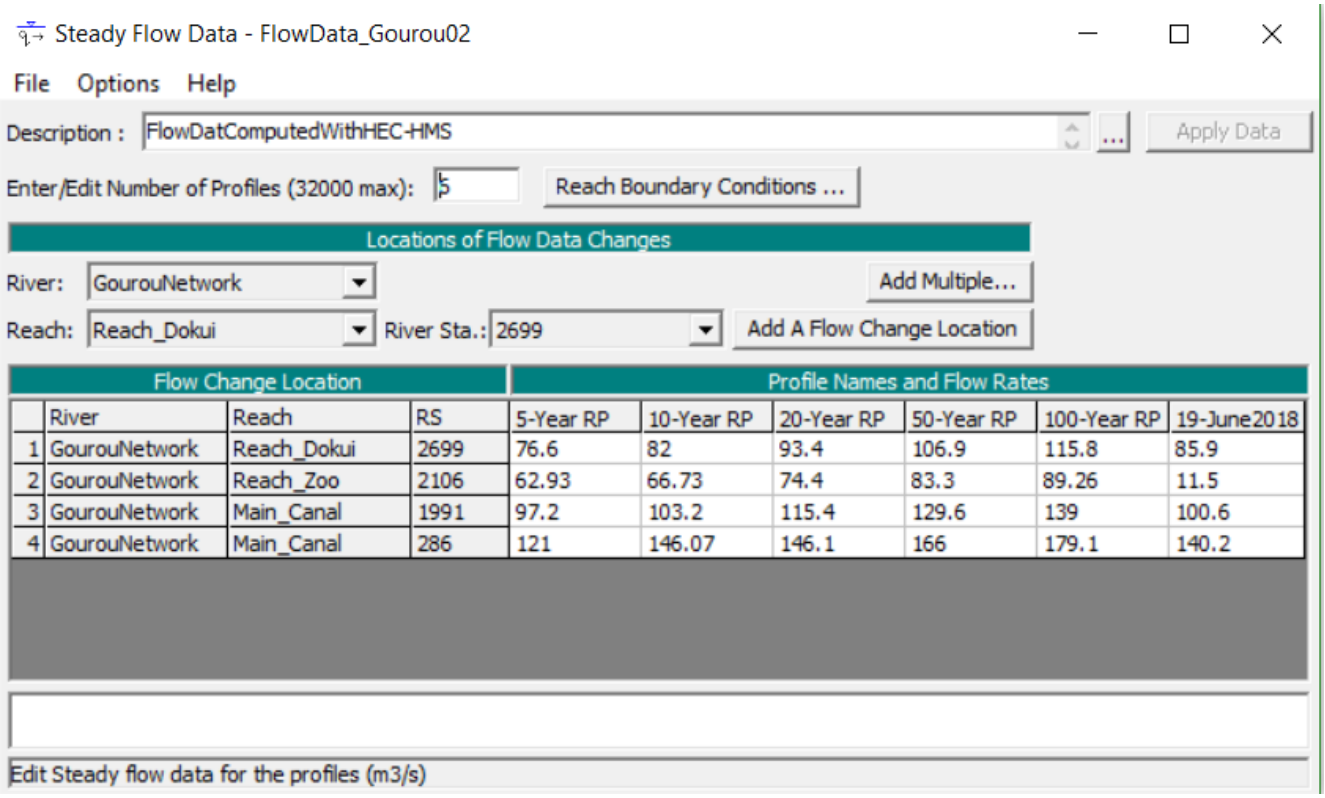

***Figure 3. 16**: Flow profiles used for simulation of the developed HEC-RAS model*

4 RESULTS AND DISCUSSION

4.1 Hydrological modeling result

4.1.1 HEC-HMS model calibration

In flood studies, peak discharge is an important aspect of the flood hydrograph (Tassew *et al.*, 2019). As said earlier, the 11th May 2018 flood event was used for calibration of the model. The result of the hydrological model showed a good fit between the observed peak flow and the simulated one after the optimization process at the point of observation (figure 4.1). The hydrograph shape and the time of peak are in general well-reproduced even though the model tends to underestimate the peak discharge.

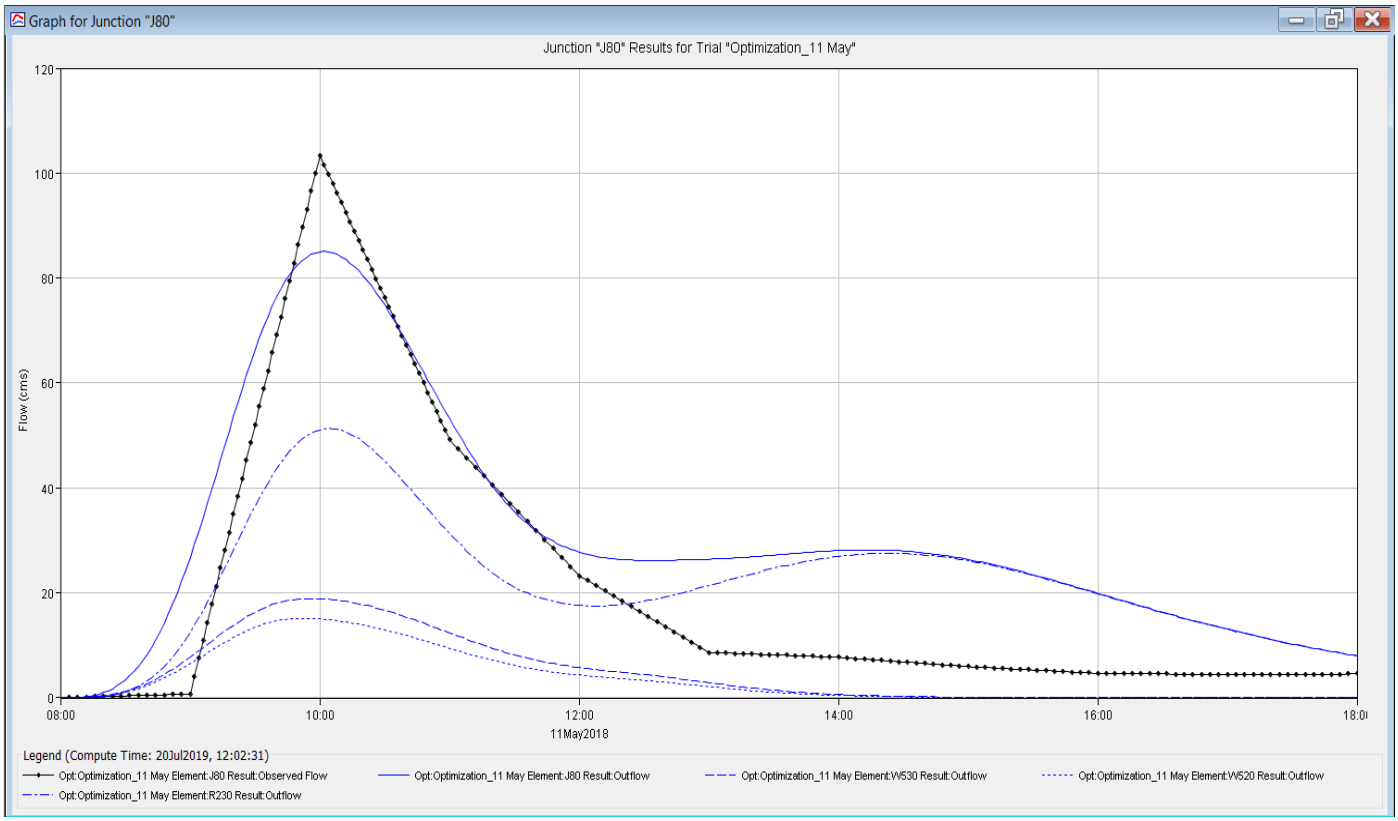

***Figure 4. 1**: Comparison between observed and simulated discharge for the calibration*

The peak discharge simulated before and after optimization, the associated volume and the NSE are mentioned in table 4.1.

Table 4. 1*: Comparison between observed and simulated discharge during the calibration*

Event	**Peak Discharge (m3/s)**			**RMS Error**	**Total Volume (mm)**			**Volume Residual**	**NSE**
11th May 2019	Simulated		Observed		Simulated		Observed		
	BOP	AOP			BOP	AOP			
	111.9	85.1	103.4	13.5	61.56	47.01	31.77	15.24	0.74

As we can see from table 4.1 the optimization process improves the quality of the model but decreases both the peak discharge and the total volume. Indeed, the NSE value of 0.74 means that the simulation results are satisfactory. However, the optimization was carried on the parameters that are susceptible to influence the model outputs. Table 4.2 summarizes the initial and optimized parameters for the watershed. The CN and Lag time of each sub-basins were optimized except for the sub-basin W620 due to the location of observation point (J80). In fact, during the optimization HEC-HMS optimized the parameters of sub-basins and reach above the observation point (Arlen, 2000).

4.1.2 HEC-HMS model validation

The model validation in this study is based on the 19th June 2018 storm event. The storm was characterized by heavy rainfall of around three (03) hours. The calibrated parameters were used for validation purpose. The simulated results of peak discharge with respect to the observed data, the RMS and the NSE during the validation are listed in table 4.3.

***Table 4. 2**: Optimized parameters*

Element	Parameters	Units	Initial Value	Optimized Value
.All Subbasins.	SCS Curve Number - Curve Number Scale Factor		1	0.96261
.All Subbasins.	SCS Curve Number - Initial Abstraction Scale Factor		1	1
W360	SCS Curve Number - Curve Number		71.91	67.68
W390	SCS Curve Number - Curve Number		72.12	67.88
W400	SCS Curve Number - Curve Number		72.80	72.8
W410	SCS Curve Number - Curve Number		72.70	99
W480	SCS Curve Number - Curve Number		74.15	73.39
W520	SCS Curve Number - Curve Number		79.43	76.61
W530	SCS Curve Number - Curve Number		76.78	74.04
W540	SCS Curve Number - Curve Number		75.64	99
R120	Muskingum - K	hr	0.15	0.34
R140	Muskingum - K	hr	0.15	0.34
R150	Muskingum - K	hr	0.18	0.41
R180	Muskingum - K	hr	0.18	0.41
R200	Muskingum - K	hr	0.15	0.34
R220	Muskingum - K	hr	0.15	0.15
R230	Muskingum - K	hr	0.1	0.1
R70	Muskingum - K	hr	0.1	0.34
R90	Muskingum - K	hr	0.1	0.76
W360	SCS Unit Hydrograph - Lag Time	hr	1.66	2.51
W390	SCS Unit Hydrograph - Lag Time	hr	2.20	3.34
W400	SCS Unit Hydrograph - Lag Time	hr	0.99	0.43
W410	SCS Unit Hydrograph - Lag Time	hr	1.42	1.33
W480	SCS Unit Hydrograph - Lag Time	hr	0.82	0.83
W520	SCS Unit Hydrograph - Lag Time	hr	1.08	1.03
W540	SCS Unit Hydrograph - Lag Time	hr	1.5	1.48
W530	SCS Unit Hydrograph - Lag Time	hr	1.09	1.05

***Table 4. 3**: Comparison between observed and simulated discharge during the validation*

Event	Peak Discharge (m3/s)		RMS Error	NSE
19th June 2019	Simulated	Observed		
	188.1	165.7	12.2	0.92

Table 4.3 showed a relatively closed fit between the observed and the simulated peak discharge with an RMS of 12.2. From the point of view of the Nash–Sutcliffe Efficiency (NSE) criteria, a good result was obtained between the simulated and the observed discharge, with NSE value of 0.92. This value can be judged as good and similar results were obtained by (Tassew *et al.*, 2019) when they used SCS-CN for rainfall-runoff simulation in Gilgel Abay catchment, Upper Blue Nile basin, Ethiopia.

4.1.3 Sensitivity analysis

A sensitivity analysis was carried out to determine which parameters of the model have more impact on the model result. It is used to classify the model parameter based on their contribution to the total error in model predictions. According to Haan, (2002) the sensitivity can be local or global. A local sensitivity analysis in determining each parameter separately by keeping the other parameters of the model constant while in global sensitivity, the model parameters are allowed to vary at the same time. Generally, one can use three types of coefficient (methods) for both local and global sensitivity analysis (Cunderlik *et al.*, 2004). We have the absolute sensitivity coefficient, the relative sensitivity coefficient and the last method which is the most used involve the perturbation of the model parameter (the method of factor perturbation). In this study, the local sensitivity analysis method was selected. In this study, the local sensitivity analysis and the method of factor perturbation were selected. The sensitivity analysis was done by changing the different parameters values in the range of $\pm 20\%$ with 5% intervals. In HEC-HMS, each parameter representing a specific hydrologic condition, three parameters were used for the sensitivity analysis. There are: Curve Number and Percentage of Impervious (parameters needed for the loss model) and the Lag-Time (parameter needed for the transform model).

4.1.3.1 Influence of each parameter on the model result

This section describes the effect of the different parameter variation on peak discharge. Only, the example of the effect of the variation of $\pm 15\%$ of the different parameters on 10-year flood hydrograph is shown. Indeed, others are similar to the presented one.

4.1.3.1.1 Influence of loss model (SCS Curve Number) parameter on model result

The SCS Curve Number (CN) and the percentage of the impervious area used to account for infiltration and interception. When increasing the CN by 15%, the peak flow also increases by 7.98% and a decrease of CN by 15% leads to a decrease in the peak flow by 7.90%. Similarly, when the percentage of impervious area is increased by 15%, the peak flow increases by 4.27% and when it is decreased by 15% the peak flow decreases by 4.23%. The figures 4.2 and 4.3 show the different hydrographs resulting from this variation of both parameters.

4.1.3.1.2 Influence of Lag-Time on model result

The basin Lag time (L) represents the time from the center of mass of excess rainfall to the hydrograph peak. It is also referred to as basin lag (Scharffenberg, 2016). When we keep the other parameters constant and we only change (L), the influence of the lag time is both on the peak runoff occurred time and the total flowrate during the storm. The following figure 4.4 is an example of the influence of the increase (decrease) of the lag time by $\pm 15\%$ on the peak flow and the occurred time. When the lag time is shortened (reducing initial lag time by 15%), the peak flow increased by 4.95% and occurred earlier (10 min earlier). The lengthened of the lag time by 15% results in a decrease of the initial peak flow by 4.39% and the peak flow occurs 15 min later comparing to the initial time.

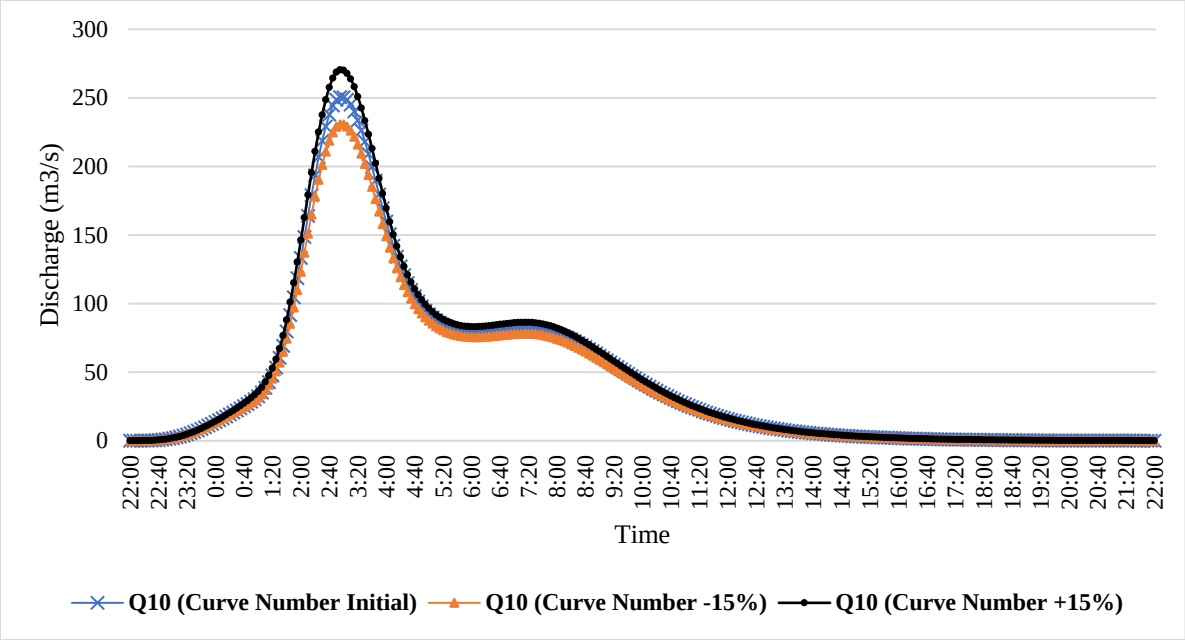

***Figure 4. 2**: Influence of ± 15% variation of curve number on 10-year flood hydrograph*

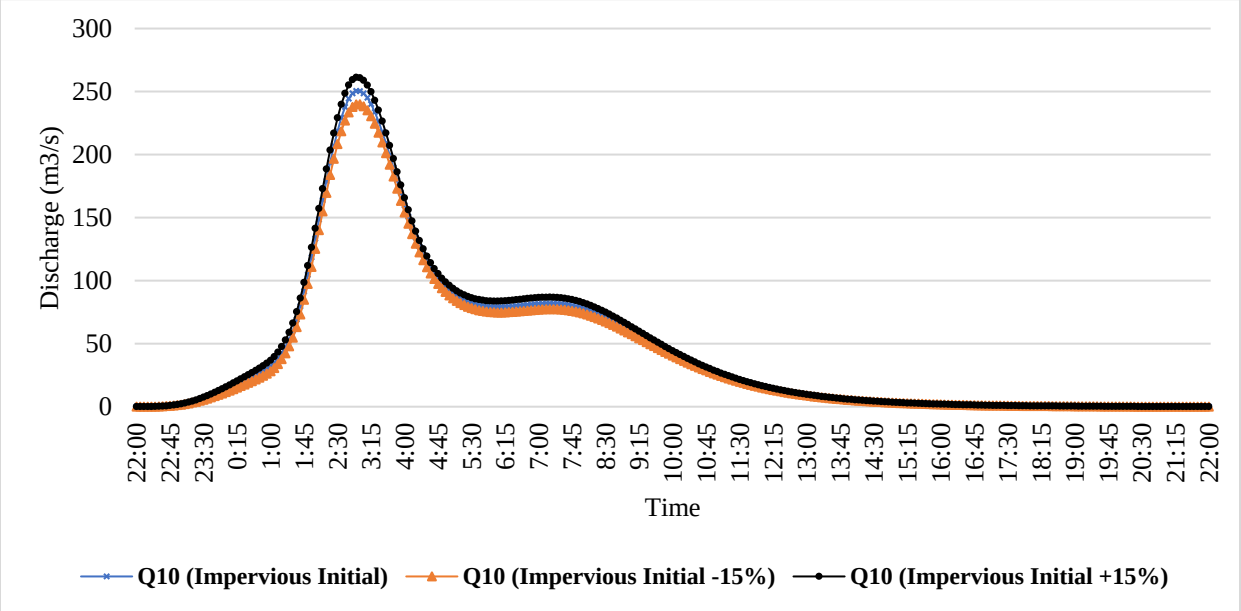

***Figure 4. 3**: Influence of ± 15% variation of percentage of Impervious area on 10-year flood hydrograph*

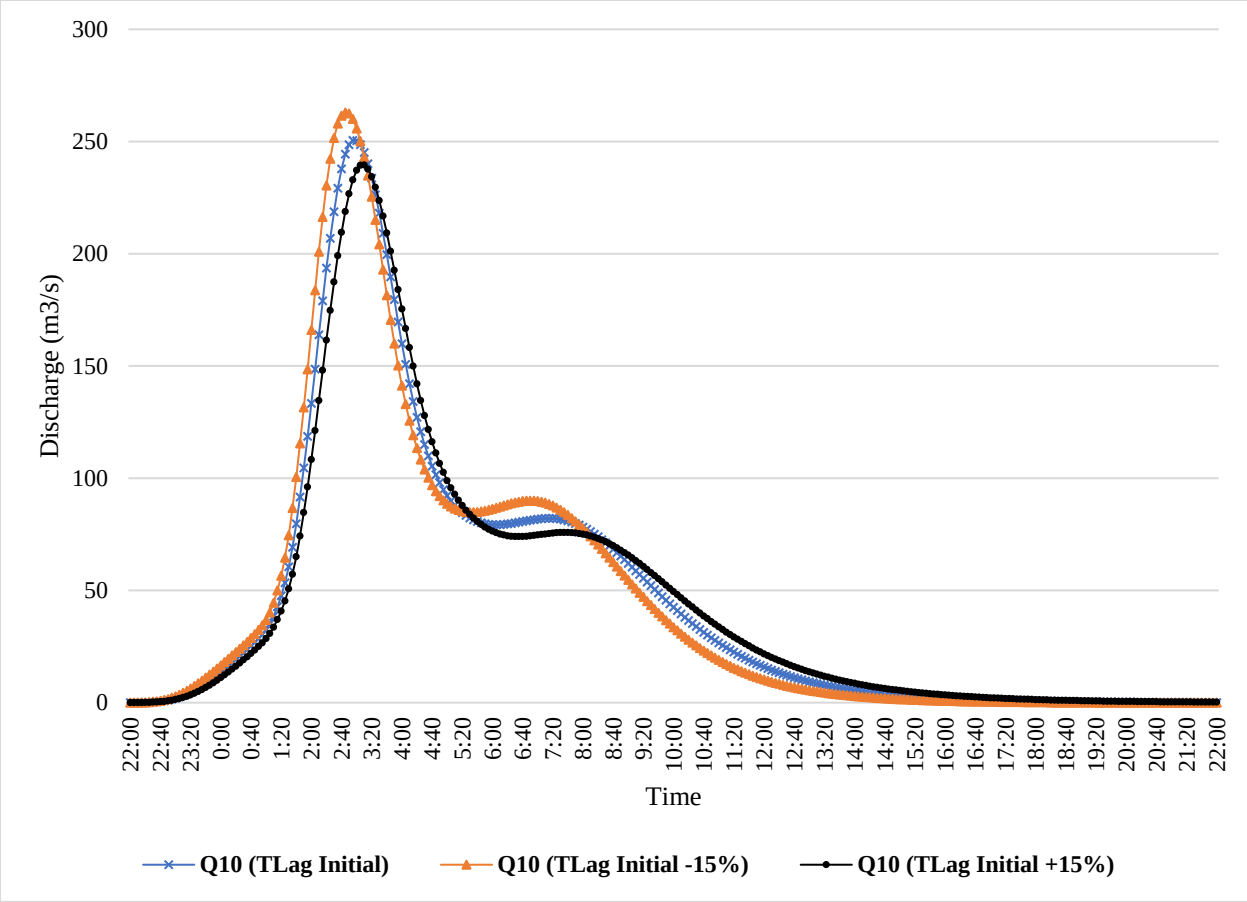

Figure 4. 4: *Influence of ± 15% variation of Lag-Time on 10-year flood hydrograph*

4.1.3.2 Identification of the most sensitive parameter

In the sensitivity analysis, different scenarios were tested for the different calibrated parameters. It was found that each parameter influences the peak flow at the outlet. In order to classify the parameter based on their impact, they were compared among them. Figure 4.5 compares the percentage error in the peak flow, PEPF, of the model results generated from the sensitivity scenarios of the change in the event model parameters for different return period. The example of 10-year return period is presented here while the others will be in appendix E. The error is highest for the scenarios of the change in the Curve Number, CN, up to 12% for the $\pm 20\%$ change scenarios. Moderate values of the PEPF measure were obtained by changing the Lag time, up to 6% for the $\pm 20\%$ change scenarios. The PEPF values change due to the variation in the percentage of impervious area is around 4%. Thus, the Curve number is the most sensitive parameter, followed

by the lag time and the percentage of impervious area. This result was also found by (Tassew et al., 2019) during their study in Lake Tana Basin. By varying the SCS Curve Number, the basin lag time and the percentage of impervious by $\pm 25\%$ with a step of 5%, they reach to the conclusion that the CN is the most sensitive parameter, followed by the lag time.

Furthermore, by analyzing the parameters influence on the peak flow variation for different return period of the storm, it was found that when the return period increase, the parameters sensitivity on the model tends to decrease. For 5-year and 10-year return period, the percentage of impervious area and the lag time seem to have the same influence on the peak flow and from 20-year return period, we can see their influence distinctly.

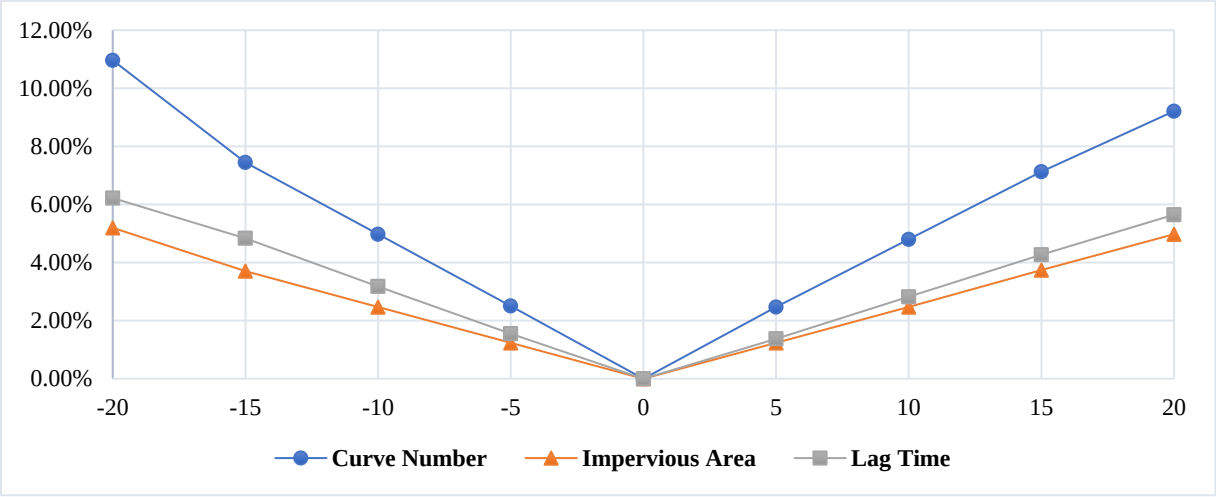

***Figure 4. 5**: Parameters influence on Peak Flow of 10-Year Return Period*

4.2 Flood hydrographs generation for different return period

After the calibration and validation based the two storms event, the model was used to simulate the flood hydrograph for different return period:1-year, 2-year, 5-year, 10-year, 20-year, 50 year and 100-year. Again, for the stability of the flow routing, a time step of 5 minutes was chosen. The storm was not defined and kept as default.

This choice implies that each sub-basin will have a different hyetograph computed automatically by HEC-HMS using the sub-basin area as the storm area. The results of the simulation are shown in the figure 4.6.

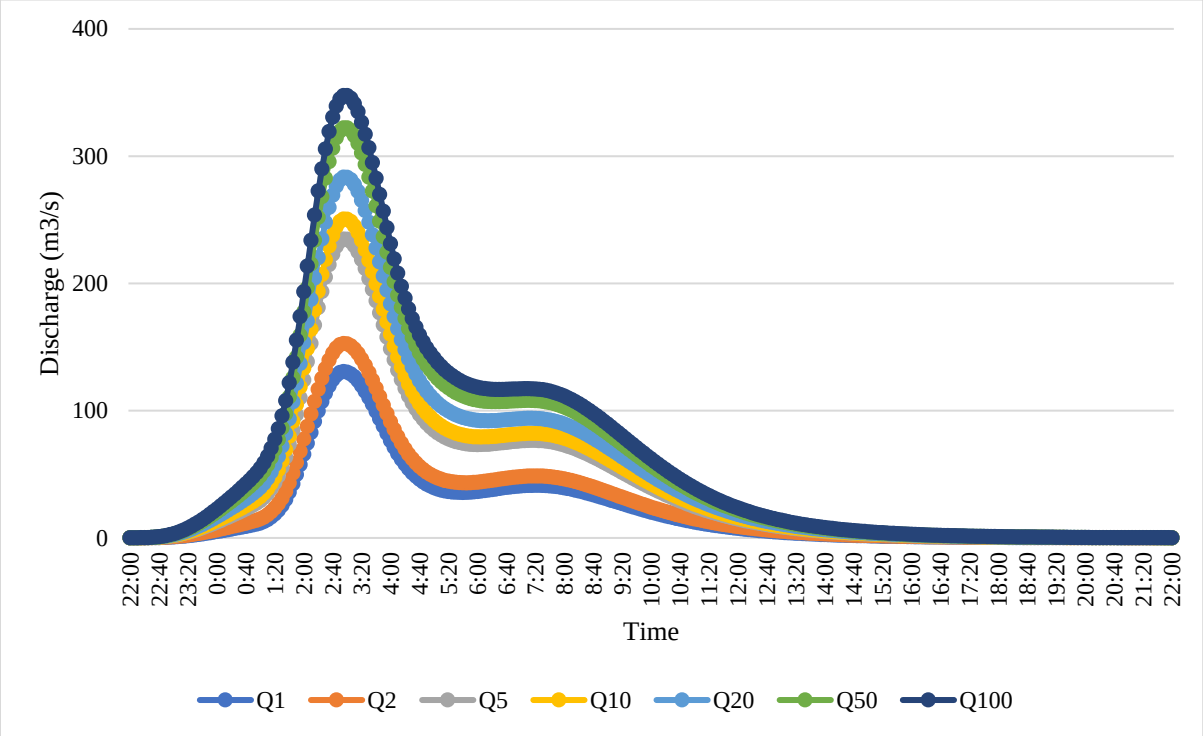

Figure 4. 6: *Flood hydrograph for different return period*

As it is common in hydrological modeling, it can be seen from the different hydrograph that the peak discharges increase when the return period increases. The shape of flood hydrograph found in this study is relatively the same as those found in (Paresh *et al.*, 2011) study when they applied HEC-HMS model for the study of Woldiya watershed, Ethiopia. From the information on previous studies done by some consulting firm, it is said that the 10-year flood hydrograph peak is around 300 m^3/s while in this study, the 10-year is between 250 m^3/s. The maximum peak discharges at the outlet of the watershed and at junctions of interest for different return period are illustrated in table 4.4 and 4.5 respectively.

***Table 4. 4**: Peak discharges at the outlet of the watershed for different return period*

Return period	**100-Year**	**50-year**	**20-year**	**10-year**	**5-year**	**2-year**	**1-year**
Maximum discharge (m^3/s)	347.6	322.2	283.4	250.5	234.7	130.6	152.7

***Table 4. 5**: Peak discharges at junctions of interest for different return period*

	100-year flood	**50-year flood**	**20-year flood**	**10-year flood**	**5-year flood**
	m^3	**m^3**	**m^3**	**m^3**	**m^3**
J104	115.8	106.9	93.4	82	76.6
W400	89.26	83.3	74.4	66.73	62.93
J92	139	129.6	115.4	103.2	97.2
J85	179.1	166	146.1	129.1	121

The global summary of HEC-HMS model result for different return period is illustrated in appendix F.

4.3 Hydraulic modeling result

4.3.1 Water surface profiles: Cross-sectional and longitudinal profiles

Hydraulics simulation was performed on the basis of geometric data, flow data and boundaries conditions in steady flow analysis. In this study, we were more interested in the water surface elevation (WSE) along the main canal (Gourou's Canal) and the flood extent for peak discharges for different return period. The manning's n values have not been calibrated due to the lack of high-quality data and aerial images of previous flood extent. The modeled network is composed of three (03) canals (Zoo Canal, Dokui Canal, and Gourou Canal which the main Canal) that are linked by a junction where floods are frequent.

Table 4.6 shows details of flow characteristic at two stations, RS 1948 (after the junction) and RS 286, at upstream and downstream respectively of the main where generally water overtopped the banks after a heavy rainfall event. The top width of the flow is high for RS 286 around 166 m (8.42 m for the left overbank, 7 m for the main channel and 149 m for the right overbank) which exceed the top width of the canal: 7m.

Table 4. 6: *Flow characteristic at River Station 1948 and 286*

Reach	**River Station**	**Profile**	**Q Total**	**Min Ch El**	**W.S. Elev**	**Flow Area**	**Top Width**
Gourou Canal (Main Channel)		10-Year RP	(m3/s)	(m)	(m)	(m2)	(m)
	1948		103.2	34	38.85	98.2	86.31
	286		146.07	23.49	26.78	167.52	165.87

One of the main advantages of using HEC-RAS is the visualization of the flow for any drawn cross-section. Figure 4.7 and 4.8**,** illustrate the water level for 5-, 10-, 20-, 50- and 100-year return period for the respective cross-section. It can be observed that the canal is overtopped by the 5 years and 10-year discharge even though those canals are designed with 10-year storm. The water surface elevation produced by 19th June 2018 flood event is closed to the 10-year flood water surface elevation, this may indicate the severity of the 19th June 2018 flood event. Therefore, as expected the water level increases when the return period also increases.

Longitudinal flow profiles were plotted (Reach in HEC-RAS) to see the variation of water surface elevation for each canal (figure 4.9 and 4.10). The water surface profile of the main channel is presented in appendix G. Because of the number of sections, it difficult to distinguish the profiles. From the profiles, we can see that the flow is characterized by an alternate of subcritical and supercritical flow regime and the WSE tend to decrease along the channel. The WSE profile of 100-year flood of Dokui canal shows an important variation near the junction with the Zoo canal.

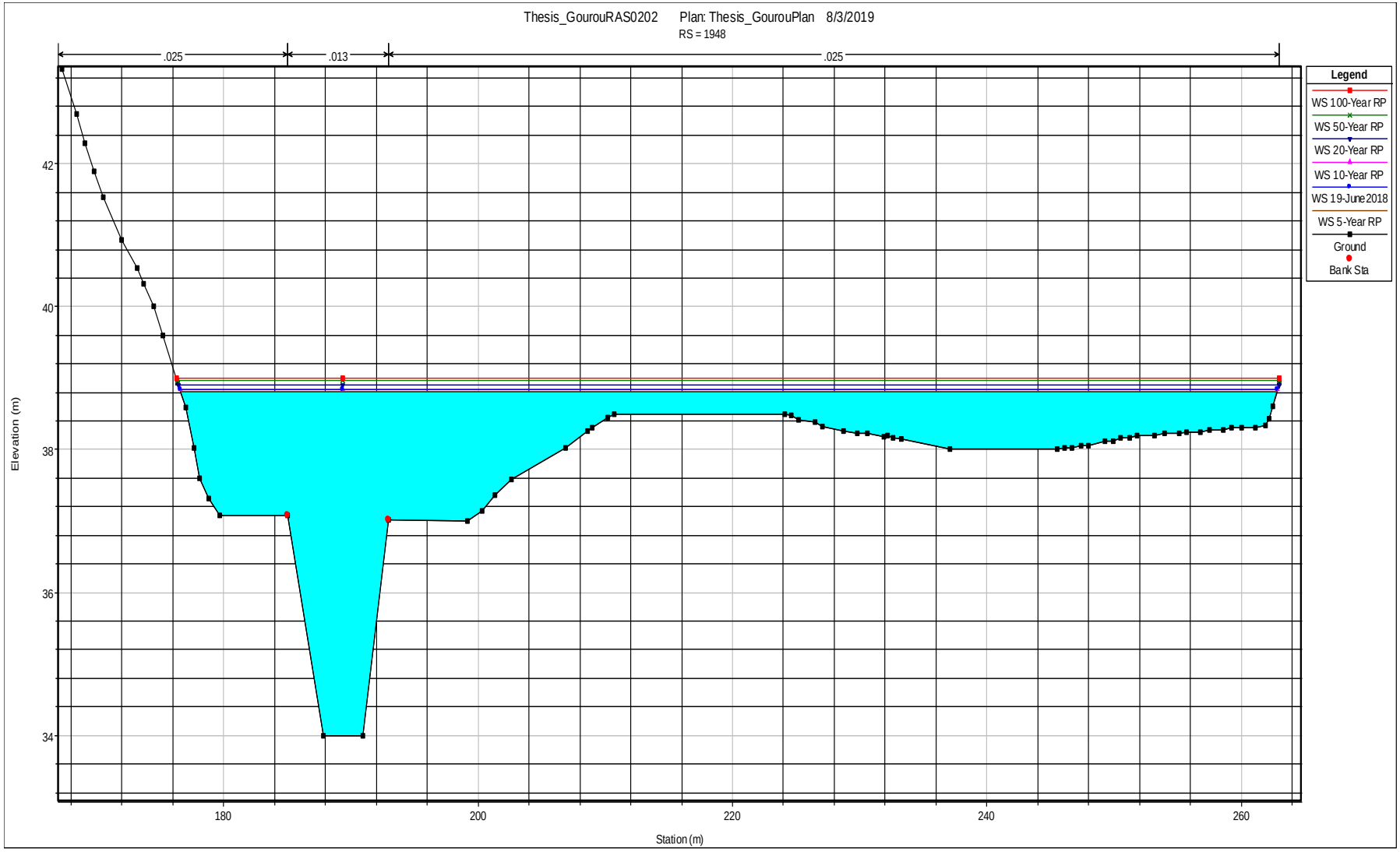

***Figure 4. 7**: Water level for cross-section RS 1948*

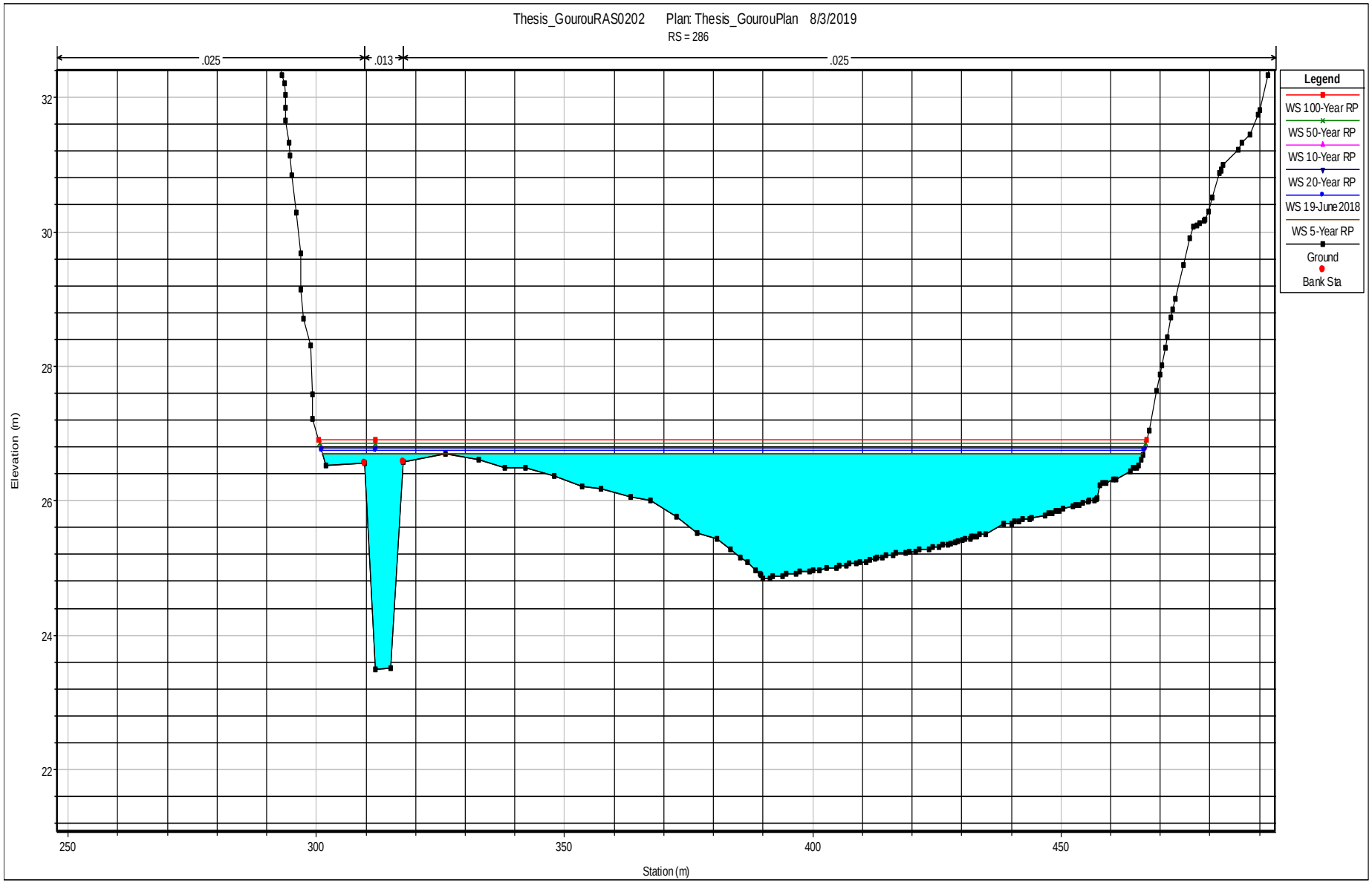

***Figure 4. 8**: Water level for cross-section RS 286*

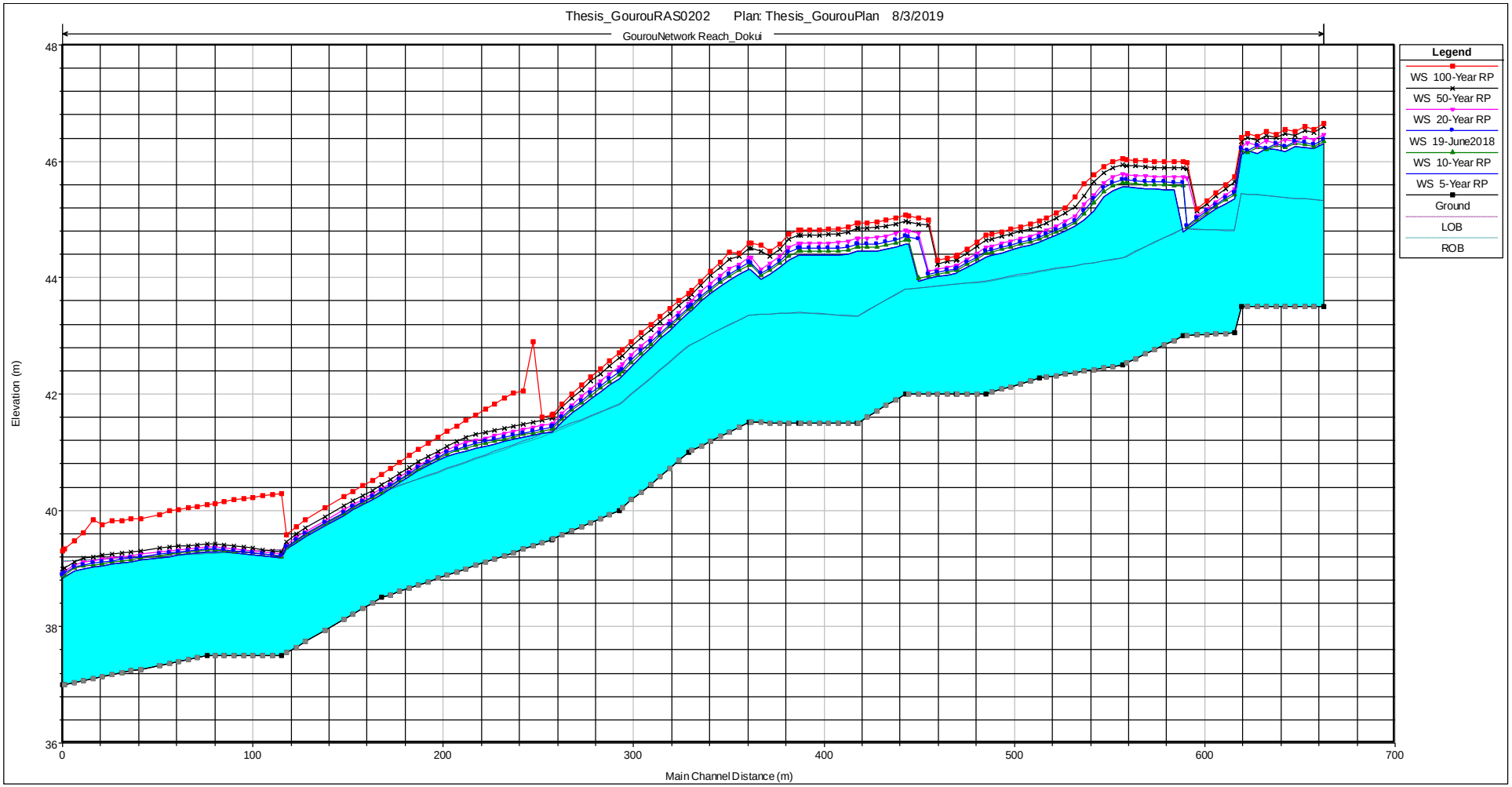

***Figure 4. 9**: Water surface elevation longitudinal profile in Dokui reac*

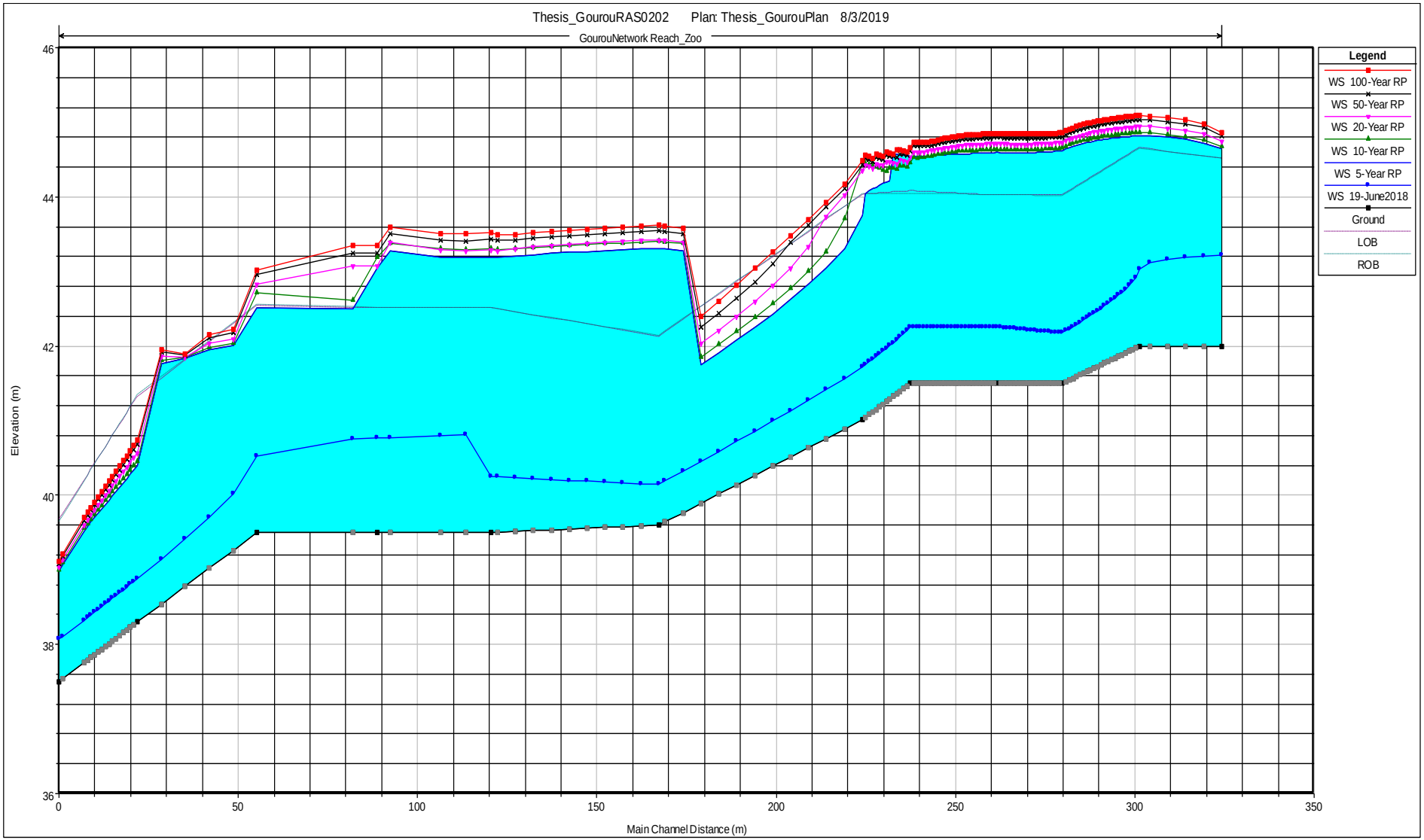

***Figure 4. 10**: Water surface elevation longitudinal profile in Zoo reach*

4.3.2 Flood inundation map

Maps are useful tools to represent the spatial distribution of flood hazard. In this study, flood hazard maps for 5-, 10-, 20-, 50-, 100-year return period were developed based on peak discharges simulated in hydrologic modeling, the TIN of the study area. The results were directly visualized in RAS Mapper. Flood maps were developed for the different return period. Figure 4.11 depicts the extent and the depth of water for different return period along the modeled canal. The water depth lies between 0 and 6 m with the maximum water depth occurring around the main channel. However, water depth decreases as it spreads gradually. The water depth and flood extent increase when the return period increases. As we can see, the water overtopped the canal banks and occupies roads around the Zoo of Abidjan, the Bus Station and some space where people are developing their businesses. The variation of water in the respective over banks will be analyzed in the following section.

The 100-year flood covers the largest inundated area of around 21 Ha along the canal. The inundated areas were estimated for different scenarios (return period) and are presented in table 4.7.

In general, for all return period, the total inundated area is less than 30 Ha and built-up area are the most inundated area.

Table 4. 7: *Inundated area in hectare (Ha)*

Affected Land Use	5-year	10-year	20-year	50-year	100-year
Forest	0.049	0.053	0.054	0.054	0.054
Mixed Agriculture and Vegetation	2.430	2.466	2.528	2.608	2.858
Built-Up Area	15.836	16.266	16.888	17.574	18.140
Total area	18.32	18.785	19.47	20.24	21.052

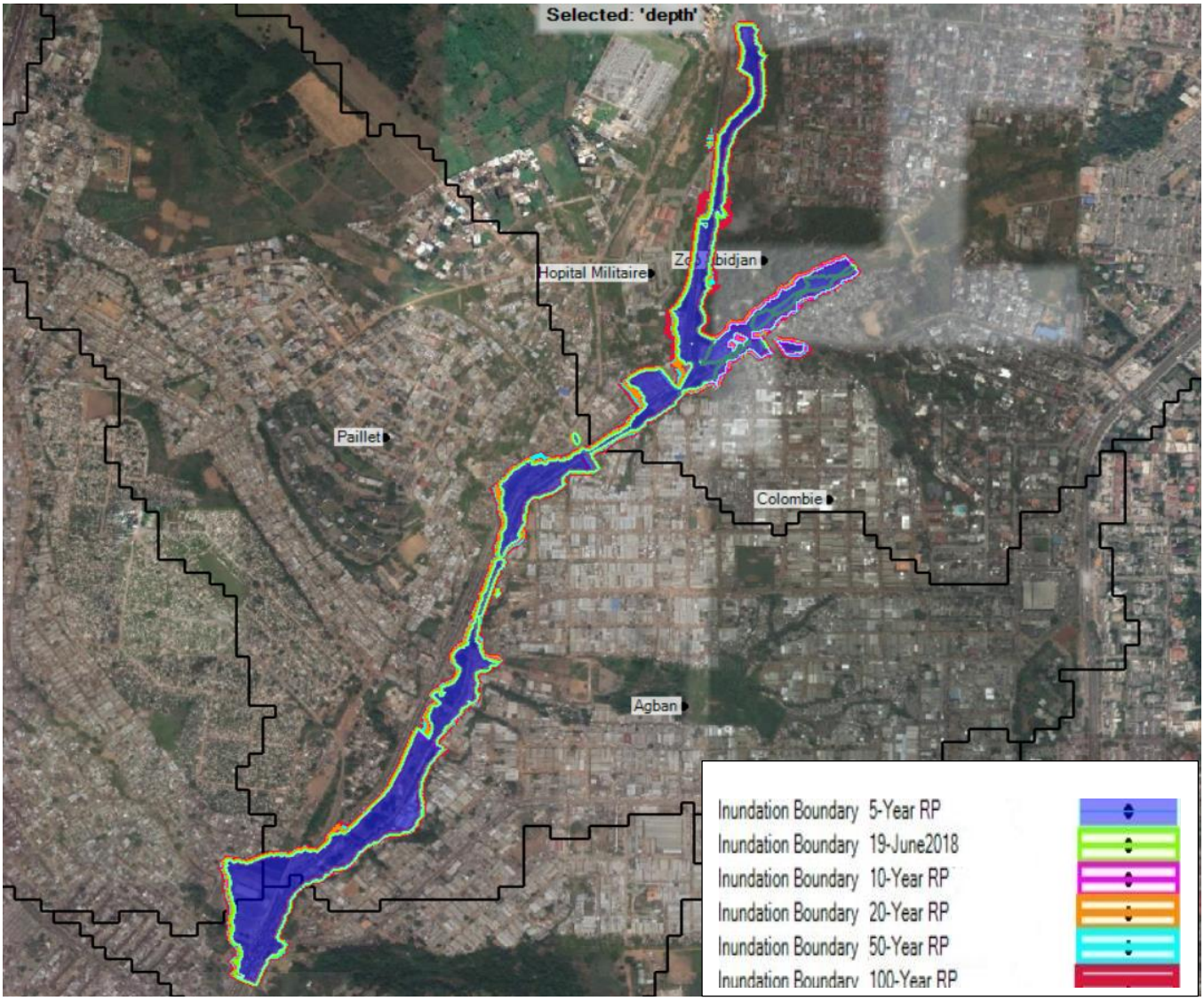

***Figure 4. 11**: Flood inundation map for the different return period*

4.3.2.1 Water depth in the overbank

The water depth in the Right Overbank (ROB) and the Left Overbank (LOB) are presented in the following figures 4.12 and 4.13 for the different return period. The water depth in the over banks seem to be higher and they increase in croissant order of the return period. The maximum water depth obtained is around 1.8 m for the ROB and 1.5 m for the LOB. The variation of the water depth in the over banks of the main channel shows that the maximum elevations occurred generally at the upstream and downstream part of the main canal.

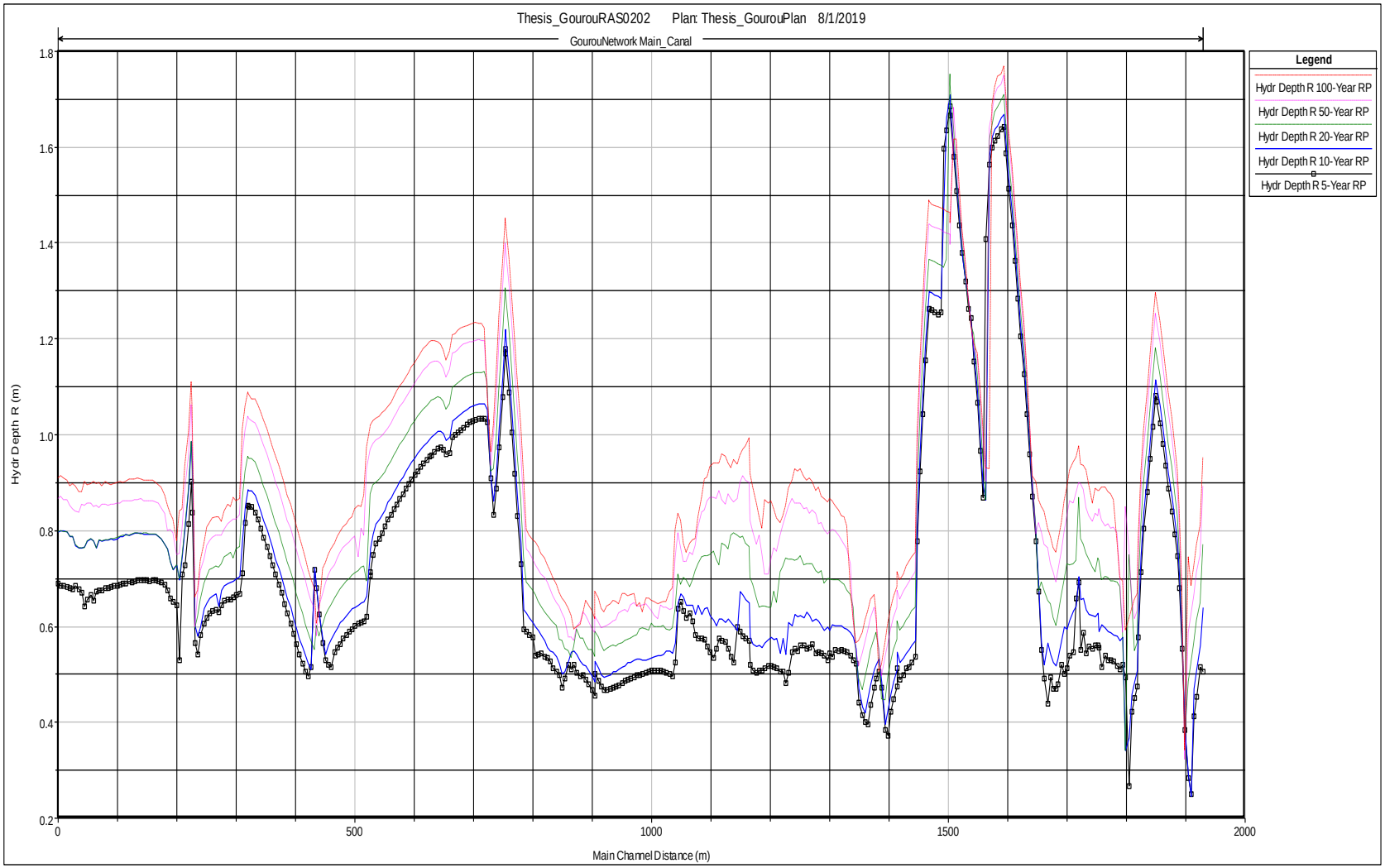

***Figure 4. 12**: Water depth in the right over bank*

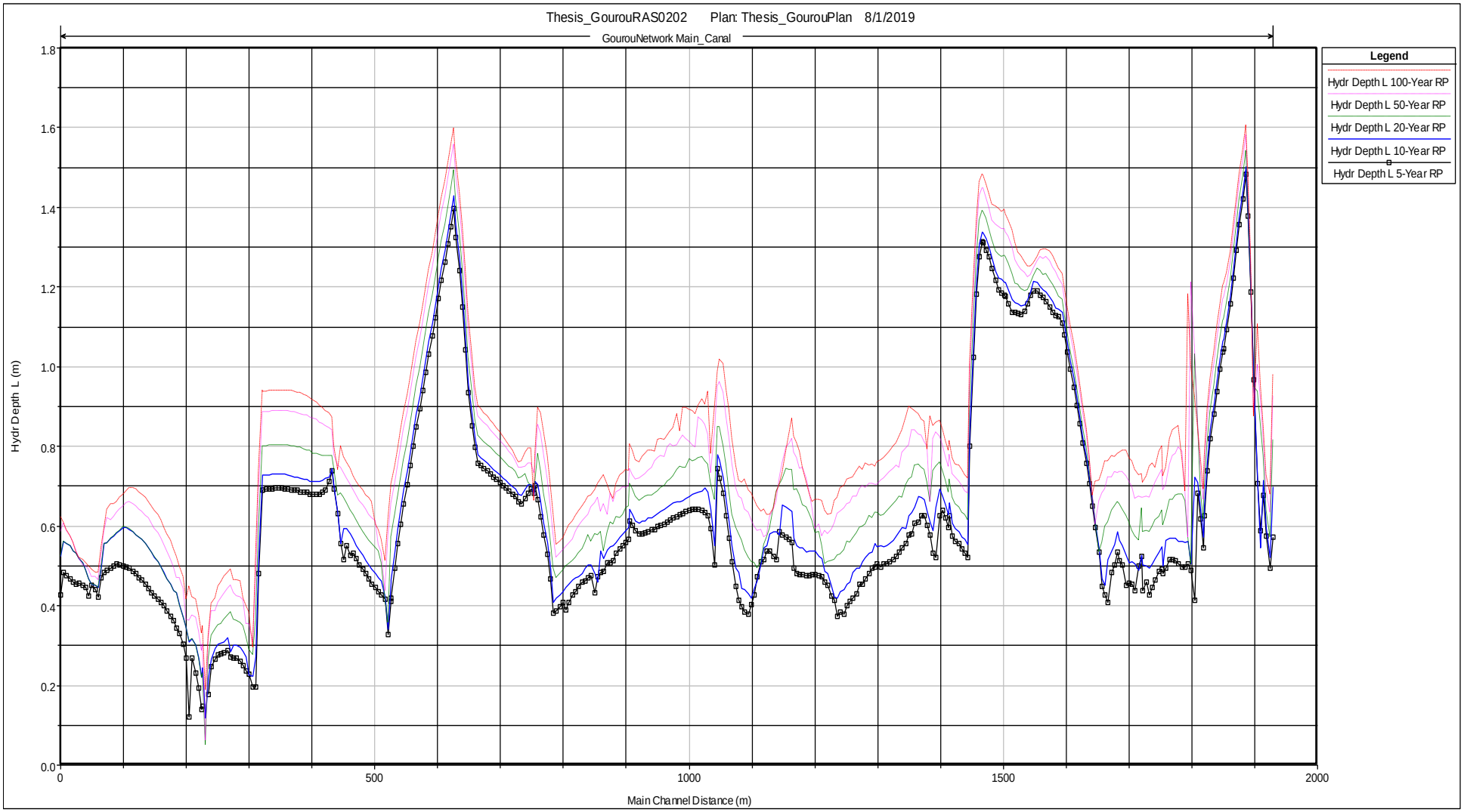

Figure 4. 13: *Water depth in the left over-bank*

4.3.2.2 Water flow velocity map

Despite the fact that water depth (maximum) is the main parameter when studying flood hazard, another parameters like velocity can also be important because, during flood event, water flows with a certain velocity which can cause some damages. It was found that the greatest velocities occurring in the main channel vary from 1.53 m/s up to 10 m/s while the velocities in the over banks (both Left and right) are less than 3.5 m/s (figure 4.17 and 4.18). Flow velocities simulated by HEC-RAS were displayed in RAS Mapper to show spatial distribution. We can see that, near the boundary of water extent, the velocities are closed to zero. A similar result was described by (Shroder et al., 2015). By using LISFLOOD model for performing hydraulic simulation for Carlisle site in United Kingdom, they found that water velocities in area where water comes into contact with people, the velocities range between 0 and 1 m/s while in the main channel it was around 3m/s. The flow velocity profile will be presented in appendix H.

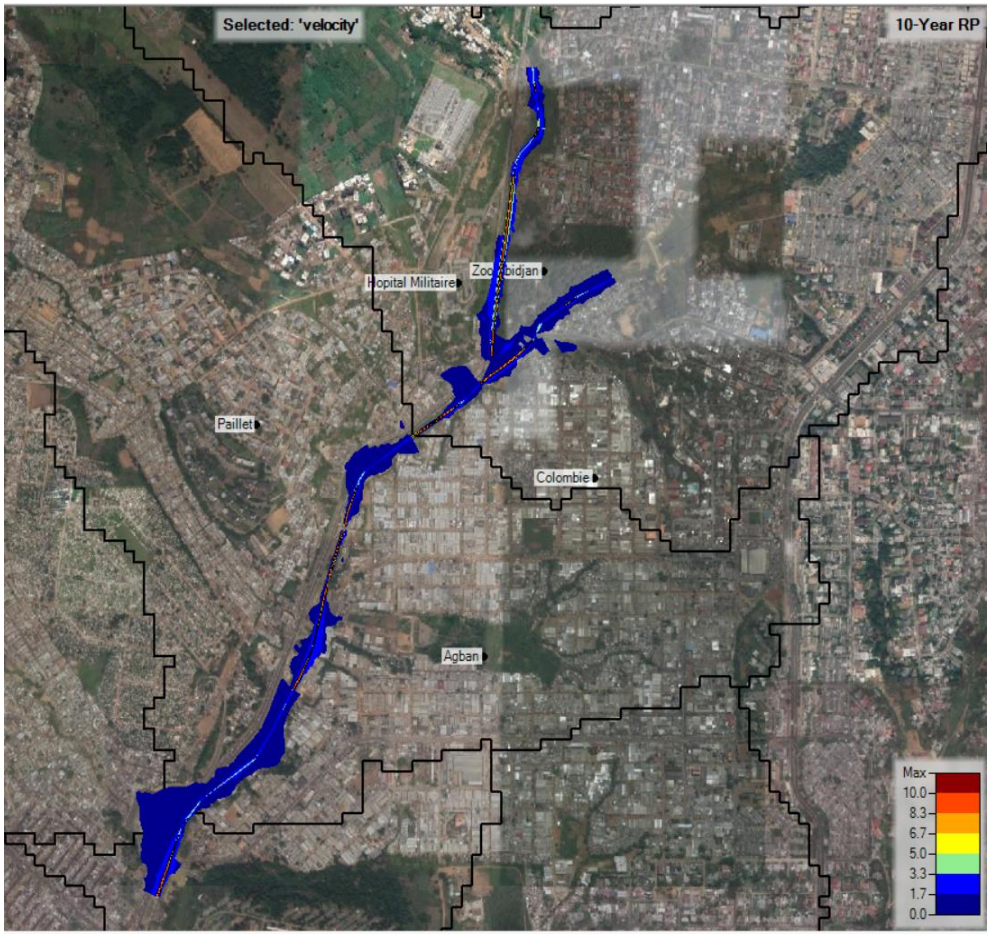

***Figure 4. 14**: Velocity map for 10-year flood*

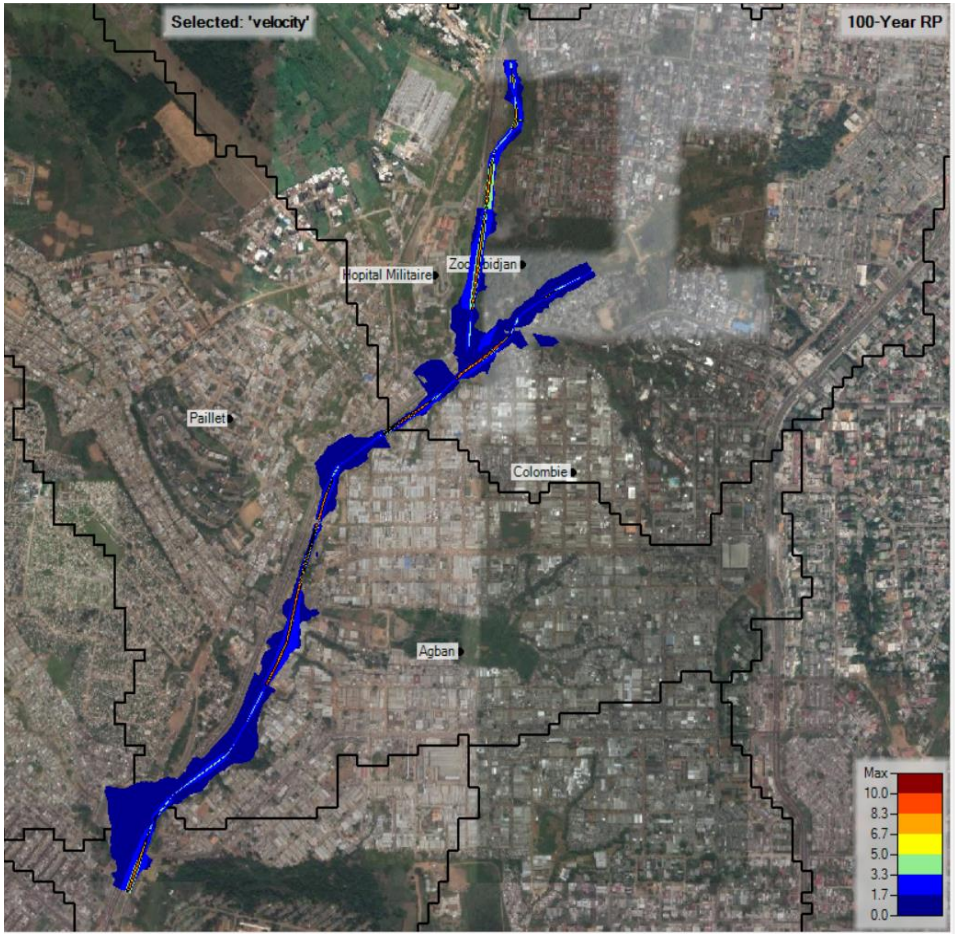

***Figure 4. 15**: Velocity map for 100-year flood*

The velocity in the maps are expressed in m/s.

4.4 Discussion

Since the recent development of hydrological models, hydrodynamic models, and GIS technologies, flood inundation modeling helps to come up with different maps showing the depth, the extent of inundated area to support the local planners, government and NGO in decision making. The main objective, when conducted this study, was to develop flood inundation map in order to improve the current practices to avert loses among communities during flooding times. The development of inundation map was support by hydrological and hydraulic modeling.

The HEC-HMS model simulated fairly well the peaks discharge though the model tends to underestimate the observed flow during the validation. The difference in the shape of the hydrograph may be attributed to the time step specified to run the modeled. Indeed, in the purpose of ensuring the stability of the Muskingum flood routing, a time step of 2 minutes was used or the observed flow data were recorded on hour basis. That why the hydrograph of observed flow is more abrupt in comparison with the simulated hydrograph. The NSE for calibration and validation were 0.74 and 0.92 respectively. A sensitivity analysis of the HEC-HMS model parameters used in this study showed that the model outputs are more sensitive to Curve Number compared to the percentage of impervious area and lag time. An underestimation of the CN (from -5% to -20%) will cause more error on prediction than an overestimation of the percent of impervious area and the lag time. As the SCS CN method has not been applied in our study are before, these results were compared to other study did in the district of Abidjan. By comparing the result with the work of Aimé, (2018). who used the SCS CN method for runoff prediction in “Rivera Palmeraie” in Abidjan, He came to the conclusion that the model is more sensitive to CN, the percent of impervious and the lag-time. He found for example that an increase of the lag time by 20% will result in a decrease in the peak flow of 5.5% which is almost equal to the result that we found. Again, these results are consistent with those obtained by (Nharo, Makurira, & Gumindoga, 2019). By applying HEC-HMS and HEC-RAS for floods mapping in the middle Zambesi basin, they reported that CN is the more sensitive parameter which influences the outputs of their model. Regarding the percentage of impervious area, it appears to be the second parameter which influences the model outputs. This finding comes to confirm the public opinion that the anarchic urbanization within the watershed yields an increase of the runoff. Similar results were obtained

in some previous study. (Chang *et al*, 2009), applied the SCS curve number method in HEC-HMS in Shihmen watershed for runoff-rainfall modeling. They found that the percentage of impervious area and the curve number were in direct proportion with the peak flow variation It means that when the CN and the percentage of impervious increase, the peak flow increase and when decreasing both parameters, the peak flow decreases.

Furthermore, the runoff hydrograph of the 10-year storm was compared to the 10-year storm used by some consulting firm (TERRABO, BRL group) for design. The peak discharge obtained in the frame of this study is 250 m^3/s while the one used by the consulting firms is 300 m^3/s. The difference can be due to the modeling approach. The past study used the rational method $\boldsymbol{Q = CIA}$ for hydrograph estimation in order to estimate the peak discharge. In most cases, this modeling approach does not account for the land use/land cover change and the heterogeneity of all watershed. Our study uses a distributed hydrological model with SCS-CN loss method for peak discharge estimation which takes into consideration some parameters like the CN, the Lag time that influences the runoff (peak discharge). Also, we should notice that generally, consulting firms used to increase the discharge by a certain amount for security purpose. Thus, we can say that the developed hydrological model is suitable for runoff prediction in the watershed.

From the result of hydrodynamics model, it was obvious that the floodplain inundated areas increase with the magnitude of flow within the modeled network confirming the high flood hazard level for settlements and activities near the main canal in Gourou watershed. The WSE profile showed a great variability as water is moving from upstream toward downstream. This result relates exactly what we observed during a rainfall event. Indeed, a field visit was done during a heavy storm. It was observed that water flow is characterized by important turbulence where the supercritical and subcritical flow are alternate. Also, the result can be accepted as we know that floods wave are characterized by great variability in time and space. Generally, the drainage systems in the country design with 10-year storm but our result showed that even 5-year flood exceeds the drainage capacity of the channel. The canal is a trapezoidal canal ($7 \times 3.18 \times 3.04$) that can accommodate a maximum discharge of 60 m3/s which is below the peak discharge of 5-year storm at the junction J92, 92.7 m^3/s. As said above, by the uncontrolled urbanization within the watershed contribute to an increase of the impervious areas and then the runoff. The canals

were constructed before the year 2000 according to a discussion with government agencies. At that time the estimated population where around 280 000 inhabitants but a recent estimation in 2014 showed that the population within the watershed is 446 267, a growth rate 2.2% which is not negligible and could significantly impact the canal capacity.

However, our HEC-RAS model tends to overestimate the water depth and underestimate the water extent due to the specified flow paths: once the water reaches the defined boundaries namely the "flow path", it cannot spread anymore, then water level raises. It can cause some errors in water depth estimation. This can be considered as a limitation of our model in estimating the inundated area/extent. This study found that the greatest velocities occurring in the main channel up to 10 m/s and decreases when the water spread in the over banks. The velocities in the over banks (both Left and right) are less than 3.5 m/s and closed to 0 m/s near the model boundary. This result is satisfactory because when looking at the velocity distribution in a trapezoidal open channel, the velocity is always higher in the center and decrease near the boundary (A. Osman, 2006).

Further investigations in the watershed may use a coupled 1D and 2D hydrodynamic model for the estimation of flood extent and flow characteristics. The 1D model will be applied in the main channel and the 2D model in the overbank. This will allow a better understanding of how water flows in the overbank because floods are usually unsteady flow.

4.5 Flood mitigation measures

Flood inundation map seems to be a vital component to defined flood mitigation measures as it allows the identification of the area where we need to concentrate the mitigation efforts. Flood mitigation is the different strategies need to be implemented to reduce damages of life and properties caused by floods. After the different analysis, it appeared that water is out of the banks for most of the flow scenarios. Thus, to keep the flood water within the extent of the bank, mitigation measure should be proposed. When dealing with flood mitigation measures, we have to types of mitigation measures: Structural measures and non-structural measures. The choice of any of these methods depends on the characteristics of the area. Considering the case of our study area, the proposed solution is to re-designed the canal in order to increase the cross-sectional area so that the drainage system will be able to drain water. Indeed, after some observation made on the

field, it is possible to widen the canal by 2 m both side and also increase the canal depth. This will result in an increase in drainage capacity.

Also, some non-structural measures can be applied. After many discussions with the community, it was found that there are not associated in the floodplain management, the decisions are of top-down type. Therefore, an integrated approach is preferable because If communities become involved in data collection for flood forecasting, and the importance of their role is understood, a sense of ownership is developed. Individuals can be appointed for the following tasks:

- caretakers of installations;
- be trained as gauge readers for manual instruments (rain gauges, water level recorders);
- radio operators to report real-time observations.

Gauge readers and observers perform a two-way role. As well as reporting information, they can use their local knowledge and understanding to report conditions. They also can have an important role in receiving information from headquarters to pass on to the community.

Trained individuals within the community should be able to gather and update information to:

- know the depth of past severe floods in the local area;
- know how quickly the waters might rise;
- know how long the floodwaters might remain in the locality;

By doing so, we can improve the data availability in the catchment and give better information to community for damages reduction.

5 CONCLUSION AND RECOMMENDATIONS

Even though extreme events cannot be prevented, a better understanding of the risk posed by such event is the first stage in building the resilience of the community. The analysis of the flood-prone area associated with flooding produces knowledge about the hazard and the vulnerability of the population at risk.

This study was carried out to construct hydrological and hydrodynamics models couple with GIS for flood inundation mapping in Gourou watershed in Côte d'Ivoire to support planners in decision making. To achieve this, two models were used in this study: the hydrological modeling was performed with Hydrologic Engineering Center-Hydrologic Modeling System (HEC-HMS) software and the hydraulic modeling of the canals was done with Hydrologic Engineering Center-River Analysis System (HEC-RAS). Digital Elevation Model (DEM) of the study was processed by HEC-GeoHMS to extract watershed physical characteristics as well as hydrologic information to prepare HEC-HMS model inputs. The discharge result obtained from HEC-HMS simulation were used to compute and produce flood inundation map for 5-, 10-, 20-, 50-, and 100-year flood.

From the hydrological result, it was fund that the discharges increase proportionally to curve number and the percentage of impervious area. A sensitivity analysis showed that the model outputs were more sensitive to curve number. Thus, the change in land use in the watershed should be monitored. However, the estimated peak discharge can be used for design purpose in the watershed. Furthermore, it is important to notice that GIS-Based hydrological modeling is useful because it allows the reduction of analysis time and improves the accuracy of hydrological studies.

On the other hand, the hydraulic modeling results showed that most parts of the right bank of Gourou canal is more vulnerable to flooding. Based on those results, and after field visit and discussion, it is worth to say that HEC-RAS can be used for flood level simulation within the watershed. The hydraulic modeling confirmed the incapacity of the drainage system to convey all the runoff from a storm beginning by 5-year storm. By using the model, the government agencies in Côte d'Ivoire can contribute to a significant reduction of flood damages.

For better management of the watershed, even though some initiatives have been taken by the government like the construction of storage area which is not sufficient, a flood emergency management strategy needs to be implemented for the settlements. This strategy should consider a communication plan of flood risk within the communities, and an evacuation plan which does not exist actually.

As no model is perfect, there is then a need to always refined the model. The current model can be refined by using a long series of discharge data to improve the quality of the calibration of the model parameters. Future studies may consider also the survey of household in the area to ameliorate the percentage of the impervious area used in hydrological modeling. HEC-RAS model was performed without the calibration of Manning's "n", it will be good to investigate the sensitivity of the model to the parameter in future work. Finally, due to time constraint, flood risk map was not developed. It will be interesting in future research to combine the water depth map and velocity map to produce a flood risk map for estimating the potential risks.

6 REFERENCES

A. Osman, A. (2006). *Open Channel Hydraulics* (First edit). Oxford: Elsevier's Science & Technology.

Ackerman, C. T., Wre, D., Jensen, M. R., & Brunner, G. W. (2010). Geospatial capabilities of HEC-RAS for model development and mapping. *2nd Joint Federal Interagency Conference*.

Aimé, K. (2018). *Urban flood modeling and floodplain mapping using ArcGIS, HEC-HMS and HEC-RAS in Abidjan City, Côte d'Ivoire-West Africa: Case Study of Bonoumin - Riviera Palmeraie Watershed*. Pan African University, Institue of Water and Energy Sciences.

Arlen D., F. (2000). Hydrologic Modeling System, HEC-HMS Technical Reference Manual. Davis, CA 95616-4687: US Army Corps of Engineers & Hydrologic Engineering Center.

Beighley, R. E., Dunne, T., & Melack, J. M. (2005). Understanding and modeling basin hydrology: Interpreting the hydrogeological signature. *Hydrological Processes*, *19*(7), 1333–1353. https://doi.org/10.1002/hyp.5567

Brunner, G. W., & CEIWR-HEC. (2016). HEC-RAS : River Analysis System User's Manual. Davis, CA 95616-4687: US Army Corps of Engineers & Institute for Water Resources & Hydrologic Engineering Center (HEC). Retrieved from www.hec.usace.army.mil

Chow, V. Te, Maidment, D. R., & Mays, L. W. (1988). *Applied Hydrology*. (B. J. Clark and John Morriss;, Ed.) (First Edit). McGraw-Hill.

Cunderlik, J., & Simonovic, S. P. (2004). *Calibration, Verification and Sensitivity analysis of the HEC-HMS Hydrologic Model*. ONTARIO.

Devia, G. K., Ganasri, B. P., & Dwarakish, G. S. (2015). A Review on Hydrological Models. *Aquatic Procedia*, *4*(Icwrcoe), 1001–1007. https://doi.org/10.1016/j.aqpro.2015.02.126

Ghalkhani, H., Golian, S., Saghafian, B., Farokhnia, A., & Shamseldin, A. (2012). Application of surrogate artificial intelligent models for real-time flood routing, *5*(2009), 1–14. https://doi.org/10.1111/j.1747-6593.2012.00344.x

Haan, C. . (2002). *Statistical methods in hydrology* (Second Edi). Iowa State Press.

Hicks, F. E., & Peacock, T. (2005). Suitability of HEC-RAS for Flood Forecasting. *Canadian Water Resources Journal*, *30*(2), 159–174. https://doi.org/10.4296/cwrj3002159

Houston, D., Werrity, A., Bassett, D., Geddes, A., Hoolachan, A., McMillan, M., … Bassett, D. (2011). Pluvial (rain-related) flooding in urban areas: the invisible hazard \textbar Joseph Rowntree Foundation, (November), 96. Retrieved from http://www.jrf.org.uk/publications/pluvial-flooding-invisible-hazard

Józsa, E., Fábián, S. Á., & Kovács, M. (2014). An evaluation of EU-DEM in comparison with ASTER GDEM, SRTM and contour-based dems over the eastern mecsek mountains. *Hungarian Geographical Bulletin*, *63*(4), 401–423. https://doi.org/10.15201/hungeobull.63.4.3

Lynn, J. (2014). GIS and Remote Sensing Applications in Modern Water Resources Engineering, 8_7. https://doi.org/10.1007/978-1-62703-595

Model, R. H., & Chang, C. (2009). *Application of SCS CN Method in HEC- HMS in Shihmen Watershed Simulation of Rainfall-Runoff Hydrologic Model*. FLORIDA STATE UNIVERSITY.

Mukolwe, M. M. (2016). Flood Hazard Mapping Uncertainty and its Value in the Decision-making Process. https://doi.org/978-1-138-03286-6

Nharo, T., Makurira, H., & Gumindoga, W. (2019). Mapping floods in the Middle Zambezi Basin using Earth observation and hydrological modeling techniques. *Physics and Chemistry of the Earth, Parts A/B/C*, (February), 0–1. https://doi.org/10.1016/j.pce.2019.06.002

Ohl, C. a, & Tapsell, S. (2000). Flooding and human health. The dangers posed are not always obvious. *BMJ (Clinical Research Ed.)*, *321*(November), 1167–1168. Retrieved from http://www.pubmedcentral.nih.gov/articlerender.fcgi?artid=1118941&tool=pmcentrez&rendertype=abstract

P. P. Mujumdar and D. Nagesh Kumar. (2012). *Floods in a Changing Climate - Hydrologic modeling*. (Cambridge University Press, Ed.) (First Edit). New York: Cambridge University Press. https://doi.org/1753-2000-2-33 [pii]\n10.1186/1753-2000-2-33

Paresh, D., Nigussie, B., & Belay, A. (2011). *GIS based HEC-HMS and HEC-RAS modeling - A study of Woldiya watershed in Ethiopia*. Saarbrucken: LAP LAMBERT Academic Publishing GmbH & Co. KG. Retrieved from info@lap-publishing.com

Saley, M. B., Kouamé, F. K., Penven, M. J., Biémi, J., & Boyossoro Kouadio, H. (2005). Cartographie Des Zones À Risque D'Inondation Dans La Région Semi-Montagneuse À Louest De La Côte D'Ivoire : Apports Des Mna Et De L'Imagerie Satellitaire. *Télédétection*, *5*(1-2–3), 53–67.

Scharffenberg, W. (2016). Hydrologic Modeling System, HEC-HMS User's Manual. Davis, CA 95616-4687: US Army Corps of Engineers & Institute for Water Resources & Hydrologic Engineering Center (CEIWR-HEC). Retrieved from https://www.hec.usace.army.mil/software/hec-hms/downloads.aspx

Shroder, J. F., Paolo, P., & Guiliano, D. B. (2015). *Hydro-Meteorological Hazards, Risks, and Disasters* (Elsevier). Amsterdam: Elsevier.

Soil Conservation Service. (1986). *Urban hydrology for small watersheds Technical Release 55*. Springfield.

Tassew, B. G., Belete, M. A., & Miegel, K. (2019). Application of HEC-HMS Model for Flow Simulation in the Lake Tana Basin : The Case of Gilgel Abay Catchment, Upper Blue Nile Basin , Ethiopia, 1–17. https://doi.org/10.3390/hydrology6010021

Tastet, J., & Aka, K. (1982). Géologie et Environnement Sédimentaires de la Marge Continentale De Côte-D 'Ivoire. In *Environnement et Ressources Aquatiques de Côte d'Ivoire* (pp. 23–56).

Timbadiya, P. V., Patel, P. L., & Porey, P. D. (2011). Calibration of HEC-RAS Model on Prediction of Flood for Lower Tapi River, India. *Journal of Water Resource and Protection*, *03*(11), 805–811. https://doi.org/10.4236/jwarp.2011.311090

Ward, R. C. (1978). Floods: A Geographical Perspective. *Macmillan*.

7 APPENDIX

APPENDIX A: Runoff Curve Numbers-Urban Areas[1]

Cover description — Cover type and hydrologic condition	Average percent impervious area[2]	Curve numbers for hydrologic soil group — A	B	C	D
Fully developed urban areas (vegetation established)					
Open space (lawns, parks, golf courses, cemeteries, etc.)[3]:					
Poor condition (grass cover < 50%)		68	79	86	89
Fair condition (grass cover 50% to 75%)		49	69	79	84
Good condition (grass cover > 75%)		39	61	74	80
Impervious areas:					
Paved parking lots, roofs, driveways, etc. (excluding right-of-way)		98	98	98	98
Streets and roads:					
Paved; curbs and storm sewers (excluding right-of-way)		98	98	98	98
Paved; open ditches (including right-of-way)		83	89	92	93
Gravel (including right-of-way)		76	85	89	91
Dirt (including right-of-way)		72	82	87	89
Western desert urban areas:					
Natural desert landscaping (pervious areas only)		63	77	85	88
Artificial desert landscaping (impervious weed barrier, desert shrub with 1- to 2-inch sand or gravel mulch and basin borders)		96	96	96	96
Urban districts:					
Commercial and business	85	89	92	94	95
Industrial	72	81	88	91	93
Residential districts by average lot size:					
1/8 acre or less (town houses)	65	77	85	90	92
1/4 acre	38	61	75	83	87
1/3 acre	30	57	72	81	86
1/2 acre	25	54	70	80	85
1 acre	20	51	68	79	84
2 acres	12	46	65	77	82
Developing urban areas					
Newly graded areas (pervious areas only, no vegetation)		77	86	91	94

[1] Average runoff condition, and $I_a = 0.2S$.

[2] The average percent impervious area shown was used to develop the composite CN's. Other assumptions are as follows: impervious areas are directly connected to the drainage system, impervious areas have a CN of 98, and pervious areas are considered equivalent to open space in good hydrologic condition. CN's for other combinations of conditions may be computed using figure 2-3 or 2-4.

[3] CN's shown are equivalent to those of pasture. Composite CN's may be computed for other combinations of open space cover type.

APPENDIX B: DEM preprocessing result

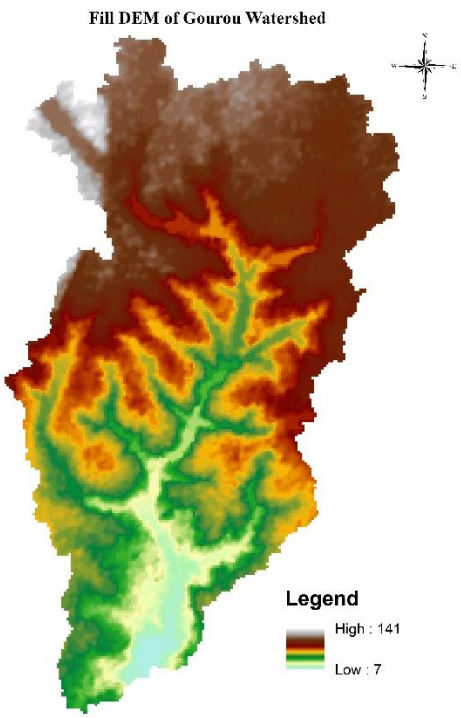

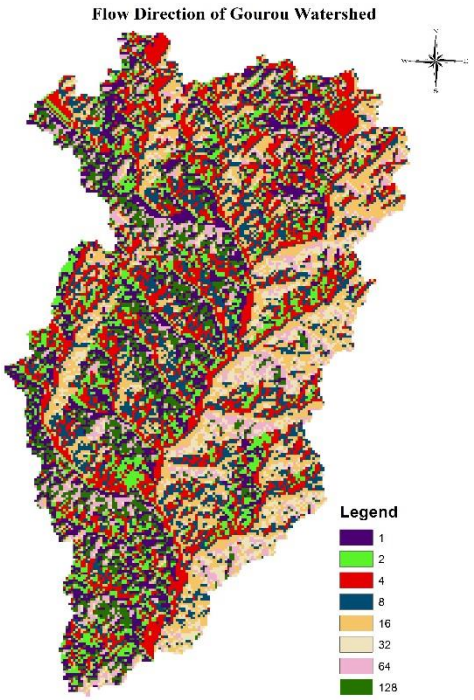

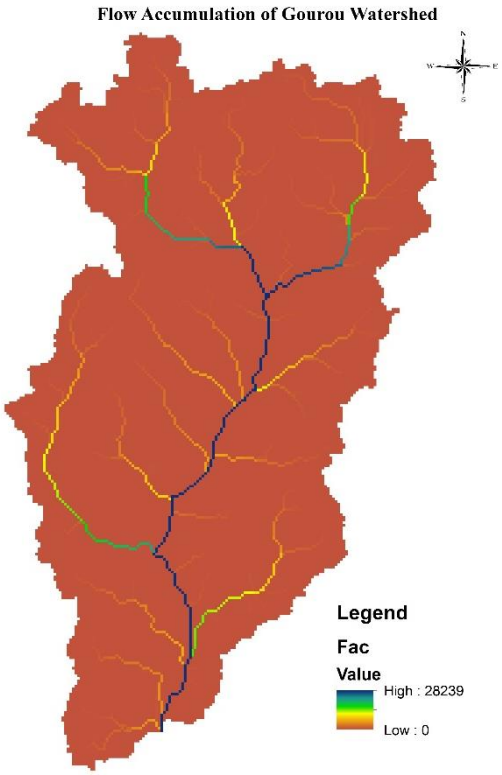

APPENDIX C: SUB-WATERSHED AND REACHES CHARACTERISTICS

Table B1: Sub-watershed characteristics

Name	BasinSlope	LossMet	TransMet	BasinCN	LagMethod	BasinLag	Area_HMS Km2	Perimeter_Km
W360	3.429	SCS	SCS	71.91297	CNLag	1.658	5.115	15.219
W390	2.497	SCS	SCS	72.11744	CNLag	2.203	4.566	14.665
W400	4.648	SCS	SCS	72.80425	CNLag	0.997	3.127	11.707
W410	4.965	SCS	SCS	72.70483	CNLag	1.423	3.241	14.234
W480	4.869	SCS	SCS	74.1465	CNLag	0.824	1.302	6.655
W520	4.049	SCS	SCS	79.42714	CNLag	1.083	1.511	8.811
W530	4.490	SCS	SCS	76.78096	CNLag	1.096	2.054	8.811
W540	4.358	SCS	SCS	75.64405	CNLag	1.580	2.909	13.987
W620	3.281	SCS	SCS	81.00638	CNLag	1.177	2.978	11.276

Table B2: Reaches characteristics

Name	Slp	ElevUP	ElevDS	RivLen	RouteMet
R10	0.022582	110	93	752.8056	Muskingum
R20	0.015865	107	93	882.4202	Muskingum
R30	0.030152	95	88	232.1582	Muskingum
R40	0.010741	100	88	1,117.22	Muskingum
R50	0.014183	93	68	1,762.65	Muskingum
R60	0.024343	99	68	1,273.45	Muskingum
R70	0.017783	68	55	731.0208	Muskingum
R80	0.020353	88	55	1,621.37	Muskingum
R90	0.011609	55	41	1,205.91	Muskingum
R100	0.0151	58	41	1,125.79	Muskingum
R110	0.022848	55	37	787.8053	Muskingum
R120	0.017926	41	37	223.1346	Muskingum
R130	0.023728	68	37	1,306.45	Muskingum
R140	0	37	37	130.7093	Muskingum
R150	0.007273	37	32	687.451	Muskingum
R160	0.022471	45	32	578.5266	Muskingum
R170	0.023101	52	31	909.0374	Muskingum
R180	0.004482	32	31	223.1346	Muskingum
R190	0.015405	43	27	1,038.65	Muskingum
R200	0.006933	31	27	576.9784	Muskingum
R210	0.01363	69	21	3,521.75	Muskingum
R220	0.008505	27	21	705.4982	Muskingum
R230	0.005528	21	13	1,447.09	Muskingum
R240	0.011553	40	13	2,336.99	Muskingum
R250	0.023455	38	10	1,193.79	Muskingum
R260	0.025435	13	10	117.9479	Muskingum
R270	0.0228	23	7	701.7604	Muskingum
R280	0.004074	10	7	736.3067	Muskingum
R290	0	7	7	21.78483	Muskingum
R300	0.02166	17	7	461.6735	Muskingum
R310	0	7	7	184.8508	Muskingum

APPENDIX D: LAND USE CLASSIFICATION RESULT: *Confusion Matrix*

Ground Truth (Pixels)

Class	ROI	#Forest_VROI	#Mixed VeROI	#_ROI_UrbROI	#Water_Va	Total
Unclassified		0	0	0	0	0
ROI #Forest_C		1226736	2220	0	169	1229125
ROI #Mixed Ve		111610	32782	5	511	144908
ROI #_Urbaniz		1060	2461	22777	2763	29061
ROI #_Water_C		8	0	0	102072	102080
Total		1339414	37463	22782	105515	1505174

Ground Truth (Percent)

Class	ROI	#Forest_VROI	#Mixed VeROI	#_ROI_UrbROI	#Water_Va	Total
Unclassified		0.00	0.00	0.00	0.00	0.00
ROI #Forest_C		91.59	5.93	0.00	0.16	81.66
ROI #Mixed Ve		8.33	87.51	0.02	0.48	9.63
ROI #_Urbaniz		0.08	6.57	99.98	2.62	1.93
ROI #_Water_C		0.00	0.00	0.00	96.74	6.78
Total		100.00	100.00	100.00	100.00	100.00

Class	Commission (Percent)	Omission (Percent)	Commission (Pixels)	Omission (Pixels)
ROI #Forest_C	0.19	8.41	2389/1229125	112678/1339414
ROI #Mixed Ve	77.38	12.49	112126/144908	4681/37463
ROI #_Urbaniz	21.62	0.02	6284/29061	5/22782
ROI #_Water_C	0.01	3.26	8/102080	3443/105515

Class	Prod. Acc. (Percent)	User Acc. (Percent)	Prod. Acc. (Pixels)	User Acc. (Pixels)
ROI #Forest_C	91.59	99.81	1226736/1339414	1226736/1229125
ROI #Mixed Ve	87.51	22.62	32782/37463	32782/144908
ROI #_Urbaniz	99.98	78.38	22777/22782	22777/29061
ROI #_Water_C	96.74	99.99	102072/105515	102072/102080

APPENDIX E: Sensitivity analysis result

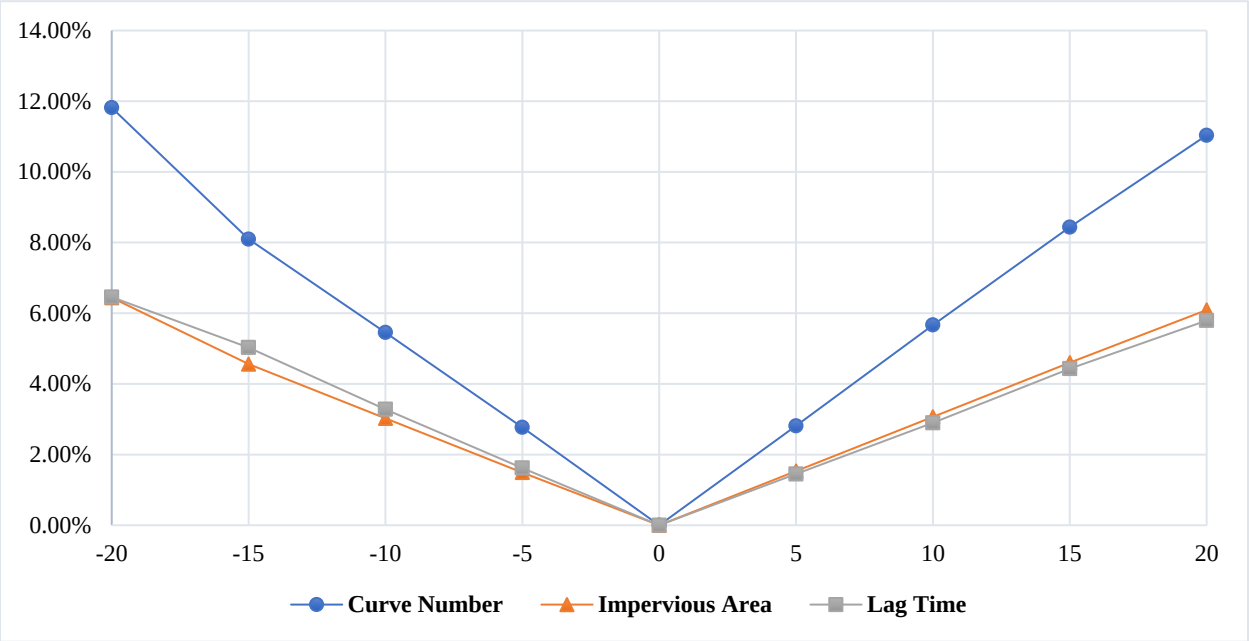

Figure F1: Parameters influence on Peak Flow of 5-Year Return Period

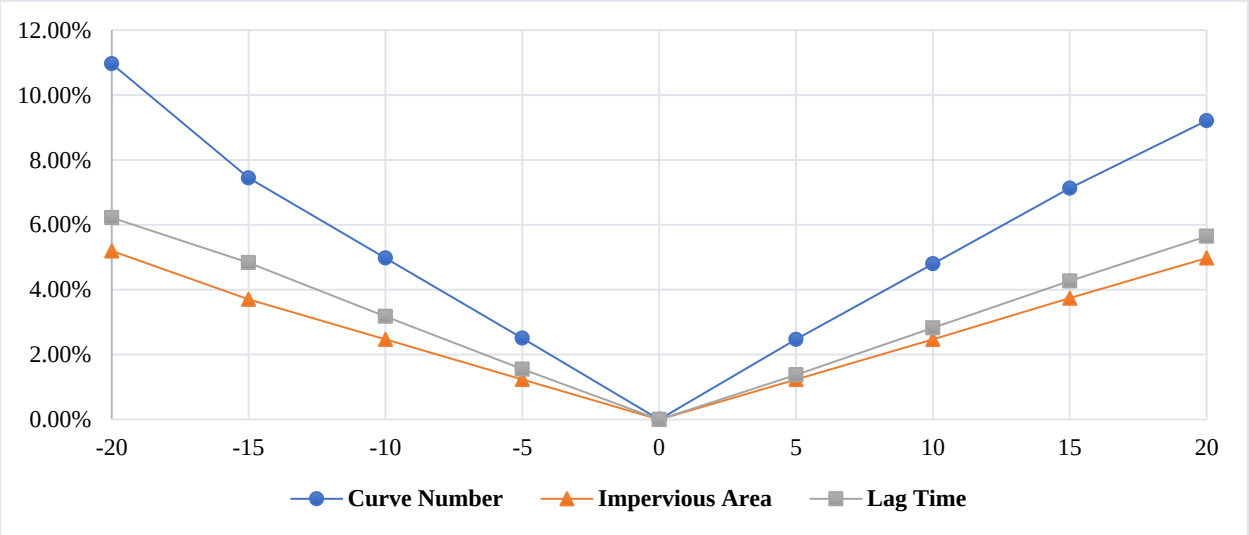

Figure F2: Parameters influence on Peak Flow of 20-Year Return Period

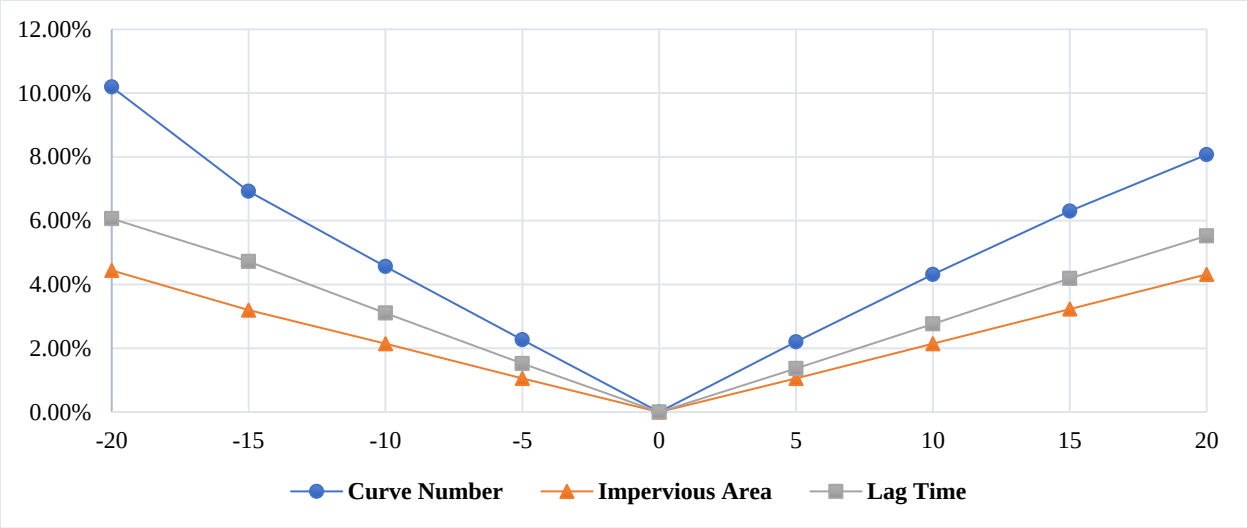

Figure F3: Parameters influence on Peak Flow of 50-Year Return Period

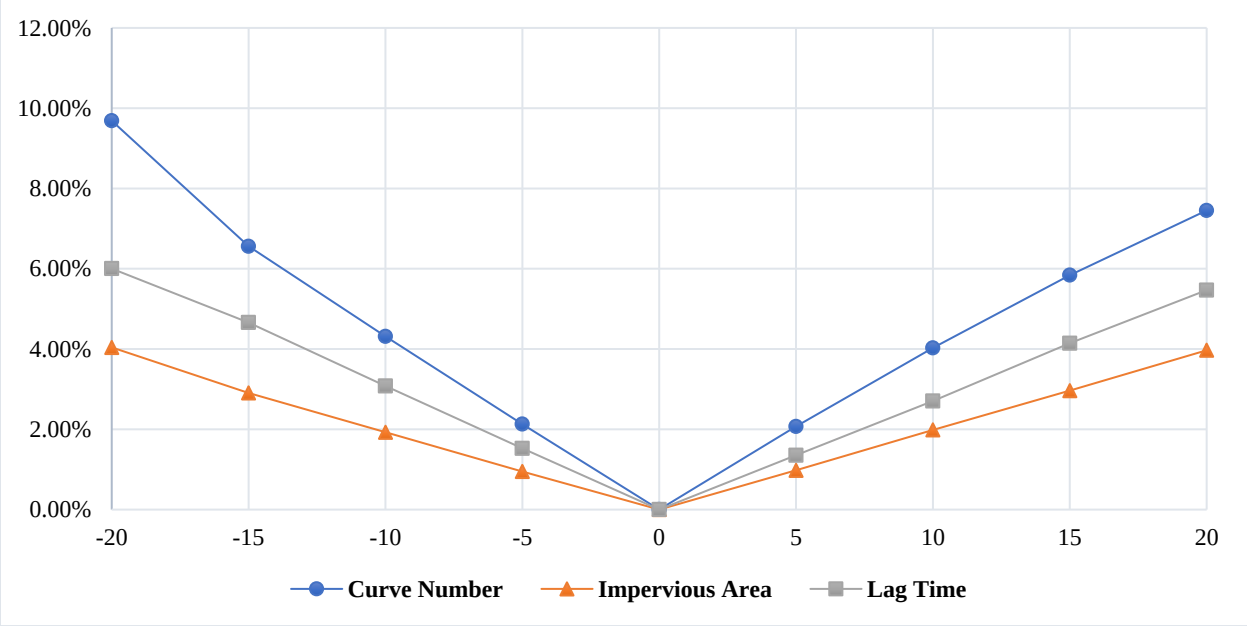

Figure F4: Parameters influence on Peak Flow of 100-Year Return Period

APPENDIX F: HEC-HMS Model result

Global Summary Results for Run "Run 3_5 Year RP"

Project: Thesis_ETCHE Simulation Run: Run 3_5 Year RP

Start of Run: 18Jun2018, 22:00 Basin Model: MasterThesisEtche_Go
End of Run: 19Jun2018, 22:00 Meteorologic Model: Met_5 Year Return Period
Compute Time: 25Jul2019, 00:29:19 Control Specifications: ControlSpe_5 year RP

Show Elements: All Elements Volume Units: (•) MM ( ) 1000 M3 Sorting: Hydrologic

Hydrologic Element	Drainage Area (KM2)	Peak Discharge (M3/S)	Time of Peak	Volume (MM)
W530	2.0540	33.6	19Jun2018, 02:10	125.66
W520	1.5111	26.3	19Jun2018, 02:10	132.11
W480	1.3022	26.2	19Jun2018, 01:55	132.54
W620	2.9775	51.0	19Jun2018, 02:15	144.62
W410	3.2414	48.4	19Jun2018, 02:25	139.23
W400	3.1275	94.4	19Jun2018, 01:30	124.23
W390	4.5664	34.1	19Jun2018, 04:35	138.67
W360	5.1150	47.5	19Jun2018, 03:40	138.46
W540	2.9092	40.8	19Jun2018, 02:35	141.13
Outlet1	26.8043	234.7	19Jun2018, 02:55	136.27
J85	17.3525	121.0	19Jun2018, 02:30	135.65
J92	12.8089	97.2	19Jun2018, 01:30	135.06
J80	23.8268	206.9	19Jun2018, 02:35	135.23
J95	9.6814	80.2	19Jun2018, 04:10	138.56
J98	5.1150	47.5	19Jun2018, 03:40	138.46
J101	20.2617	160.6	19Jun2018, 02:40	136.44
J104	9.6814	76.6	19Jun2018, 05:00	138.56
J106	9.6814	76.0	19Jun2018, 05:20	138.56
J109	12.8089	74.6	19Jun2018, 06:05	135.06
J111	12.8089	73.8	19Jun2018, 06:30	135.06
J116	23.8268	206.2	19Jun2018, 02:40	135.23
J118	23.8268	203.2	19Jun2018, 02:50	135.23
J120	23.8268	202.6	19Jun2018, 03:00	135.23
R70	5.1150	47.0	19Jun2018, 04:00	138.46
R90	9.6814	76.6	19Jun2018, 05:00	138.56
R120	9.6814	76.0	19Jun2018, 05:20	138.56
R140	9.6814	75.4	19Jun2018, 05:40	138.56
R150	12.8089	74.6	19Jun2018, 06:05	135.06
R180	12.8089	73.8	19Jun2018, 06:30	135.06
R200	12.8089	73.3	19Jun2018, 06:50	135.06
R220	17.3525	119.9	19Jun2018, 02:40	135.65
R230	20.2617	160.2	19Jun2018, 02:45	136.44
R260	23.8268	206.2	19Jun2018, 02:40	135.23
R280	23.8268	203.2	19Jun2018, 02:50	135.23
R290	23.8268	202.1	19Jun2018, 03:05	135.23
R310	23.8268	202.6	19Jun2018, 03:00	135.23

Figure E1: Global Summary Result of HEC-HMS Model for 5 years return period

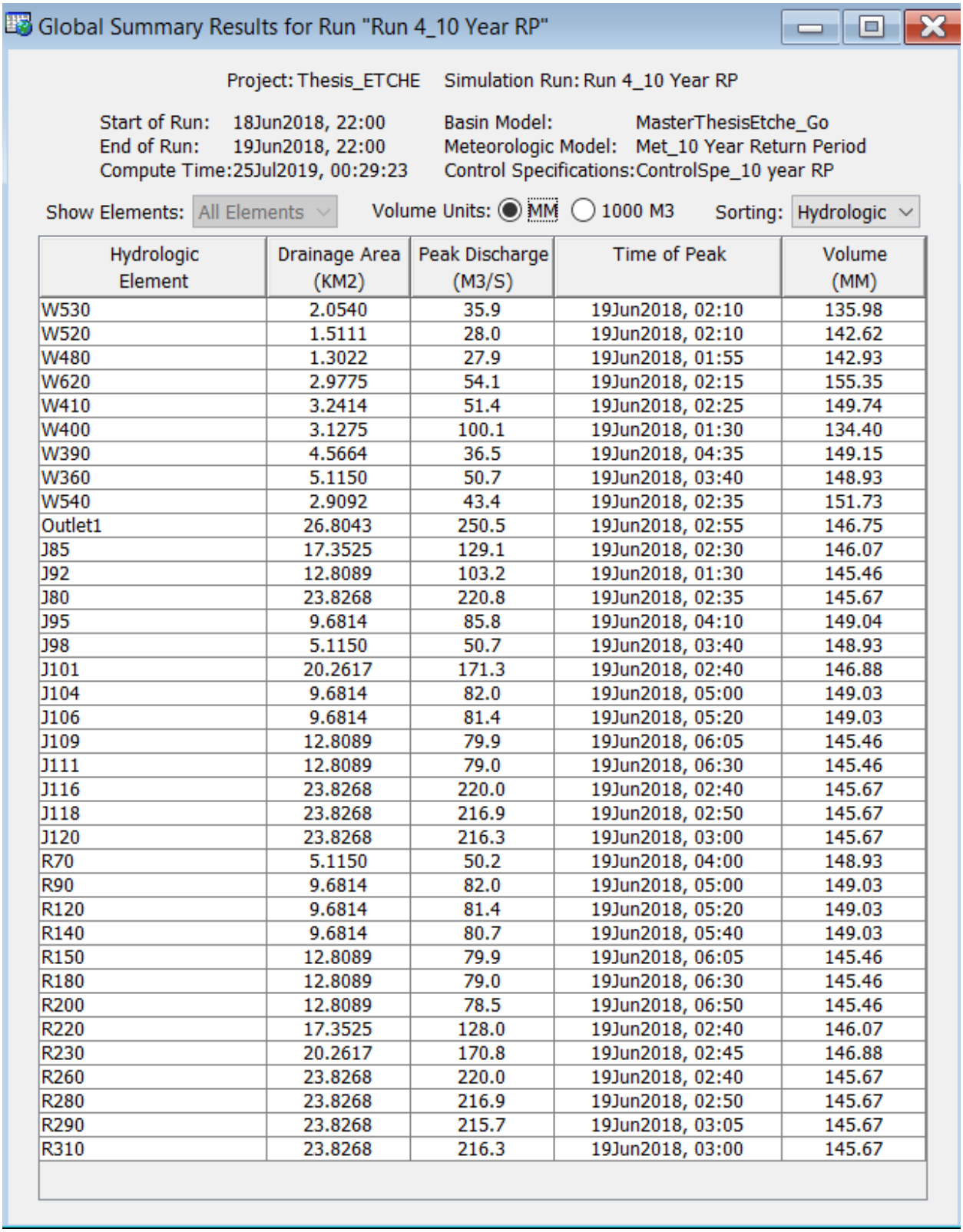

Hydrologic Element	Drainage Area (KM2)	Peak Discharge (M3/S)	Time of Peak	Volume (MM)
W530	2.0540	35.9	19Jun2018, 02:10	135.98
W520	1.5111	28.0	19Jun2018, 02:10	142.62
W480	1.3022	27.9	19Jun2018, 01:55	142.93
W620	2.9775	54.1	19Jun2018, 02:15	155.35
W410	3.2414	51.4	19Jun2018, 02:25	149.74
W400	3.1275	100.1	19Jun2018, 01:30	134.40
W390	4.5664	36.5	19Jun2018, 04:35	149.15
W360	5.1150	50.7	19Jun2018, 03:40	148.93
W540	2.9092	43.4	19Jun2018, 02:35	151.73
Outlet1	26.8043	250.5	19Jun2018, 02:55	146.75
J85	17.3525	129.1	19Jun2018, 02:30	146.07
J92	12.8089	103.2	19Jun2018, 01:30	145.46
J80	23.8268	220.8	19Jun2018, 02:35	145.67
J95	9.6814	85.8	19Jun2018, 04:10	149.04
J98	5.1150	50.7	19Jun2018, 03:40	148.93
J101	20.2617	171.3	19Jun2018, 02:40	146.88
J104	9.6814	82.0	19Jun2018, 05:00	149.03
J106	9.6814	81.4	19Jun2018, 05:20	149.03
J109	12.8089	79.9	19Jun2018, 06:05	145.46
J111	12.8089	79.0	19Jun2018, 06:30	145.46
J116	23.8268	220.0	19Jun2018, 02:40	145.67
J118	23.8268	216.9	19Jun2018, 02:50	145.67
J120	23.8268	216.3	19Jun2018, 03:00	145.67
R70	5.1150	50.2	19Jun2018, 04:00	148.93
R90	9.6814	82.0	19Jun2018, 05:00	149.03
R120	9.6814	81.4	19Jun2018, 05:20	149.03
R140	9.6814	80.7	19Jun2018, 05:40	149.03
R150	12.8089	79.9	19Jun2018, 06:05	145.46
R180	12.8089	79.0	19Jun2018, 06:30	145.46
R200	12.8089	78.5	19Jun2018, 06:50	145.46
R220	17.3525	128.0	19Jun2018, 02:40	146.07
R230	20.2617	170.8	19Jun2018, 02:45	146.88
R260	23.8268	220.0	19Jun2018, 02:40	145.67
R280	23.8268	216.9	19Jun2018, 02:50	145.67
R290	23.8268	215.7	19Jun2018, 03:05	145.67
R310	23.8268	216.3	19Jun2018, 03:00	145.67

Figure E2: Global Summary Result of HEC-HMS Model for 10 years return period

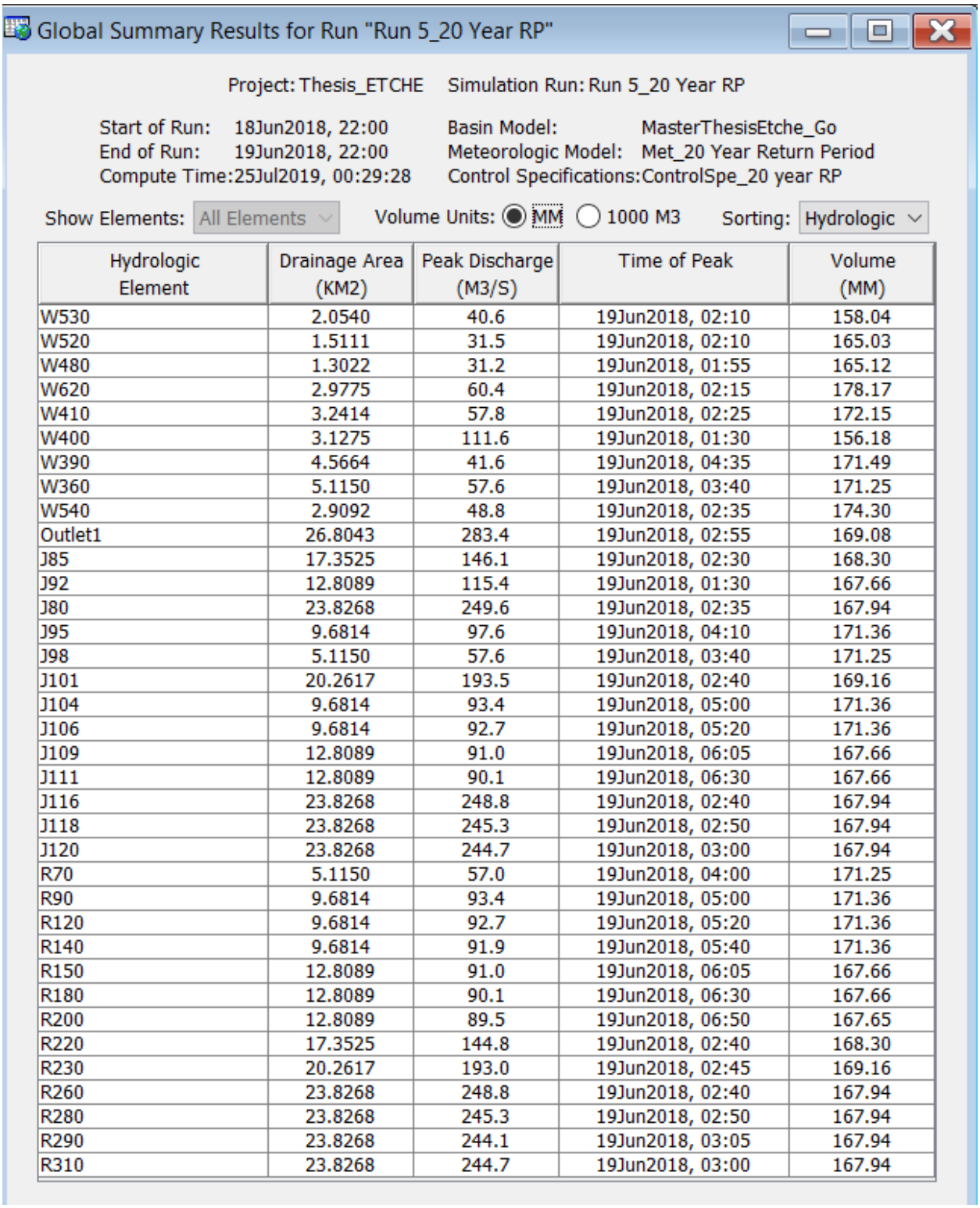

Hydrologic Element	Drainage Area (KM2)	Peak Discharge (M3/S)	Time of Peak	Volume (MM)
W530	2.0540	40.6	19Jun2018, 02:10	158.04
W520	1.5111	31.5	19Jun2018, 02:10	165.03
W480	1.3022	31.2	19Jun2018, 01:55	165.12
W620	2.9775	60.4	19Jun2018, 02:15	178.17
W410	3.2414	57.8	19Jun2018, 02:25	172.15
W400	3.1275	111.6	19Jun2018, 01:30	156.18
W390	4.5664	41.6	19Jun2018, 04:35	171.49
W360	5.1150	57.6	19Jun2018, 03:40	171.25
W540	2.9092	48.8	19Jun2018, 02:35	174.30
Outlet1	26.8043	283.4	19Jun2018, 02:55	169.08
J85	17.3525	146.1	19Jun2018, 02:30	168.30
J92	12.8089	115.4	19Jun2018, 01:30	167.66
J80	23.8268	249.6	19Jun2018, 02:35	167.94
J95	9.6814	97.6	19Jun2018, 04:10	171.36
J98	5.1150	57.6	19Jun2018, 03:40	171.25
J101	20.2617	193.5	19Jun2018, 02:40	169.16
J104	9.6814	93.4	19Jun2018, 05:00	171.36
J106	9.6814	92.7	19Jun2018, 05:20	171.36
J109	12.8089	91.0	19Jun2018, 06:05	167.66
J111	12.8089	90.1	19Jun2018, 06:30	167.66
J116	23.8268	248.8	19Jun2018, 02:40	167.94
J118	23.8268	245.3	19Jun2018, 02:50	167.94
J120	23.8268	244.7	19Jun2018, 03:00	167.94
R70	5.1150	57.0	19Jun2018, 04:00	171.25
R90	9.6814	93.4	19Jun2018, 05:00	171.36
R120	9.6814	92.7	19Jun2018, 05:20	171.36
R140	9.6814	91.9	19Jun2018, 05:40	171.36
R150	12.8089	91.0	19Jun2018, 06:05	167.66
R180	12.8089	90.1	19Jun2018, 06:30	167.66
R200	12.8089	89.5	19Jun2018, 06:50	167.65
R220	17.3525	144.8	19Jun2018, 02:40	168.30
R230	20.2617	193.0	19Jun2018, 02:45	169.16
R260	23.8268	248.8	19Jun2018, 02:40	167.94
R280	23.8268	245.3	19Jun2018, 02:50	167.94
R290	23.8268	244.1	19Jun2018, 03:05	167.94
R310	23.8268	244.7	19Jun2018, 03:00	167.94

Figure E3: Global Summary Result of HEC-HMS Model for 20 years return period

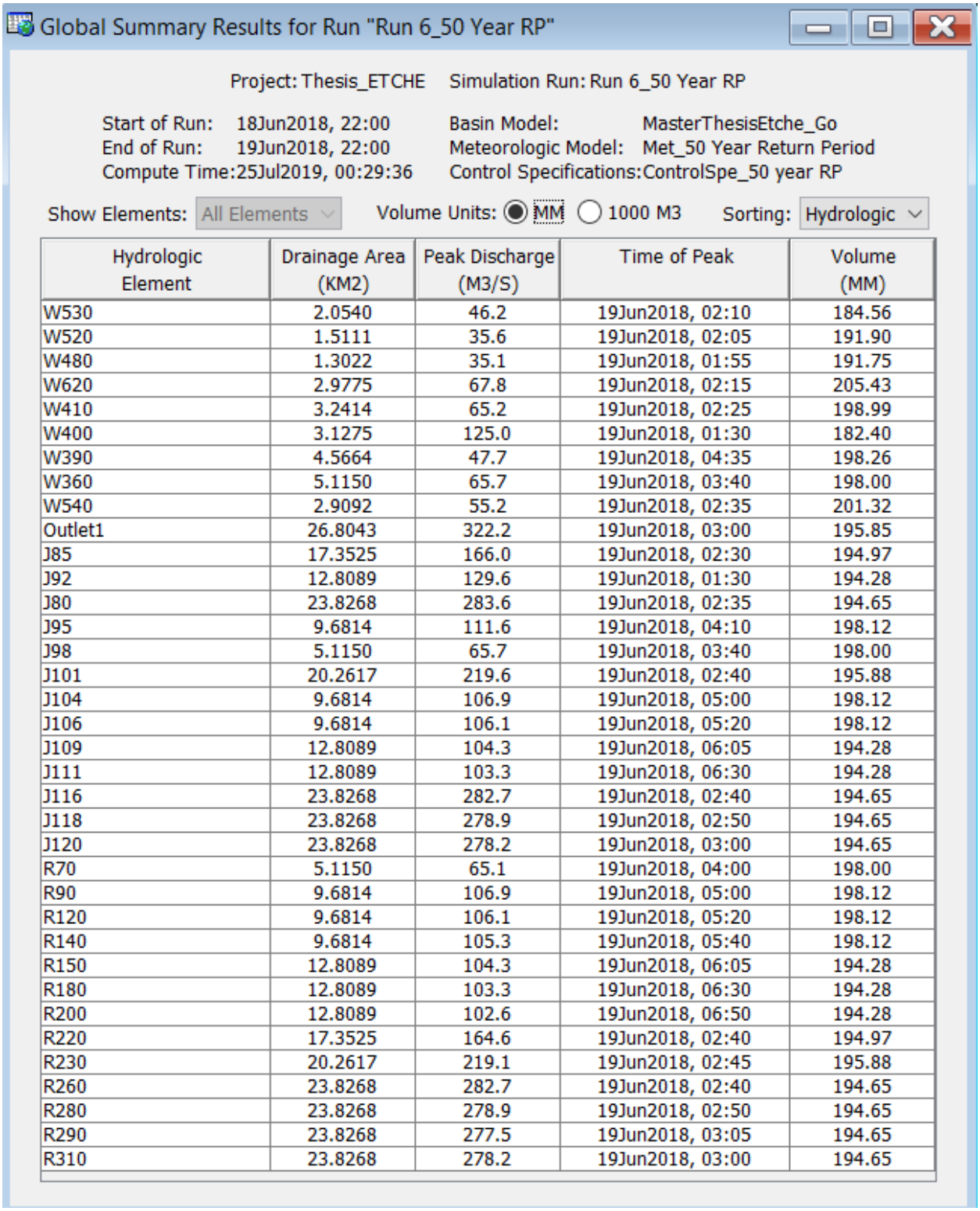

Global Summary Results for Run "Run 6_50 Year RP"

Project: Thesis_ETCHE Simulation Run: Run 6_50 Year RP

Start of Run: 18Jun2018, 22:00 Basin Model: MasterThesisEtche_Go
End of Run: 19Jun2018, 22:00 Meteorologic Model: Met_50 Year Return Period
Compute Time: 25Jul2019, 00:29:36 Control Specifications: ControlSpe_50 year RP

Show Elements: All Elements Volume Units: MM 1000 M3 Sorting: Hydrologic

Hydrologic Element	Drainage Area (KM2)	Peak Discharge (M3/S)	Time of Peak	Volume (MM)
W530	2.0540	46.2	19Jun2018, 02:10	184.56
W520	1.5111	35.6	19Jun2018, 02:05	191.90
W480	1.3022	35.1	19Jun2018, 01:55	191.75
W620	2.9775	67.8	19Jun2018, 02:15	205.43
W410	3.2414	65.2	19Jun2018, 02:25	198.99
W400	3.1275	125.0	19Jun2018, 01:30	182.40
W390	4.5664	47.7	19Jun2018, 04:35	198.26
W360	5.1150	65.7	19Jun2018, 03:40	198.00
W540	2.9092	55.2	19Jun2018, 02:35	201.32
Outlet1	26.8043	322.2	19Jun2018, 03:00	195.85
J85	17.3525	166.0	19Jun2018, 02:30	194.97
J92	12.8089	129.6	19Jun2018, 01:30	194.28
J80	23.8268	283.6	19Jun2018, 02:35	194.65
J95	9.6814	111.6	19Jun2018, 04:10	198.12
J98	5.1150	65.7	19Jun2018, 03:40	198.00
J101	20.2617	219.6	19Jun2018, 02:40	195.88
J104	9.6814	106.9	19Jun2018, 05:00	198.12
J106	9.6814	106.1	19Jun2018, 05:20	198.12
J109	12.8089	104.3	19Jun2018, 06:05	194.28
J111	12.8089	103.3	19Jun2018, 06:30	194.28
J116	23.8268	282.7	19Jun2018, 02:40	194.65
J118	23.8268	278.9	19Jun2018, 02:50	194.65
J120	23.8268	278.2	19Jun2018, 03:00	194.65
R70	5.1150	65.1	19Jun2018, 04:00	198.00
R90	9.6814	106.9	19Jun2018, 05:00	198.12
R120	9.6814	106.1	19Jun2018, 05:20	198.12
R140	9.6814	105.3	19Jun2018, 05:40	198.12
R150	12.8089	104.3	19Jun2018, 06:05	194.28
R180	12.8089	103.3	19Jun2018, 06:30	194.28
R200	12.8089	102.6	19Jun2018, 06:50	194.28
R220	17.3525	164.6	19Jun2018, 02:40	194.97
R230	20.2617	219.1	19Jun2018, 02:45	195.88
R260	23.8268	282.7	19Jun2018, 02:40	194.65
R280	23.8268	278.9	19Jun2018, 02:50	194.65
R290	23.8268	277.5	19Jun2018, 03:05	194.65
R310	23.8268	278.2	19Jun2018, 03:00	194.65

Figure E4: Global Summary Result of HEC-HMS Model for 50 years return period

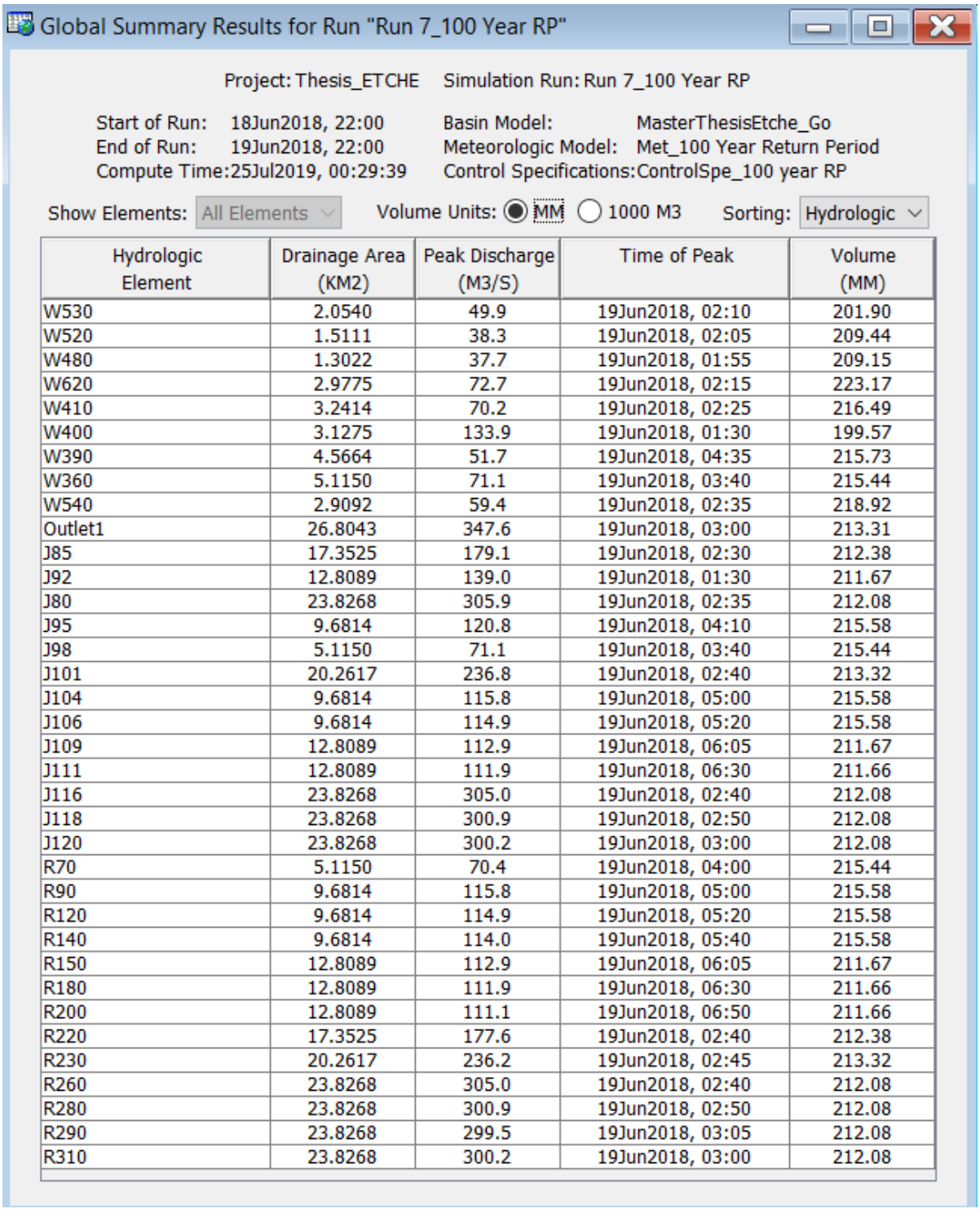

Hydrologic Element	Drainage Area (KM2)	Peak Discharge (M3/S)	Time of Peak	Volume (MM)
W530	2.0540	49.9	19Jun2018, 02:10	201.90
W520	1.5111	38.3	19Jun2018, 02:05	209.44
W480	1.3022	37.7	19Jun2018, 01:55	209.15
W620	2.9775	72.7	19Jun2018, 02:15	223.17
W410	3.2414	70.2	19Jun2018, 02:25	216.49
W400	3.1275	133.9	19Jun2018, 01:30	199.57
W390	4.5664	51.7	19Jun2018, 04:35	215.73
W360	5.1150	71.1	19Jun2018, 03:40	215.44
W540	2.9092	59.4	19Jun2018, 02:35	218.92
Outlet1	26.8043	347.6	19Jun2018, 03:00	213.31
J85	17.3525	179.1	19Jun2018, 02:30	212.38
J92	12.8089	139.0	19Jun2018, 01:30	211.67
J80	23.8268	305.9	19Jun2018, 02:35	212.08
J95	9.6814	120.8	19Jun2018, 04:10	215.58
J98	5.1150	71.1	19Jun2018, 03:40	215.44
J101	20.2617	236.8	19Jun2018, 02:40	213.32
J104	9.6814	115.8	19Jun2018, 05:00	215.58
J106	9.6814	114.9	19Jun2018, 05:20	215.58
J109	12.8089	112.9	19Jun2018, 06:05	211.67
J111	12.8089	111.9	19Jun2018, 06:30	211.66
J116	23.8268	305.0	19Jun2018, 02:40	212.08
J118	23.8268	300.9	19Jun2018, 02:50	212.08
J120	23.8268	300.2	19Jun2018, 03:00	212.08
R70	5.1150	70.4	19Jun2018, 04:00	215.44
R90	9.6814	115.8	19Jun2018, 05:00	215.58
R120	9.6814	114.9	19Jun2018, 05:20	215.58
R140	9.6814	114.0	19Jun2018, 05:40	215.58
R150	12.8089	112.9	19Jun2018, 06:05	211.67
R180	12.8089	111.9	19Jun2018, 06:30	211.66
R200	12.8089	111.1	19Jun2018, 06:50	211.66
R220	17.3525	177.6	19Jun2018, 02:40	212.38
R230	20.2617	236.2	19Jun2018, 02:45	213.32
R260	23.8268	305.0	19Jun2018, 02:40	212.08
R280	23.8268	300.9	19Jun2018, 02:50	212.08
R290	23.8268	299.5	19Jun2018, 03:05	212.08
R310	23.8268	300.2	19Jun2018, 03:00	212.08

Figure E5: Global Summary Result of HEC-HMS Model for 100 years return period

APPENDIX G: Water surface profile of the main channel

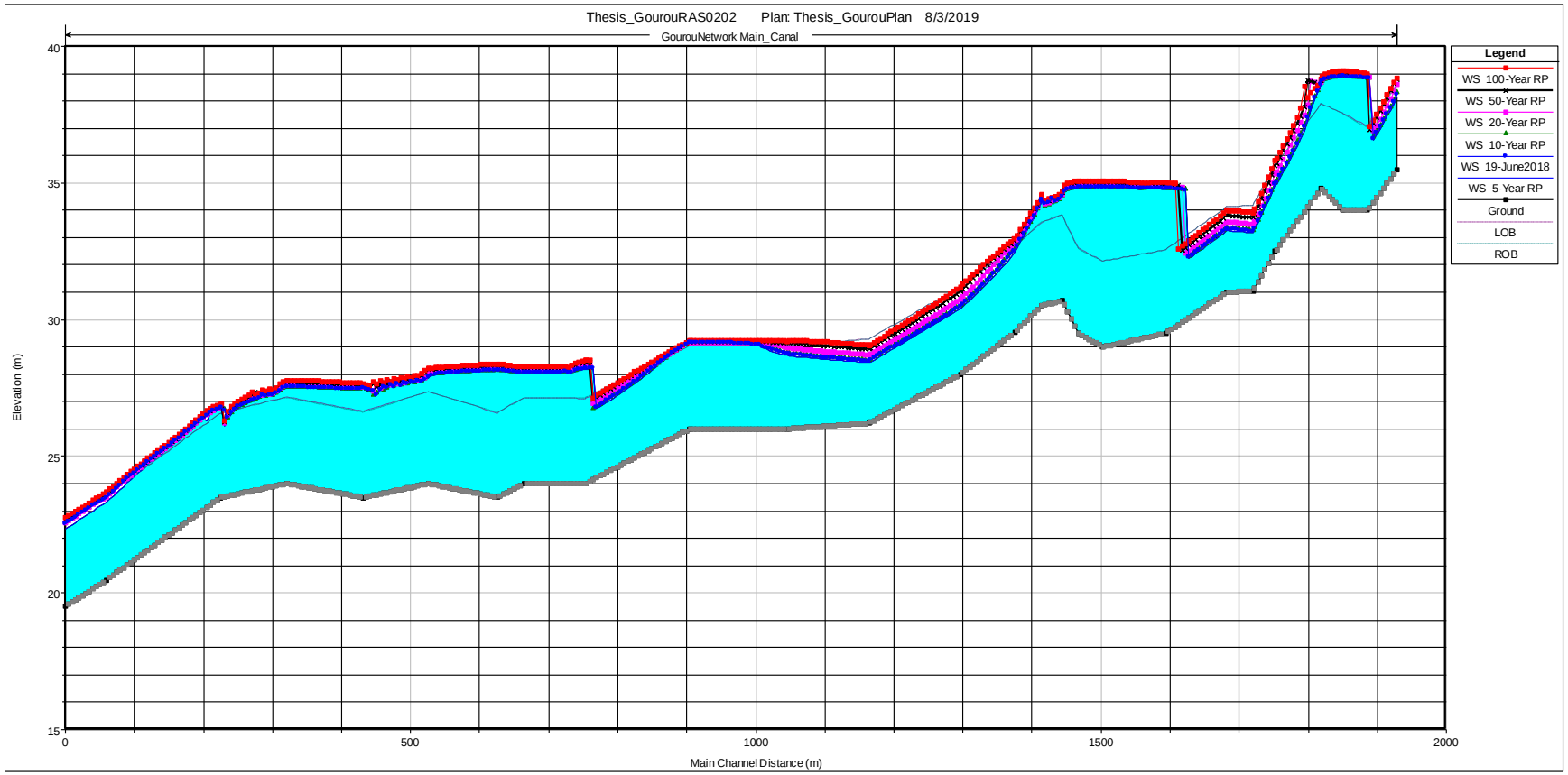

APPENDIX H: Water velocity profile